Alma Mater Studiorum - Università di Bologna

DOTTORATO DI RICERCA IN

MECCANICA E SCIENZE AVANZATE DELL'INGEGNERIA

Ciclo 35

Settore Concorsuale: 09/C1 - MACCHINE E SISTEMI PER L'ENERGIA E L'AMBIENTE

Settore Scientifico Disciplinare: ING-IND/08 - MACCHINE A FLUIDO

STUDY OF LOW GRADE TEMPERATURE CCHP SYSTEMS FOR THE
REALIZATION OF ZERO POWER BUILDINGS

Presentata da: Walter Lombardo

Coordinatore Dottorato

Lorenzo Donati

Supervisore

Andrea De Pascale

Co-supervisori CNR-ITAE

Salvatore Vasta
Alessio Sapienza

Esame finale anno 2023

INDEX

LIST OF FIGURES

NOMENCLATURE

CCHP	Combined Cooling, Heating and Power	
NZEB	Nearly Zero Energy Building	
SHP	Separate Heat and Power	
ORC	Organic Rankine Cycle	
AC	Adsorption Chiller	
HP	Heat Pump	
TES	Thermal Energy Storage	
ICE	Internal Combustion Engine	
HVAC	Heating, Ventilation, And Air Conditioning	
ACP	Average Cooling Power	kW
SCP	Specific Cooling Power	kW/kg
VCP	Volumetric Cooling Power	kW/m^3
S/V	Surface to volume ratio	m^{-1}
S	Net floor area	m^2
s	Thickness	m
U	Stationary thermal transmittance	$W/m^2\,K$
U_g	Glass thermal transmittance	$W/m^2\,K$
U_f	Frame thermal transmittance	$W/m^2\,K$
HDD	Heating daily Degree Days	
FPC	Flat Plate Collectors	
PV	Photovoltaic	
A	Area of the collectors	m^2
c_p	Specific heat,	$J/kg\,K$
P_e	Electric power	kW_e

4

Q_c	Cooling Power	kW_e
Q_{th}	Thermal Power	kW_t
E	Annual energy	kW_h
I	Solar radiation	W/m^2
$\dot{m}$	Mass flow rate	kg/h
$\dot{V}$	Volumetric flow rate	m^3/h
t	Time	s
h	Hour	
h_n	Specific enthalpy at point n of the cycle,	$kJ/kg\ K$
T	Temperature	$°C$
T_{TES}	Average temperature of the TES	$°C$
SPB	Simple Pay Back Period	y
COP	Coefficient Of Performance	
PES	Primary Energy Saving	
NPV	Net Present Value	
GWP	Global Warming Potential	
FESR	Fuel Energy Saving Ratio	
IC	Investment Cost	$€$
f_{CO2}	Italian CO_2 emission factor	kg_{CO2}/kWh

Subscripts

a	Ambient
m	Mechanical
el	Electrical
in	Inlet
out	Outlet
c	Cooling
h	Heating
exp	Expander
iso	Isentropic
p	Pump
Rec	Recuperator
SH	Superheating degree
L	Low
M	Medium
H	High
glob	global

Greek Symbols

ρ	Density	kg/m^3
η	Efficiency	$\%$

ACKNNOWLEDGEMENT

Walter Lombardo

ABSTRACT

   Combined Cooling Heat and Power Generation (CCHP) or trigeneration has been considered worldwide as a suitable alternative to traditional energy systems in terms of significant energy saving and environmental conservation. A renewable energy resource-fueled CCHP would deliver even more environmental benefits than a fossil fuel-driven system. Solar is one of the renewable energy resources that plays an important role to the world primary energy supplies and can be used to fuel CCHP systems. In particular, solar driven microscale CCHP (1-10 kW$_c$) which is suitable for building applications has been yet commercialized or demonstrated. The development and evaluation of a solar driven micro-CCHP system based on a ORC cogenerator and an Adsorption Chiller (AC) experimental prototypes has been the focus of this PhD research.
The specific objectives of the overall project are:

- To design, construct and evaluate an innovative Adsorption Chiller in order to improve the performance of the AC subsection.
- To thermodynamically model the proposed micro-scale solar driven CHP system and to prove that the concept of trigeneration through solar energy combined with an organic Rankine turbine cycle (ORC) and an adsorption chiller (AC) is suitable for residential applications.

Following the introduction of relevant background of this research, Chapter 1 describes the International, European, and Italian regulatory framework respectively to outline the context the study has been carried out in.
Chapter 2 presents the state of the art in the literature of these systems. In particular, two innovative technologies are studied in depth: absorption machines and low temperature ORC systems. Both have to reach technological maturity, be studied and optimized. The study of these systems, coupled together in a CCHP configuration, was carried out following two parallel paths.
Chapter 3 describes the development of an innovative two bed solid adsorption chiller. The particularity of this proposal mainly concerns the materials used for the adsorbent bed and the management system, described later in detail.
In Chapter 4, the micro-scale solar CCHP system conceived for the residential sector has been investigated by means of a dynamic model in TRNSYS. In particular, the system is composed of a 60 m^2 flat plate solar thermal collectors' field, a 10 kW$_e$ photovoltaic plant, a 2 m^3 Thermal Energy Storage (TES), a 3 kW$_e$ micro-Organic Rankine Cycle (micro-ORC) prototype, a 4.4 kW$_c$ thermally driven Adsorption Chiller (AC) coupled with a 6 kW$_c$ auxiliary Heat Pump (HP). The dynamic performances of the considered system have been evaluated with respect to a real "nearly zero energy building" (NZEB) located in three different cities representative of the Italian climatic zones: Messina, Rome and Milan.
The energy, environmental and economic performances of the proposed system are presented as results in Chapter 5 and compared with those achieved by the reference system based on separated energy production.
The conclusions, discussed in Chapter 6, highlights the potential of solar driven micro-CCHP systems for residential applications, and their characteristics; moreover, the proposed model can be adopted as a tool for the design and the verify the feasibility of similar systems by redefining the different subsystems according to the desired technology.

1. REGULATORY FRAMEWORK

1.1.   Global energy trends

In the last years, the increasing global energy demand and, thus, the energy-related environment pollution, has led to looking for new strategies in several sectors including manufacturing, transports, buildings, services. Energy efficiency plays an essential role in accelerating clean energy transitions and achieving global climate and sustainability goals.

According the Global CO_2 emissions from energy combustion and industrial processes [1] rebounded in 2021 to reach their highest ever annual level. A 6% increase from 2020 pushed emissions to 36.3 gigatons (Gt), an estimate based on the IEA's detailed region-by-region and fuel-by-fuel analysis, drawing on the latest official national data and publicly available energy, economic and weather data. The Covid-19 pandemic had far-reaching impacts on energy demand in 2020, reducing global CO_2 emissions by 5.1%, as showed in Figure 1. However, the world has experienced an extremely rapid economic recovery since then, driven by unprecedented fiscal and monetary stimulus and a fast – although uneven – roll-out of vaccines. The recovery of energy demand in 2021 was compounded by adverse weather and energy market conditions, which led to more coal being burnt despite renewable power generation registering its largest ever annual growth. Emissions increased by over 2.0 Gt from 2020 levels. This puts 2021 above 2010 as the largest ever year-on-year increase in energy-related CO_2 emissions in absolute terms. The rebound in 2021 more than reversed the pandemic-induced decline in emissions of close to 1.9 Gt experienced in 2020. CO_2 emissions in 2021 rose to around 180 megatons (Mt) above the pre-pandemic level of 2019.
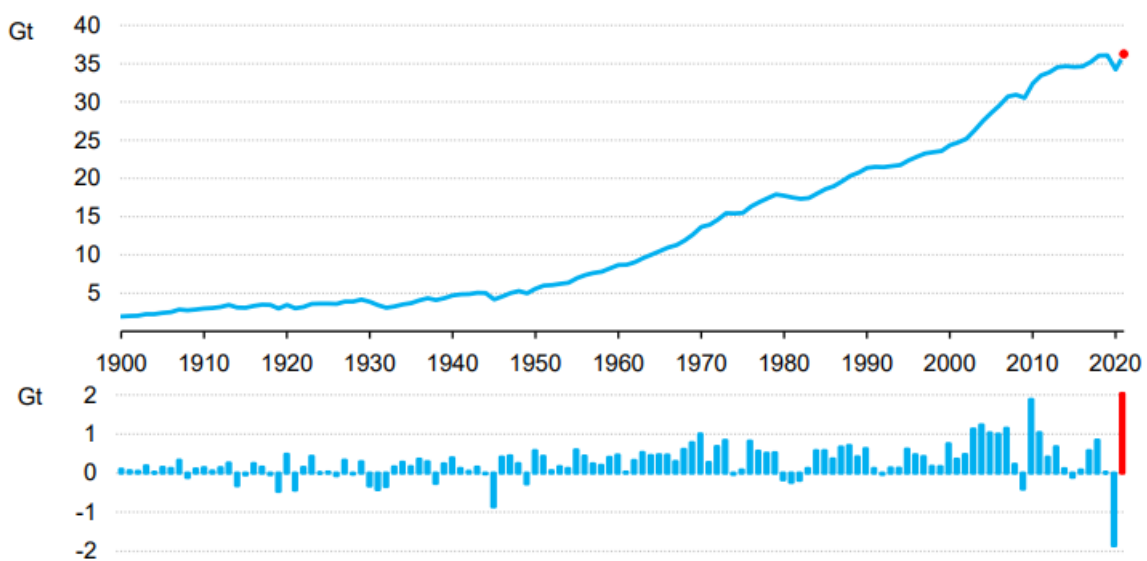
Figure 1 Total CO_2 emissions from energy combustion and industrial processes and their annual change, 1900-2021 [1]

Global energy demand is expected to increase by about 4% in the next years, returning to pre-pandemic levels as economic activity rebounds. The previous year was one of the worst ever for efficiency improvement, as energy demand and prices fell, technical efficiency enhancements slowed and the balance of economic activity shifted away from less energy-intensive services, such as hospitality and tourism. With disruptions due to Covid-19 shaping global energy and economic trends in 2020 and 2021, it is still unclear whether this year's improved energy intensity will signal the start of a sustained recovery. However, increased investment trends, rising government spending on

efficiency - in large part related to recovery plans enacted in response to Covid-19 crisis, new announcements of higher climate ambition and other policy measures offer some encouraging signals [2].
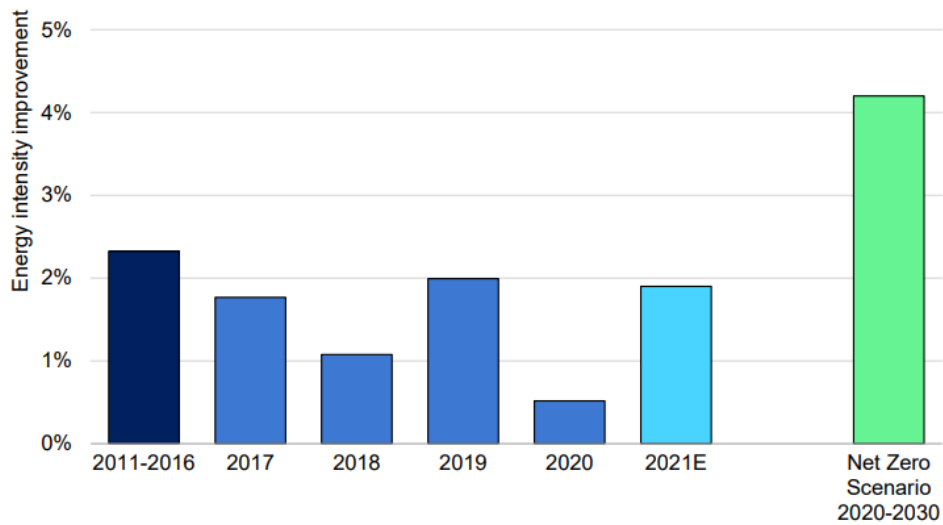
Figure 2 Primary energy intensity improvement, 2011-2021

The economic recovery in China appears to be particularly energy intensive. The China's Global energy intensity (GDP) between 2019 and 2021 improved by an average of only 1% annually, compared with 1.2% between 2008 and 2010 when China enacted huge economic stimulus, and an average improvement rate of 3.7% from 2010 to 2019. China's energy intensity in 2021 was impacted primarily by evolutions in the electricity sector. With rapid GDP growth and additional electrification of energy services, electricity demand in China grew by 10% in 2021, faster than economic growth at 8.4%. The increase in demand of almost 700 TWh was the largest ever experienced in China. With demand growth outstripping the increase of low emissions supply, coal was called on to fill 56% of the rise in electricity demand. This was despite the country also seeing its largest ever increase in renewable power output in 2021. Electricity generation from renewables in China neared 2500 TWh in 2021, accounting for 28% of total generation in the country. CO_2 emissions in India rebounded strongly in 2021 to rise 80 Mt above 2019 levels, led by growth in coal use for electricity generation. Coal-fired generation reached an all-time high in India, jumping 13% above the level in 2020 when coal generation had declined by 3.7%. This was in part because the growth of renewables slowed to one-third of its average rate of the previous five years.
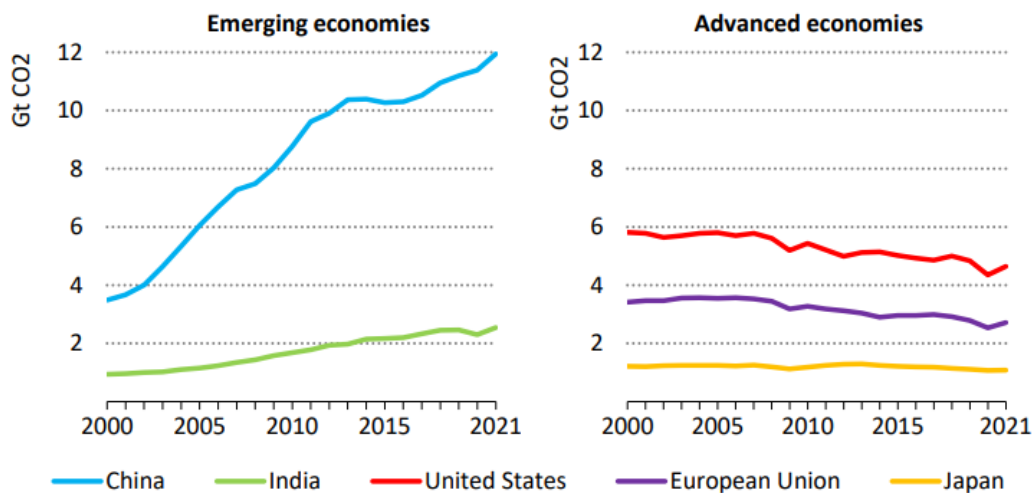
Figure 3 CO₂ emissions in selected emerging and advanced economies, 2000-2021 [1]

9

Global economic output in advanced economies recovered to pre-pandemic levels in 2021, but CO_2 emissions rebounded less sharply, signaling a more permanent trajectory of structural decline. CO_2 emissions in the United States in 2021 were 4% below their 2019 level. In the European Union, they were 2.4% lower. In Japan, emissions dropped by 3.7% in 2020 and rebounded by less than 1% in 2021. Across advanced economies overall, structural changes such as increased uptake of renewables, electrification and energy efficiency improvements avoided an additional 100 Mt of CO_2 emissions in 2021 compared with 2020.

Dividing the total emissions into the related sources, Coal accounted for over 40% of the overall growth in global CO_2 emissions in 2021, as showed in Figure 4. Coal emissions now stand at an all-time high of 15.3 Gt, surpassing their previous peak (seen in 2014) by almost 200 Mt. CO_2 emissions from natural gas also rebounded well above 2019 levels to 7.5 Gt, as demand increased in all sectors. At 10.7 Gt, emissions from oil remained significantly below pre-pandemic levels because of the limited recovery in global transport activity in 2021.

Coal-fired power plants were called upon to meet half of the increase in global electricity demand in 2021, with coal's share of total generation rebounding above 36%. CO_2 emissions from coal power plants rose to a record 10.5 Gt, which is 800 Mt above their 2020 level and more than 200 Mt above their previous peak in 2018. Without supply constraints and high prices that affected China and India during certain periods of the year, global coal use for electricity generation in 2021 would have been even higher.
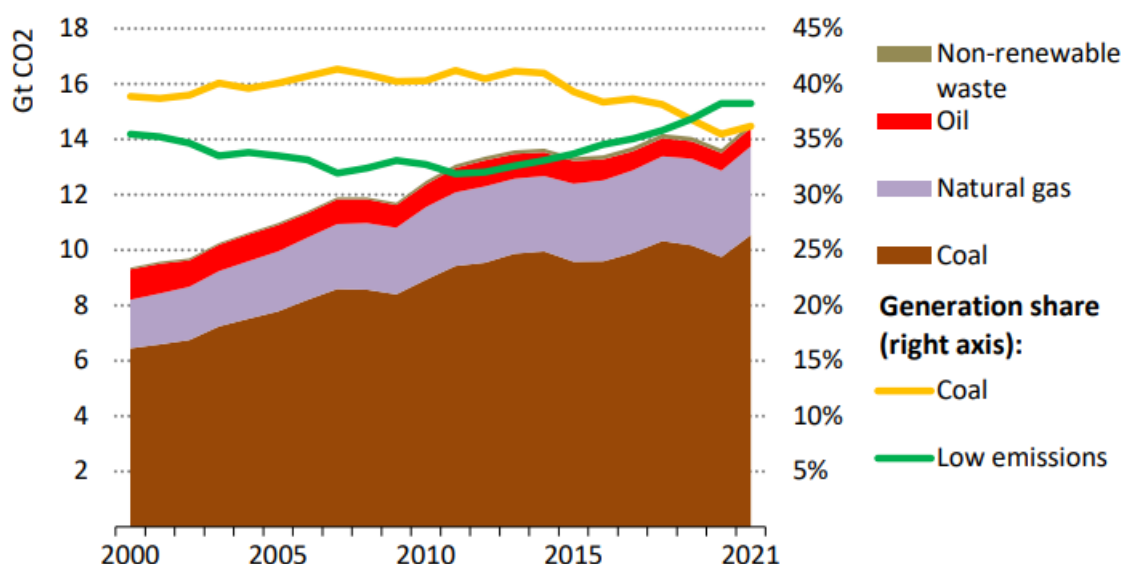
Figure 4 CO2 emissions from electricity and heat production by fuel, and share by fuel, 2000-2021 [1]

The biggest increase in CO_2 emissions by sector in 2021 took place in electricity and heat production, where they jumped by more than 900 Mt. This accounted for 46% of the global increase in emissions since the use of all fossil fuels increased to help meet electricity demand growth. CO_2 emissions from the sector neared 14.6 Gt, their highest-ever level and around 500 Mt higher than in 2019. China accounted for almost all of the global increase in electricity and heat sector emissions between 2019 and 2021. A small decline from the rest of the world was insufficient to offset the increase in China. Global CO_2 emissions from the buildings and industry sectors rebounded back to their 2019 levels, driven by increases in both advanced economies and emerging market and developing economies. China was the notable exception, with lower coal use in industry pushing CO_2 emissions from the industry sector below their 2019 level for the second year in a row. Transport was the only sector in which global CO_2 emissions remained well below 2019 levels.
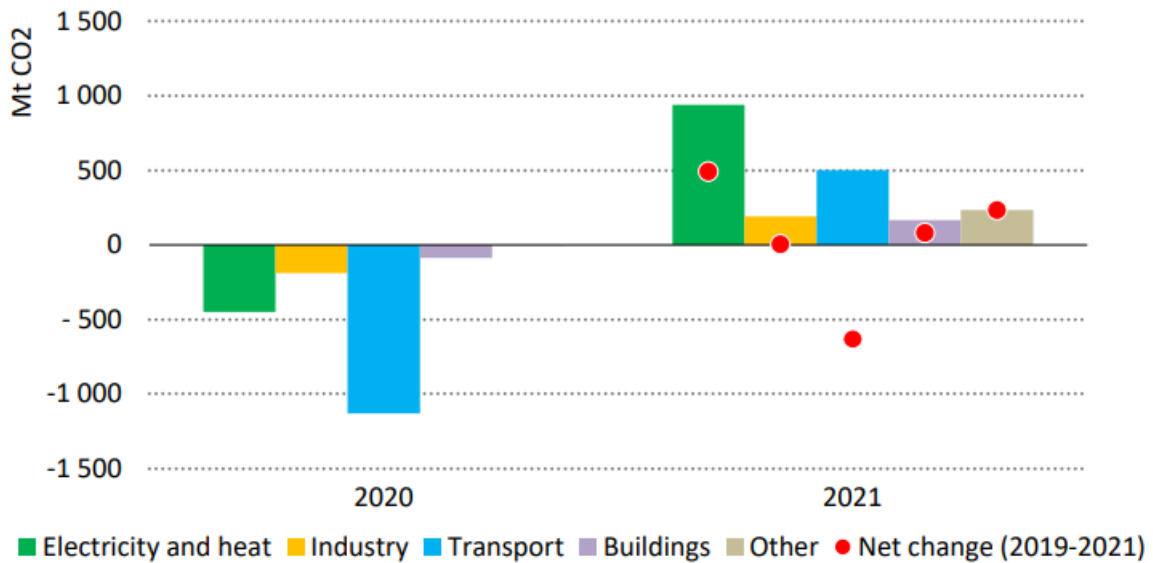
Figure 5 Annual change in CO2 emissions by sector, 2020-2021 [1]

The transport sector as a whole accounted for the highest share of final energy consumption in 2018 (35%), followed by the manufacturing industry (24%) and the residential sector (20%) as described in Figure 6 [3].
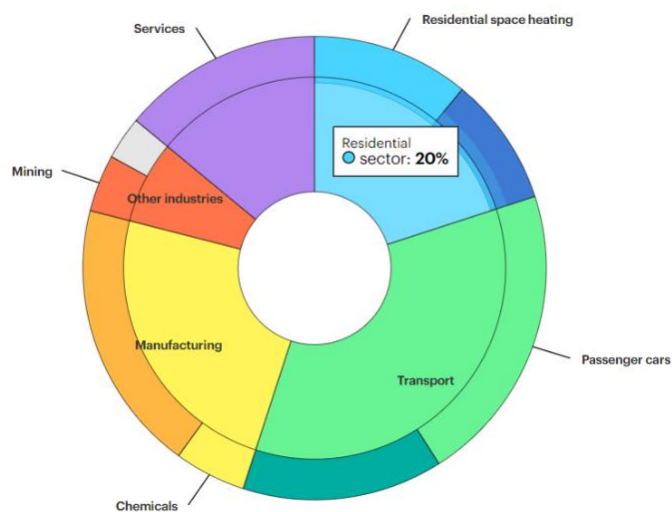
Figure 6 Largest end-uses of energy by sector in selected IEA countries, 2018 [1]

In particular, in the residential sector, energy efficiency improvements for space heating have occurred across IEA countries, mostly due to better insulation of buildings, refurbishment of old buildings, and improvements in heating equipment. The effects are tracked by trends in residential space heating intensity – defined as energy consumption per floor area – which significantly decreased in most IEA countries. As described in Figure 7, space heating accounted for more than half of the IEA energy consumption in the residential sector, with the highest shares in European countries (73% in Belgium and 72% in Hungary) and typically the lowest shares in Asia and Oceania (Japan 26% and New Zealand 30%).
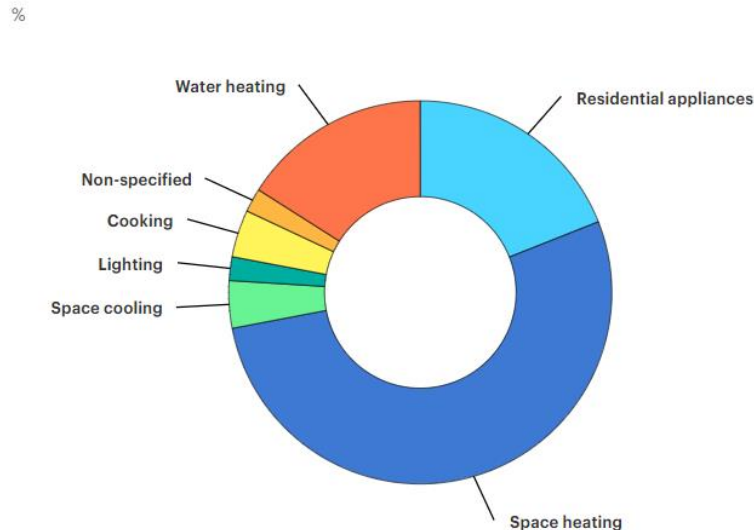
Figure 7 Shares of residential energy consumption by end use in selected IEA countries, 2018 [1]

Warmer countries generally have lower space heating intensities, as less energy is needed on average to keep the indoor temperature at a comfort level.

Furthermore, energy demand about the air conditioning has been assessed as the 65% of residential sector requirements [4].

In this context, the report "Climate Change 2022", the Intergovernmental Panel on Climate Change (IPCC) stressed that to contain the increase in warming within the limit of 2°C, beyond which the risks of a collapse ecosystems are very high, greenhouse gas emissions reductions of the order of 60-80% must be implemented within the century. This means that extending the current energy structure into the future, with the foreseeable increases in demands and emissions, is simply not compatible with the future of the planet and, only through the adoption of adequate technical solutions supported by adequate political decisions, can it be reversed the current trend and ensure sustainable development [5].

In 2020, the IEA and the COP26 presidency launched the COP26 Product Efficiency Call to Action to help countries raise ambition more quickly, more easily and at a lower cost. G7 leaders endorsed the Call to Action at the 2021 Summit in Cornwall. The objectives of the Call to Action are to:

- Set countries on a trajectory to double the efficiency of key products sold globally by 2030 – industrial motors systems, general lighting service lamps, residential air conditioners and residential refrigerators/freezers.
- Support the delivery of national climate change targets.
- Provide consumers and businesses with more efficient products that are affordable and cost-effective to own and operate.
- Stimulate innovation and provide businesses with export opportunities.
- Promote a dual course of action making products both energy efficient and climate-friendly by reducing the use of refrigerants in cooling appliances.

1.2.   European policies

In Europe, the goal is to achieve climate neutrality in the EU by 2050, including the intermediate target of at least a 55% net reduction in greenhouse gas emissions by 2030 by adopting a series of legislative proposals. In particular, the application of EU Directives on energy efficiency has significantly improved the energy performance of new constructions with the concept of Zero Energy Building (ZEB).

The building sector is crucial for achieving the EU's energy and environmental goals. At the same time, better and more energy efficient buildings will improve the quality of citizens' life and alleviate energy poverty while bringing additional benefits, such as health and better indoor comfort levels, green jobs, to the economy and the society.

To boost the energy performance of buildings, the EU has established a legislative framework that includes the Energy Performance of Buildings Directive 2010/31/EU [6] and the Energy Efficiency Directive 2012/27/EU [7].

Together, the directives promote policies that will help to:

- achieve a highly energy efficient and decarbonised building stock by 2050.
- create a stable environment for investment decisions.
- enable consumers and businesses to make more informed choices to save energy and money.

Following the introduction of energy performance rules in national building codes, buildings consume only half as much today, compared to typical buildings from the 1980s.

Both directives were amended in 2018 and 2019, as part of the Clean energy for all Europeans package [8]. The agreement on this new energy rulebook marked a significant step towards implementing the energy union strategy, published in 2015. Based on Commission proposals published in 2016, the package consists of 8 new laws. Following political agreement by the EU Council and the European Parliament (finalised in May 2019) and the entry into force of the different EU rules, EU countries have 1-2 years to convert the new directives into national law.

The new rules will bring considerable benefits for consumers, the environment, and for the economy. By coordinating these changes at the EU level, the legislation also underlines EU leadership in tackling global warming and makes an important contribution to the EU's long-term strategy of achieving carbon neutrality (net-zero emissions) by 2050.

The Directive amending the Energy Performance of Buildings Directive (2018/844/EU) [9] introduced new elements and sent a strong political signal on the EU's commitment to modernise the buildings sector in light of technological improvements and to increase building renovations.

The main rationale for Directive (EU) 2018/844 on the energy performance of buildings has been tapping the potential for decarbonization that the EU building stock offers: as the European Commission web page on buildings points out, approximately 40% of energy consumption and 36% of CO_2 emissions in the EU originate from buildings. However, a few provisions of the new Directive have a direct bearing on the adaptation of the energy sector. The new Directive reinforces the policy framework on energy efficiency so far set by the Energy Efficiency Directive of 2012 (EED) and by the Energy Performance of Buildings Directive of 2010 (EPBD). The main developments brought about by the amendment are, according to the cited website:
- The obligation for EU countries to establish stronger long-term renovation strategies.
- A common European scheme for rating the smart readiness of buildings.
- The further promotion of smart technologies, including on devices that regulate temperature at room level.
- The support of e-mobility through minimum requirements for large buildings' car parks and for smaller buildings.
- the obligation of cross-national comparability of national energy performance requirements.

- the promotion of health and well-being of building users.

In October 2020, the Commission presented its Renovation wave strategy [10], as part of the European Green Deal [11]. It contains an action plan with concrete regulatory, financing and enabling measures to boost building renovation. Its objective is to at least double the annual energy renovation rate of buildings by 2030 and to foster deep renovation. A revision of the Energy Performance of Buildings Directive is one of its key initiatives.

In December 2021, the Commission proposed a revision of the Directive [12]. It upgrades the existing regulatory framework to reflect higher ambitions and more pressing needs in climate and social action, while providing EU countries with the flexibility needed to take into account the differences in the building stock across Europe.

It also sets out how Europe can achieve a zero-emission and fully decarbonized building stock by 2050. The proposed measures will increase the rate of renovation, particularly for the worst-performing buildings in each country. The revised directive will modernize the building stock, making it more resilient and accessible. It will also support better air quality, the digitalization of energy systems for buildings and the roll-out of infrastructure for sustainable mobility. Crucially, the revised directive facilitates more targeted financing to investments in the building sector, complementing other EU instruments supporting vulnerable consumers and fighting energy poverty. To make sure that buildings are fit for the enhanced climate ambition, as presented in the 2030 Climate Target Plan, the Commission's new proposal aims to contribute to reaching the target of at least -60% emission reductions by 2030 in the building sector in comparison to 2015 and achieve climate neutrality by 2050. It will work hand in hand with other initiatives of the European Green Deal package, in particular with the review of the proposed new emissions trading system for fuels used in buildings, the Energy Efficiency Directive, the Renewable Energy Directive, as well as the Alternative Fuels Infrastructure Regulation.

The main measures in the new proposal are:
- the gradual introduction of minimum energy performance standards to trigger renovation of the worst-performing buildings.
- a new standard for new buildings and a more ambitious vision for buildings to be zero-emission.
- enhanced long-term renovation strategies, to be renamed national Building Renovation Plans
- increased reliability, quality and digitalization of Energy Performance Certificates; with energy performance classes to be based on common criteria.
- a definition of deep renovation and the introduction of building renovation passports
- modernization of buildings and their systems, and better energy system integration (for heating, cooling, ventilation, charging of electric vehicles, renewable energy)

The proposed revision of the directive is now being considered by the Council and the European Parliament. EU countries must for example establish strong long-term renovation strategies, aiming at decarbonising the national building stocks by 2050, with indicative milestones for 2030, 2040 and 2050. The strategies should contribute to achieving the national energy and climate plans (NECPs) energy efficiency targets.

The directive also requires that EU countries set cost-optimal minimum energy performance requirements for new buildings, for existing buildings undergoing major renovation, and for the replacement or retrofit of building elements like heating and cooling systems, roofs and walls.

As of 2021, all new buildings must be nearly zero-energy buildings (NZEB) and since 2019, all new public buildings should be NZEB.

Net or nearly zero energy buildings (NZEB) are highly efficient buildings with extremely low energy demand, which is met by renewable energy sources. Such buildings produce as much energy as they consume, accounted for annually. In order to achieve their net zero energy goals, NZEBs must first

sharply reduce energy demand using energy efficient technologies, and then utilize renewable energy sources (RES) to meet the residual demand. In such buildings, efficiency gains enable the balance of energy needs to be supplied with renewable energy technologies. This is the most logical approach to reach NZEB goal.

However, this broad definition leaves plenty of room for interpretations and for misunderstandings among owners, architects, and other stakeholders in the NZEB project. Agreeing to a common definition of NZEB boundaries and metrics is essential to developing design goals and strategies.

About another of the other statements of the Directive, when a building is sold or rented, energy performance certificates must be issued and inspection schemes for heating and air conditioning systems must be established.

The directive supports electro-mobility by introducing minimum requirements for car parks over a certain size and other minimum infrastructure for smaller buildings.

There is also an optional European scheme for rating the smart readiness of buildings and smart technologies are promoted. The directive introduced requirements on the installation of building automation and control systems, and on devices that regulate temperature at room level. It addresses health and well-being of building users, for instance through the consideration of air quality and ventilation [13]. EU countries must also draw up lists of national financial measures to improve the energy efficiency of buildings.

1.3.   The Italian situation

Italy has aligned itself with this policy starting with Legislative Decree no. 192 of 19 August 2005 [14] (Implementation of Directive 2002/91/EC relating to energy performance in buildings), as integrated and amended by Legislative Decree 311/2006 [15] and made operational, in its main aspects, by the Decree of the President of the Italian Republic 59/2009 [16] and by the Inter-Ministerial Decree of 26 June 2009 (containing the National Guidelines for the Energy Certification of buildings) [17].

The publication of "Urgent provisions for the transposition of Directive 2010/31/EU of the European Parliament and the Council of 19 May 2010, on the energy performance of buildings for the definition of infringement procedures initiated by the European Commission, as well as other provisions on social cohesion", in the Official Gazette of 3 August 2013, is the last official act of the Italian legislative process on the subject of redevelopment and energy efficiency of the Italian public and private real estate assets. Result of the need to avoid an aggravation of the infringement procedure against Italy, due to the failure to transpose Directive 2010/31/EU, Law no. 90/2013 involved a structural evolution of the Italian legislation on energy performance, since once the implementing decrees have been issued, the methodology for calculating the energy performance of buildings, the minimum requirements and the areas of intervention will change [18].

In particular, starting from 31 December 2018, new buildings occupied by public administrations and owned by the latter, and from 1 January 2021 all new buildings, including school buildings, must be almost zero energy buildings (nZEB).

In Italy institutions also provide incentives to promote cogeneration and trigeneration to achieve the following objectives:
- a reduction of environmental impact due to lower emissions and residual heat released into the environment (lower thermal pollution and atmospheric pollution);
- lower transmission and distribution losses for the electrical national system due to the location of the production system close to users or self-consumption of the produced energy;
- replacement of less efficient and more polluting technologies.

To benefit from these economic incentives, some characteristics are required. There are two types of incentives regarding energy efficiency:

- "Cogenerazione ad Alto Rendemento'' (CAR): incentives for high efficiency cogeneration [19];
- "Titoli di efficienza energetica'' (TEE) or "Certificati Bianchi'' (CB): denote how many tons of equivalent oil (toe) are saved, thanks to determined intervention, done to make more efficient the energy production process [20].

In Directive of February 11, 2004 of the European Parliament and of the Council n. 2004/8/CE: the UE prefixed the goal to increase the energetic efficiency and enhance the security of fuel supply, in the internal market, of the "Cogenerazione ad Alto Rendimento''[21]. This directive defines the concept of useful heat. The Legislative Decree No. 20 of February 8, 2007, which took effect on January 1, 2011, implemented the directive in Italy. The criteria used to determine CAR is based on PES (Primary Energy Saving), which represents the primary energy savings that cogeneration makes possible compared to producing the same amount of electric and thermal energy separately.

 The Decree of the Ministry of Economic Development of August 4, 2011 completes the directive 2004/8/CE and legislative decree 8 February 2007. The aforementioned decree explains how to grade a unit's operation as CAR. It specifies, based on the type of technology and the annual first principle efficiency, when the production of electric energy from combined production can be considered wholly from cogeneration. If the production unit exhibits a first principle efficiency below the threshold values, it defines a way to divide the electrical energy produced in two portions, of which one can be quantified as cogeneration. The order continues by saying that the PES index is used to identify CAR systems. The PES must be greater than 10%; however, for small or micro cogeneration units (i.e., those with power below 1MW and 50kW, respectively), a positive PES is sufficient.

The requirements and procedures to enter the cogeneration support program are established by the Decree of the Ministry of Economic Development dated September 5, 2011. According to this regulation, new or renovated cogeneration units are eligible to receive II type "Titoli di Efficienza Energetica" (or "Certificati Bianchi") certificates in proportion to the amount of energy savings realized for each year that they meet the CAR standards (RISP). According to Article 4 of the Ministerial Decree of September 5, 2011, a producer's annual entitlement to "Certificati Bianchi" is determined. Subsequently, with the Guidelines of the Decree of the Ministry of Development Economic September 5, 2011 the calculation method of the relevant quantities for the purposes of CAR recognition and the access mechanism of "Certificati Bianchi'' has been simplified.

The Decree of the Ministry of Economic Development March 16, 2017, finally applied to high efficiency micro-cogeneration units and to micro-cogeneration units fueled by renewables sources. The current regulation aims to reduce producers' burdens and standardize information sharing between municipalities, network operators, and GSE about the implementation, connection, and operation of these kinds of systems.

2. CHP – CCHP SYSTEMS LITERATURE REVIEW

2.1. Combined Heating and Power systems (CHP)

The working principle of a Combined Heat and Power (CHP) system, which is also called "cogeneration", is basically the use of a heat engine or a power station to sequentially or simultaneously generate both electricity and useful heat. CHP is a well-developed concept which can date back to the 1880s, when steam was a primary source of energy in industry and electricity was beginning to be used. On-site industrial power plants with cogeneration of power and heat were the main power systems in the early 19th. Then the development of large central power plants with higher efficiency and reliable utility grids, together with the low fuel costs and advances in technology, drove the electricity prices down and contributed to the decline of cogeneration. However, over the past decades, the increases in the world fossil energy price, the uncertainty with the fuel supplies, the deteriorating environment and the predicted global climate change have become serious problems, and this results in CHP gaining attention again because of its potentials for fuel savings and low GHG emissions. Today, CHP represents a series of proven, reliable, and cost-effective technologies that are already making an important contribution to meeting global heat and electricity demands. Due to the enhanced energy supply efficiency and utilization of waste heat and low-carbon renewable energy resources, CHP, particularly together with district heating and cooling (DHC), is an important part of national and regional GHG emissions reductions strategies [22].

The overall efficiency of electricity generation has been improved over time, but the transition from primary energy such as fossil, biomass or nuclear fuels to electricity is still an inefficient process. According to the Second Law of Thermodynamics, thermal power systems inevitably reject heat into the environment and the thermal efficiency of a heat engine cannot be 100%. In fact, the maximum thermal efficiency of any heat engine cycle is the efficiency of a reversible Carnot heat engine [23], expressed in (1):

$$\eta_{Carnot} = 1 - \frac{T_L}{T_H} \qquad\qquad (1)$$

Where T_H is the maximum temperature available (e.g. the metallurgical limit) and T_L is the lowest temperature available (e.g. cooling water temperature for the condenser of a steam-Rankine cycle-based power plant). Further, the power generation efficiency of most engines and power plants are much lower than the potential maximum efficiency. For instance, the power generation efficiency of gas turbines varies from 20% to about 40%, which indicates 60% to 80% of the heat supplied into gas turbines via burning of fuels is wasted. While some modem power plants can achieve nearly 60% power generation efficiency, most operate closer to 30% and smaller or older units may reach only 20% [24]. Putting these percentages in another way, about 40% to 80% of all the primary energy input is always wasted with any power generation unit. Figure 8 shows that about 63 % of the thermal input is wasted in the global electricity generation system [25]. The wasted energy from power plant emerges as heat and is dumped in different ways. Sometimes it ends up in cooling water, but most often it is dissipated into the atmosphere. This waste heat can be considered not only a large account of energy lost but also a form of pollution.
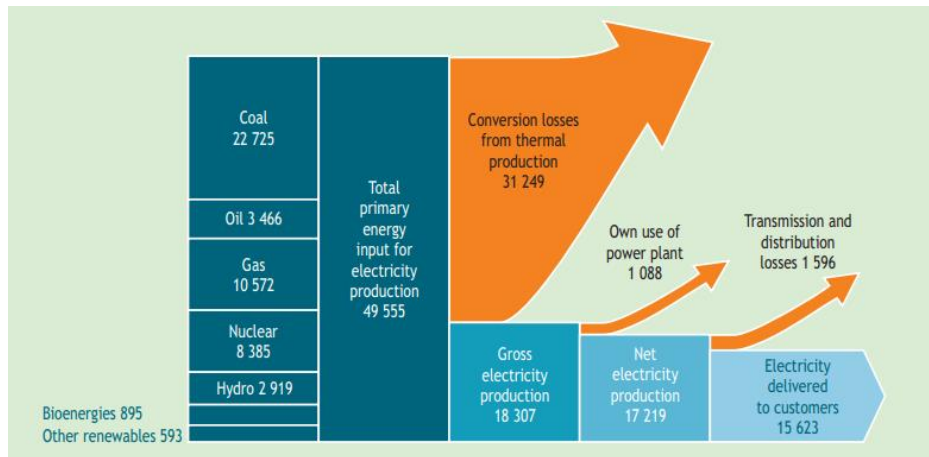
Figure 8 Energy flows in the global electricity system (TWh)

With the CHP technology, most of this considerable amount of low-grade waste heat from an electricity generation process will not be wasted. Although the waste heat energy cannot be used to generate electricity, it can be used to produce hot water or for space heating or cooling. In this way, the waste heat from power generation replaces a high-grade energy resource such as gas, oil or even electricity that is used to generate thermal energy needed for hot water, space heating or cooling. Therefore, cogeneration represents a significant improvement in overall energy efficiency compared with conventional power generation plants. CHP systems can operate with an energy efficiency of up to 90%, leading to a major saving in fuel costs and a significant reduction in greenhouse gas emissions and other environmental pollutants.

CHP systems also reduce network and transport losses because they are mostly sited near the end users. The efficiencies of CHP systems may vary to some extent, mainly depending on the design of the systems, technologies, and fuel sources. Figure 9 compares the overall efficiencies of an example CHP system and a conventional "separate heat and power" generation scheme. It illustrates the potential efficiency gains of a typical CHP system:

- to produce 80 units of useful energy, the conventional generation with separate heat and power systems uses 130 units of energy which consists of 75 units of energy for electricity production with a highly efficient gas power plant (48% efficiency) and 55 units of energy to produce heat by an efficient gas boiler (80% efficiency), resulting in an overall efficiency of 60% and 75 units of energy loss.
- however, the CHP system needs only 100 units of energy to produce the same 80 units of useful energy from a single fuel source, resulting in a total system efficiency of 80% and an energy loss of 20 units which is less than half of the energy loss of the conventional separate power and heat generation.

While the benefits of CHP are widely recognized, the implementation of CHP remains low. Despite the existence of various energy policies such as EU Cogeneration Directive 2004/8/EC [21] which promoted CHP in Europe, the United States, Japan and other countries, the share of CHP in global power generation has remained stagnant for the past several years at around 9% [26].

18
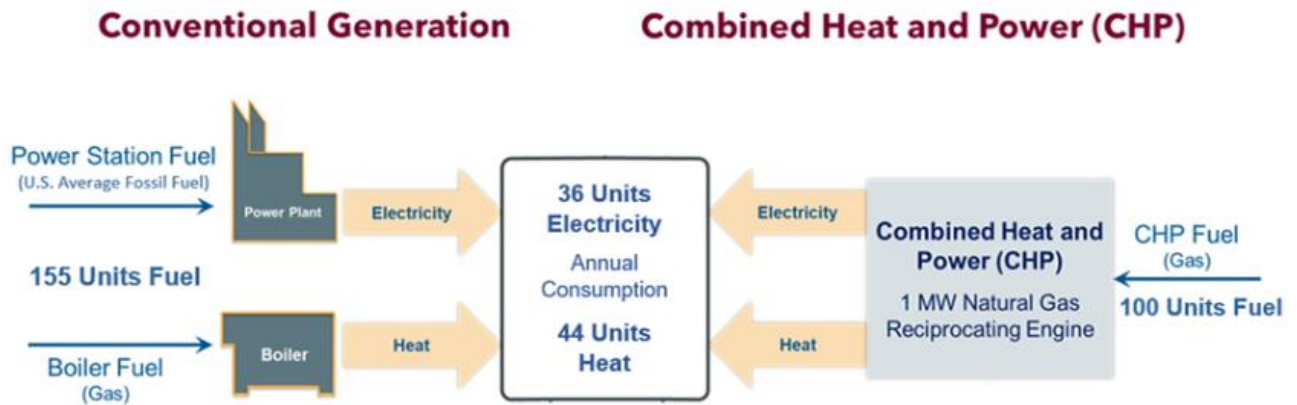
Figure 9 Conventional Generation vs Combined Heat and Power Generation

A typical CHP system consists of four basic elements:
- a prime mover (an engine or a drive system),
- an electricity generator,
- a heat recovery system,
- a management and control system.

Although each of these four elements can have a significant impact on the performance of a CHP system, the prime mover is the most critical element of a CHP system.

There are several different technologies to convert fuels into useful forms of energy (mostly electricity and heat) that have been developed and researched for CHP applications. Although quite a few new technologies appear to be promising, the conversion process based on combustion and subsequent conversion of heat into mechanical energy, which then drives a generator for electricity production, is still the dominant technical route. Reciprocating internal combustion engines, steam turbines and combustion turbines which are based on this technical route are the most widely used prime movers [27]. New developments with prime movers include those of fuel cells, Stirling engines and micro-turbines. These CHP technologies has been considered as suitable to operate with renewable energy resources with an acceptable capital cost in the future [28]. The current CHP research and development is primarily focused on improving performance, reliability, modular and smaller units, and lower GHG emissions (for example, using biomass). Although there are several ways to classify CHP system, such as based on the fuel used or the capacity range, they are generally classified by the type of the prime mover equipment which in some extent determine possibilities and availability of other related technologies. The technologies of the following prime movers will be discussed in this chapter, with specific respect to their ability to run as CHP: steam turbines, reciprocating engines, gas turbines, micro-turbines, and fuel cells. A synopsis of the major parameters and performance of these prime movers is shown in Table 1. As the topic of the present PhD research is the development of a biomass-fired microscale CHP, the discussions below will also focus on the technologies related to micro-CHPs that are below 50 kW$_e$, where possible.

Table 1 Different CHP technologies

Technology	Fuel	Capacity (MW)	Electrical efficiency (%)	Overall Effciency (%)
Steam turbine	Any combustible	0.5-500	17-35	60-80
Reciprocating engines	Gaseous & liquid	0.003-10	25-45	65-92
Gas turbine	Gaseous	0.25-50+	25-42	65-87
Micro-turbines	Gaseous & liquid	0.03-0.25	15-30	60-85
Stirling engines	Any combustible	0.003-1.5	30-40	65-85
Fuel cells	Gaseous	0.003-3+	37-50	85-90

Steam turbine-based CHP

Steam turbines are the most common power generation technology used in commercial electric power plants and industries. Usually, fuel is combusted within a boiler, releasing heat which is used to generate high-pressure steam. The high-pressure steam is transferred to the steam turbine, driving the turbine that is coupled with a generator to produce electric power. Because of steam turbine units have separate heat source and do not directly convert fuel to electric energy, they can operate with large variety of fuels with suitable combustion devices, from natural gas to solid waste, including all types of coal, wood, wood waste, and agricultural byproducts. The thermodynamic cycle of steam turbines is based upon the well-known Rankine cycle. As illustrated in Figure 10, the working liquid (water) evaporates in the boiler when heated and then expands in the turbine to produce shaft work [22]. The mechanical energy of the shaft work is turned into electricity with a generator. The exhaust vapor from the steam turbine passes through a condenser for condensation or a heat exchanger for heat extraction and then pumped back the boiler to complete the cycle.
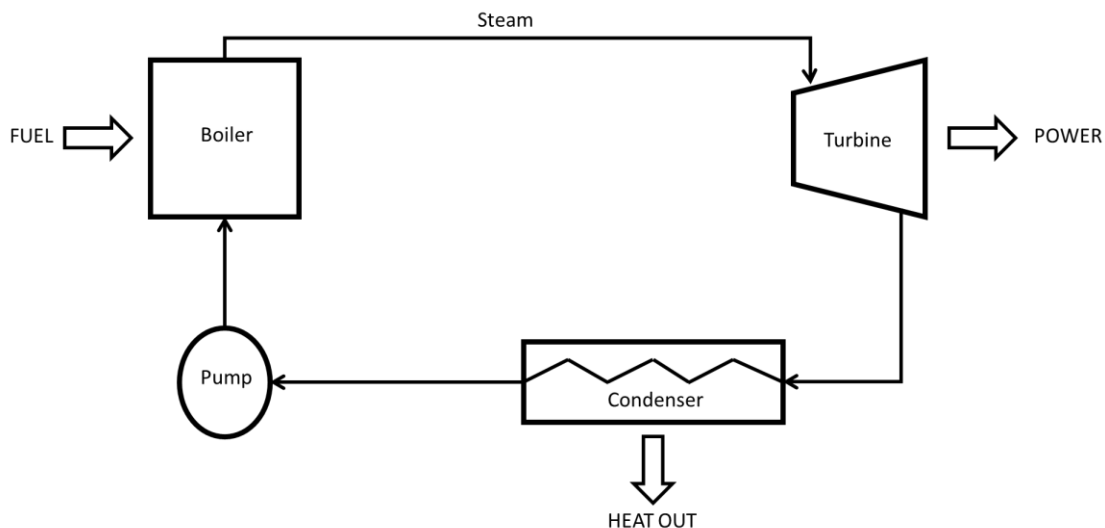
Figure 10 Schematic of a simple Steam Turbine Power Cycle

Depending on the exit pressures of the steam turbines, steam turbines fall into two types: backpressure turbines and condensing turbines. [29]. A backpressure turbine operates with an exit pressure equal or higher than atmospheric pressure, whereas a condensing turbine operates with an exit pressure

lower than atmospheric pressure. Condensing turbines have the advantages of high-power generation efficiency and being able to change electrical and thermal power independently when in cogeneration mode of operation. Power generation using steam turbines is one of the oldest power generation technologies and is still in commercial production. As a matter of fact, conventional steam turbine power plants currently generate most of the electricity around the world. The capacity of steam turbines ranges from a few hundred kW for small units to several hundred MW for large power plants. As steam turbines are more suitable for large-scale power generation, they are widely used for large-scale and industrial-scale CHP applications. Small-scale steam turbines have relatively low electrical conversion efficiency, deteriorating rapidly with smaller capacity and therefore they are generally considered not suitable for micro-CHP applications [30].

Reciprocating internal combustion engines
Reciprocating engines, also called internal combustion engines or endothermic engines, are well-known for cars and other vehicles. Reciprocating engines can operate on a wide range of liquid and gaseous fuels but not solid fuels. The reciprocating shaft power can produce either electricity through a generator or drive loads directly. The reciprocating engine CHP is a conventional internal combustion engine coupled with generators and heat exchanger to recover the heat of the exhaust gas and the cooling cycle. As a well-known and widespread technology, reciprocating engines are available for power generation applications in sizes ranging from a few kW to more than 10 MW and can be fired on a wide variety of fuels [31]. In addition, reciprocating engines have high power generation efficiencies even in small sizes, making them suitable for small-scale CHP applications [22].

Reciprocating IC engines are widely used m small power generating plants because they allow compact modular systems to suit various application needs. Besides, reciprocating engines are also well-proven technology that eases maintenance. Driven by economic and environmental pressures, reciprocating engine technology has improved dramatically with the development of engine research worldwide and heat recovery technology over the past decades. A typically reciprocating engine CHP is illustrated in Figure 11. Heat can be recovered not only from the exhaust, but also from the jacket water and the engine oil, which leads to notable increase of fuel efficiency and reduction of emissions [32]. There are two basic types of reciprocating engines currently in use: Spark ignition engines and Compression engines [33]. Spark ignition engines are operated mainly with natural gas as the preferred fuel, although biogas, gasoline, and landfill gas can also be used. The capacity of spark ignition engines ranges between 3 kWe and 6 MWe. Compression ignition engines, often called diesel engines, operate on petroleum diesel and biodiesel as well as other petroleum products such as heavy fuel oil [34].

Compression ignition engines can also be set up to run in a dual-fuel configuration that bums primarily natural gas or biogas with a small amount of diesel pilot fuel [32]. Compression ignition engine CHP presents a higher power-to-heat ratio compared to spark ignition engine CHP, and has a large range of capacity from a very small size of a few kWe for small systems to a power equivalent of some tens of MWe for large systems [33].

Although reciprocating engines have been proved to be suitable for numerous cogeneration applications in residential, commercial, institutional, and small-scale industrial loads, they still have obvious drawbacks including relatively high vibration noises, a large number of moving parts and high cost for frequent maintenance. Moreover, compared to other CHP technologies, the relatively high emissions of reciprocating engines, particularly in nitrogen oxides and particulate matter, need to be reduced.
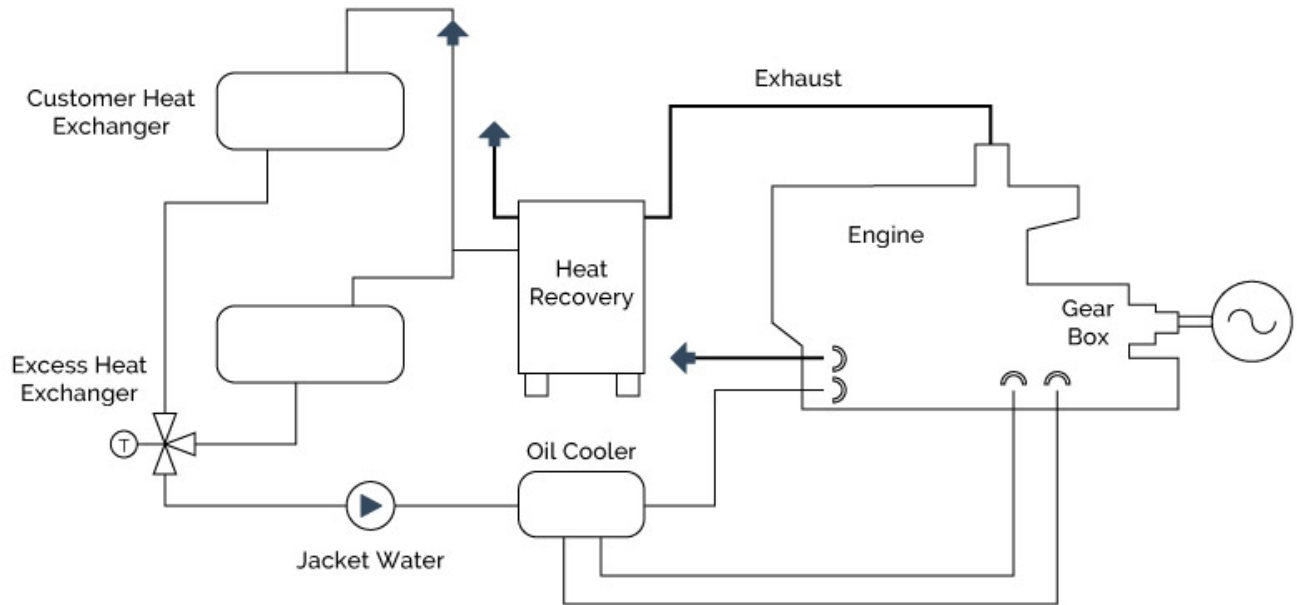
Figure 11 Closed-Loop Heat Recovery System for a Rciprocating IC Engine CHP [22]

Gas turbine-based CHP

Combustion turbines, or gas turbines, have been used for power generation for decades and are now the frequently used prime movers in larger-scale cogenerations due to their high reliability and large range of power capacity. Compared with the other two most widely used prime mover technologies (steam turbines and reciprocating engines), combustion turbines are easier to install with lower capital costs than steam turbines and have lower costs in maintenance and lower emissions than reciprocating engines [33].

A gas turbine is an internal combustion engine that operates with rotational motion rather than reciprocating motion. Observably, a gas turbine is only fueled by a gaseous fuel such as natural gas or biogas. Gas turbines range in size from 30 kWe (micro turbines) to 250 MWe (large-scale power plant units) and can be used in a variety of power cycle configurations. CHP operation of a gas turbine is built up with a simple-cycle gas turbine and a heat recovery. The heat from the turbine exhaust is recovered and converted into useful thermal energy, mostly in the form of steam or hot water. However, because of the high temperature of combustion turbine exhaust gases, typically around 540°C, the exhaust gases can be used to support the combustion of additional fuel and this technology is called supplementary firing, ln some cases, high-pressure steam is generated from the recovered heat of the turbine exhaust and used to generate additional power with a steam turbine, and this can be called a combined cycle CHP system [22].

Micro turbines are the extension of combustion turbine technology, making the gas turbines smaller and more efficient units. The capacity of currently available micro turbines can be as low as 30 kWe. Micro turbines are primarily fueled with natural gas, but now they can operate with wider variety of fuels, including diesel, gasoline and even biogas [35]. Micro turbine devices have now achieved almost the same electrical efficiency as internal combustion engines. Additionally, they have environmental advantages, such as lower emission levels of NOx and CO and less noise over an engine of comparable size.

The basic components of a micro turbine CHP are shown in Figure 12 in its versions without or with internal heat recuperation. The key part of a micro turbine CHP system is the compressor-turbine package, with single shaft turbines commonly used on electric generators. The shaft of a micro turbine can work in high rotational speed up to 120,000 rpm. In a typical micro turbine CHP system, the inlet air is compressed and preheated in the recuperator with turbine exhaust heat. Then, the heated air

mixed with fuel is sent into the combustor and ignited there. The hot combustion gas is then expanded in one or more turbine sections, producing rotating mechanical power to drive the compressor and the electric generator [22].

As a recently developed technology, micro turbines have started initial commercial service only from 1999. Hence at this stage there are few track records of this technology, and they are offered by only a small number of suppliers. Besides, micro turbines are more expensive than internal combustion engines of equivalent sizes in capital costs. However, because it contains few moving parts, the operation and maintenance costs of a micro-turbine can be lower than that of an internal combustion engine. A micro turbine can be used in power-only generation or in a CHP system. With distributed generation applications it can be used by power producers and consumers, including industrial, institutional, commercial, and even residential users in the future. Micro turbines' high outlet temperature (> 500 DC) is suitable for other high value applications, such as producing low-pressure steam or hot water for on-site requirements; furthermore for cooling applications including absorption systems [33].

a)   b)
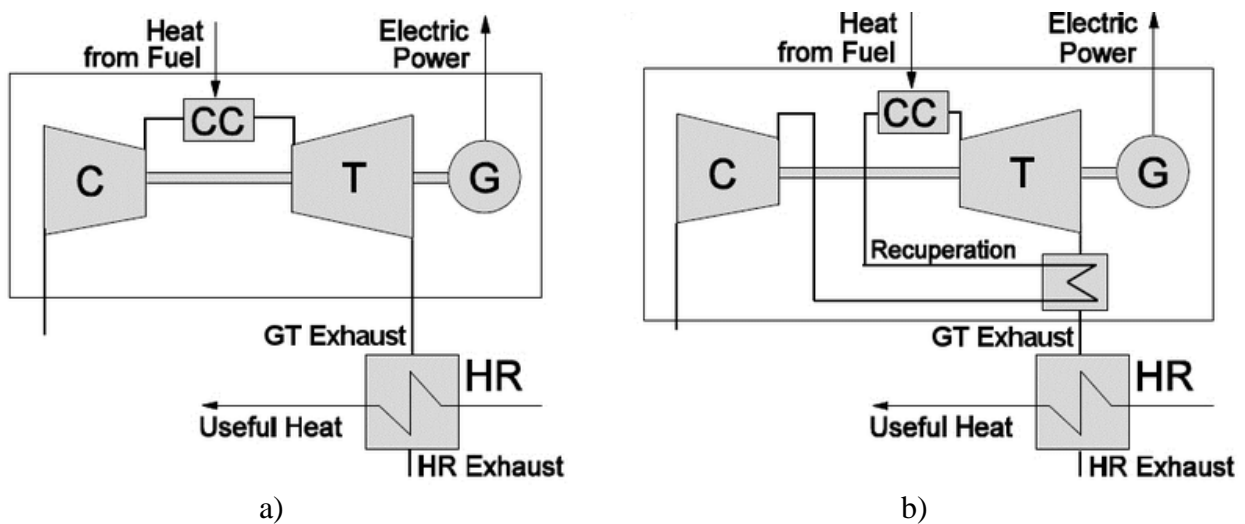
Figure 12 Scheme of gas turbine cycle with CHP: a) a gas turbine with the basic thermodynamic cycle, b) a gas turbine with internal heat recuperation [36]

Stirling Engine-based CHP

Compared to a conventional internal combustion engine, a Stirling engine is an external combustion device, which can produce either electricity through a generator or drive loads directly [22]. As an external combustion engine, a Stirling engine generates heat externally in a separate combustion chamber. Due to this characteristic, Stirling engines can operate on almost any fuel. With external combustion that facilitates the control of the combustion process, Stirling engines have obvious advantages such as low noise and low air emission levels. Presently the electrical efficiency of Stirling engines can be as high as 40%, which is much higher than other prime movers' technologies, with 50% a possibility in the future, whereas the overall CHP efficiency of a Stirling engine cogeneration system is within in the range of 65-85% [34]. A Stirling cycle has the potential of achieving higher efficiency than Rankine cycle or Joule cycle as it more closely approaches the Carnot Cycle [34]. Besides, Stirling engines also have good capability to operate under part-load conditions. It is expected that while the full load electrical efficiency can be 35-50%, the electrical efficiency at 50% load can be expected to be in the 34-39% range [37]. Figure 13 shows the schematic of a micro-scale biomass Stirling engine CHP system.
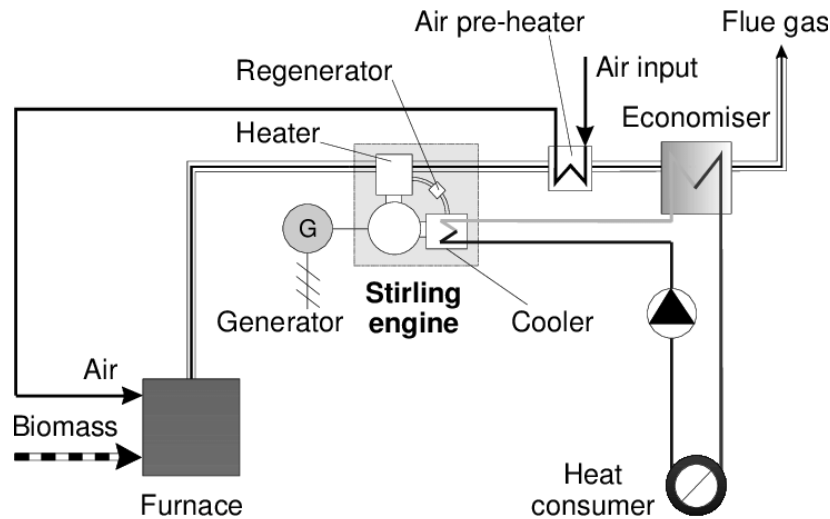
Figure 13 Scheme of a Stirling Engine based CHP [38]

Although there are some demonstrations of Stirling engine systems, they are still under development and not commercially available today, and for this reason almost no statistical data on reliability, availability or prices of Stirling engine systems are available. Nevertheless, because of their good performance at partial load and capability to operate with different fuels, Stirling engines are particularly well-suited to micro-scale CHP applications.

Fuel-cell based CHP

Fuel cells are an entirely different technique to generate electricity than traditional prime mover technologies and are still in the research and develop phase presently. Fuel cells take in hydrogen (or hydrogen-rich fuels) and oxygen to create electricity, heat, and water. Figure 14 shows the key system components of a fuel cell. Basically, a fuel cell consists of a stack of layers arranged around a central electrolyte: an anode at which the hydrogen is oxidized; a cathode at which the oxygen is reduced; and bipolar plates, which feed the gases, collect the electrons, and conduct the reaction heat.
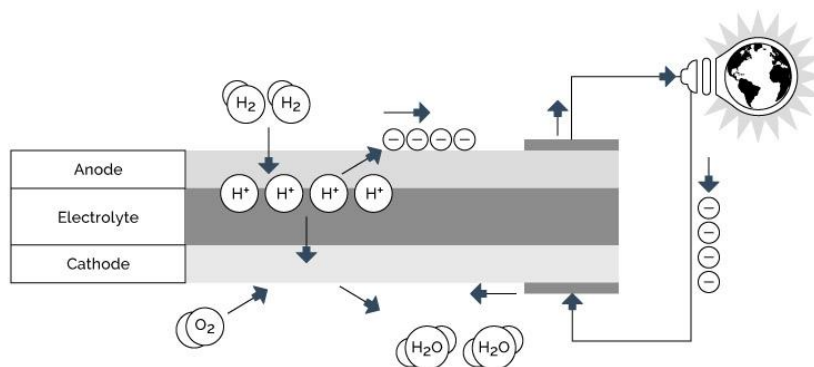
Figure 14 Basic components and electrochemical process of a fuel cell

Fuel cells can be sized for a wide variety of applications - from laptop computers (50 to 100 W_e) to vehicles (50 to 85 kW_e) and to central power generation (0.2 to 2 MW_e) [34]. Hydrogen-fueled fuel cells do not produce CO_2, the main greenhouse gas in the atmosphere. Because there is no combustion and no moving parts, fuel cells are quiet and can achieve electric efficiencies up to two times greater than internal combustion engines [22]. The transportation sector is now the major market for the application of fuel cells. Four main types of fuel cells listed below appear to have the most attractive prospects: phosphoric acid fuel cell (PAFC), proton exchange membrane fuel cell (PEMFC), molten

carbonate fuel cell (MCFC), and solid oxide fuel cell (SOFC). However, power generation seems to be another promising market in which fuel cells could be quickly commercialized. The typical layout of fuel cells based on hydrogen is shown in Figure 15 [32].
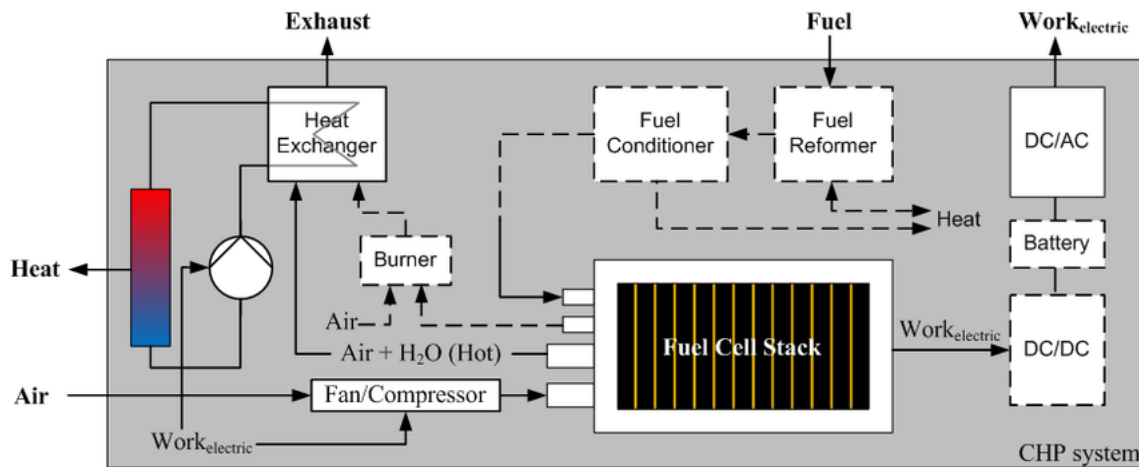
Figure 15 Simplified layout of a fuel cell based CHP supplied with hydrogen [39]

PEMF based residential CHP systems have reached demonstration stage, with a variety of FC developers reporting on their latest products, including Ebara Ballard's 1 kW_e stationary CHP system, Plug Power's GenSys 5 system (5 kW_e, 9 kW_{th}) and Hpower's 4.5 kW RCU [37]. In addition, solid oxide fuel cells (SOFC) are suitable for residential CHP applications because they run efficiently at high temperatures and have a favourable thermal/electric ratio. A 3.5 kW_e SOFC CHP system for residential and commercial applications with an electrical efficiency of approximately 50% and overall CHP efficiency of approximately 80% has been developed by Hydrovolt, and a 2 kW_e SOFC CHP system suitable for single family house application with an overall efficiency of about 85% and a 10 kW SOFC system with an overall efficiency of about 85% have been developed by Global Thermoelectric, Inc. [37]. Typical performance and CHP characteristics of fuel cells are showed in Table 2.

Since fuel cell are still under research, development and demonstration [40], there are several disadvantages for their commercialization. Fuel cells are currently more expensive than internal combustion engines and cost more on maintenance. There are only a handful of fuel cell installation on operating and therefore their long-term operational experience with fuel other than pure hydrogen such as natural gas and biomass-derived gaseous fuels are limited. Besides relatively short lifetime of fuel cell systems is another main drawback [33]. However, fuel cell' high electrical efficiency, low noise during operation and low emissions makes them particularly suitable for residential, commercial, and institutional building applications.

Table 2 Fuel cells' performances and CHP characteristics

PERFORMANCES CHARACTERISTICS				
Fuel cell type	PAFC	MCFC	PEM	SOFC
Normal electric capacity (kW)	200	250	200	100
Commercial status	Commercial	Commercial	Demonstration	Demonstration
Electrical efficiency, HHV(%)	36	43	35	45
CHP CHARACTERISTICS				
Total CHP efficiency, HHV (%)	75	65	72	70
Power/Heat Ratio	0.92	1.95	0.95	1.79

2.2. Combined Cooling, Heating and Power systems (CCHP)

Trigeneration, or Combined Cooling, Heat and Power (CCHP), is a particular field of cogeneration systems, in which, besides producing electrical energy, it allows to use part of the thermal energy recovered, through an absorption chiller, to produce refrigeration power, that can be used for air conditioning or industrial processes. The conceptual scheme of trigeneration is presented in Figure 16. First fuel and excess air are burned to drive a prime mover, which in turn drives an electrical generator, that produces electricity for final use. The energy of high-temperature exhaust, from the prime mover, is mainly recovered using a heat recovery unit. Using a convenient heat transfer fluid, the recovered heat can be used in specific heating processes, and in case of trigeneration, also to drive a cooling unit, for cooling purposes according to the site demands.
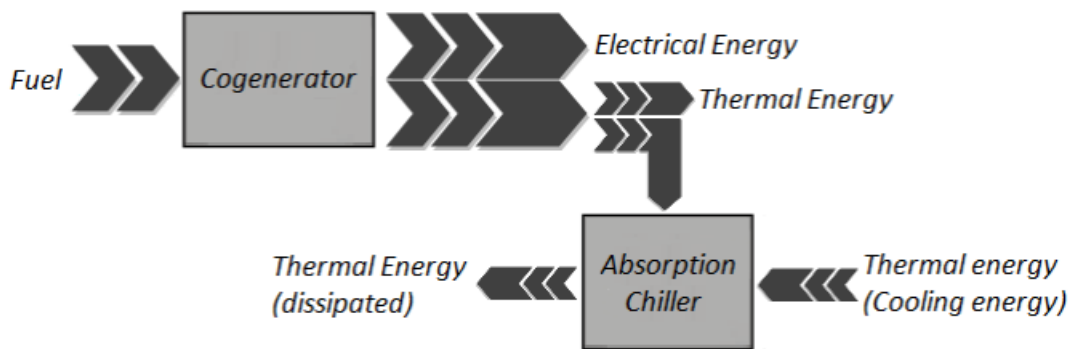
Figure 16 Conceptual scheme of a CCHP system

Trigeneration extends the possibilities of cogeneration, that are limited by the necessity to have contemporaneity among electric and thermal use to have an efficient system. This factor represents a constraint, where the need of thermal power is limited to the winter period, while during summer, the cogeneration system must be stopped, or left work dissipating the heat produced. Instead, matching a cogenerator with a dedicated absorption chiller, that can generate cooling power using heat as a source, rather than electricity, it is possible to exploit the cogeneration implant also in the hotter months; when the request for air conditioning is very high, or in the industrial sectors, in which cooling systems are needed.

The use of waste heat to supply the required heat of the chillers has always been considered by many researchers.

Liu et al.'s investigation of the power output of a hybrid chiller and cogeneration system has been carried out in both limited and unlimited modes. Their findings demonstrated that using a cogeneration system reduces expenses by 50% when compared to using a separate production system [41]. The performance of a cogeneration system, in which the combustion products were employed to supply the necessary heat for the chiller, was examined by Bruno et al. [42] at varied capacities of micro-gas turbines. Additionally, they increased the cooling production capacity by injecting natural gas into combustion products. The results for four different micro-turbine capacities demonstrated that, as a result of the rise in temperature, the natural gas injection enhances the COP and cooling production capacity.

A cogeneration system based on a fuel cell and an ammonia absorption chiller was researched by Oro et al. [43]. Finally, results demonstrated that the fuel cell's power production ranges from 600 to 1400 W and its cooling output can reach 400 W. The use of a gas engine as the primary mover and a water-ammonia absorption chiller as the refrigeration cycle of a cogeneration system was suggested by Colonna et al. [44]. They assessed the impact of evaporator temperature on chiller COP before looking at the system performance from an economic angle.

A water-ammonia absorption refrigeration cycle with a cooling capacity of 10.5 kW has been numerically modelled by Le Lostec et al [45]. In order to investigate how evaporator temperature and generator temperature affect system performance, researchers used mass and energy balance equations in steady state conditions. In [46] a data centre has been cooled using waste heat. The poor quality of the heat in this investigation was one of its difficulties. In this case, the issue was resolved by using a heat pump.

A mass recovery procedure was used to build and experimentally study a silica gel-water adsorption chiller by Pan et al. under the condition of driving hot water temperature less than 80 °C. The results show that the silica gel-water adsorption chiller for waste heat utilization at extra-low temperatures performs well.

Another global concern that poses a threat to human life in the modern world is the rise in greenhouse gas emissions and related environmental problems. Utilizing waste heat can significantly minimize the creation of pollutants because it uses less fuel. To cut down on pollutants emissions from the cogeneration system, Fumo et al. presented an operating approach for emissions [47]. In this study, the operational emission strategy was used to minimize primary energy consumption and carbon dioxide emissions. The data were then compared to those from the primary energy consumption strategy. It has been demonstrated that using the operational emission strategy reduces carbon dioxide emissions by 18.7% for the city of Minneapolis. This is in comparison to using the primary energy consumption plan. This suggests that, in order to lower greenhouse gas emissions, it is desirable to follow the emission operating approach for cogeneration systems.

By comparing the CCHP system to the separate production (SP) system, Wang et al. [18] examined three indicators of primary energy savings, energy efficiency, and CO_2 emission reduction in a CCHP system for a commercial building in Beijing. The energy and environmental performances of CCHP systems are primarily impacted by the power production efficiency and cooling mode performance coefficient, which have significant effects on CO_2 emission reduction, according to a feasibility study and sensitivity analysis [48].

Kong et al. [49] worked on the optimization of a cogeneration system composed of a gas turbine, an absorption chiller and a heat recovery boiler. Their findings demonstrated that operating load has a significant impact on the ideal point. To significantly reduce energy usage and CO_2 emissions, Yang et al. [50] designed and optimized a solar cogeneration system under five different operating scenarios. Song et al. [51] looked into the data centre's use of a cogeneration system with cold storage. Following thermal load (FTL) and following electrical load (FEL) methodologies were used to operate the suggested system. It was discovered that adopting FTL strategy rather than FEL method results in greater CO_2 emissions and energy consumption reductions. According to Haeseldonckx et al. [52], using a thermal storage system allows a cogeneration system to run at full capacity for a longer period. The recovery of waste heat from a gas engine for a water-ammonia chiller was studied by Garimella et al. [53]. To provide the heat needed for the chiller, they used direct combustion products. Finally, they demonstrated that by varying the ambient temperature between 40 and 52 °C, the COP ranges between 0.38 and 0.3. They also investigated the impacts of ambient temperature on the performance of this cycle. A summary of the studies about using the waste heat of CCHP systems for cooling purposes is listed in Table 3.

Table 3 Some of the related studies about the use of CCHP waste heat for cooling.

Ref.	Year	System description	Analysis type	Main results
Nami et al. [54]	2019	Applied absorption chiller and ORC cycle	energy, exergy	better performance and decreased payback period
Wegener et al. [55]	2020	Used biomass and solar energy combined cooling, heating, power and heat pump for different climate	energy, environment, economic and optimization	Decreased net present cost and emissions
Deymi-Dashtebayaz and Norani [56]	2021	Used CCHP system in data center and investigated two different scenarios	Sustainability assessment, energy analysis	Calculating energy consumption, selecting best scenario based on sustainability index,
Li et al. [57]	2020	Used CCHP system in high-speed railway and investigated different strategy	energy, environment, economic and optimization	improved primary energy consumption rate, CO_2 emission reduction rate, operating cost savings rate and comprehensive performance matching
Zare et al. [58]	2020	Used geothermal driven CCHP system, ejector transcritical CO_2 cycle is integrated with conventional Rankine cycle and replaced the gas cooler with an internal heat exchanger.	energy and exergy	increased the exergy efficiency, net output power and output cooling
Dehghani et al. [59]	2020	Used wastewater of the textile industry for producing biofuel and using biofuel driven CCHP.	energy, economic and optimization	the methane content of biofuel was enhanced and improved power efficiency of CCHP
Soltani et al. [60]	2020	Applied CCHP system with gas engine and used water- ammonia absorption chiller for producing cooling.	energy, economic and optimization	reduced of fuel consumption and system operating costs
Wang et al. [61]	2020	Investigated different waste heat recovery on performance of cogeneration, also applied absorption chiller for cooling.	energy and optimization	The simulation results of the static and dynamic models have no evident difference, and the maximal error is only approximately 0.5 %.
Cho et al. [62]	2009	Optimization of the operation of CCHP systems for different climate conditions based on operational cost, primary energy consumption and carbon dioxide emissions.	energy, environment, economic and optimization	The only cities that show reduction of primary energy consumption while also reducing the carbon dioxide emissions are Columbus.
Tayyeban et al. [63]	2021	Applied refrigeration cycle (REC), ORC cycle and multi-effect desalination (MED)	energy and exergy	Proposing a new multi-generation system, determining the best operating condition

2.3.   Micro-Trigenerative Systems (Micro-CCHP)

The micro-CCHP concept is referred to cogeneration plants with electrical power output below 50 kW. Although several issues have limited their widespread use so far, the potential market for system of this size is considered huge [64,65]. Indeed, the global efficiency of micro-CHP systems is greater than 75%, and, depending on the features and parameterization of the equipment, it can exceed 90%. The current research is focused on the optimization of CCHP systems to reduce primary energy consumption and increase the share of renewable energy. To this aim, several authors introduced their recent breakthroughs in the field: Akisawa et al. analyzed the optimal configuration of CCHP systems minimizing the primary energy consumption as an objective function. They found that absorption chillers can be worthier than compression chillers even though the latter generally assure a higher COP value [66]. Cardona et al. designed hybrid CCHP-heat pump systems to adapt power-to-heat systems ratios to demand [67]. Angrisani et al. analyzed a gas-fired micro-CHP system in two different buildings: a tertiary building and a residential building; comparing the results in two different Italian locations and highlighting the potential benefits of the thermal load-sharing approach [68]. From a thermodynamic point of view, micro-CCHP systems can be easily simulated in steady-state conditions. However, the actual use of these applications often requires an analysis of the transient processes involved. Indeed, the same authors performed a thermo-economic analysis of a CCHP desiccant-based air handling unit, which is dynamically simulated using TRNSYS software considering Southern Italy climatic conditions. The inputs of this model are empirical data, and parametric analysis is performed to obtain the output quantities [69].

2.4.   ORC Systems

The interest in low-grade heat recovery has been growing for the last decades, due to the increasing concern over energy shortage and global warming. Among the novel solutions, the Organic Rankine Cycle (ORC) system is the most interesting. This ORC process is similar to the cycle of a conventional steam turbine, except for the working fluid that drives the turbine, which is a high molecular mass organic fluid. The ORC system involves parts of the same components as a conventional steam power system: a work-producing expansion device, condenser, and pump. However, there always is an evaporator in replacement of a boiler to vaporize working fluid in relatively lower evaporating temperatures, as shown in Figure 17.
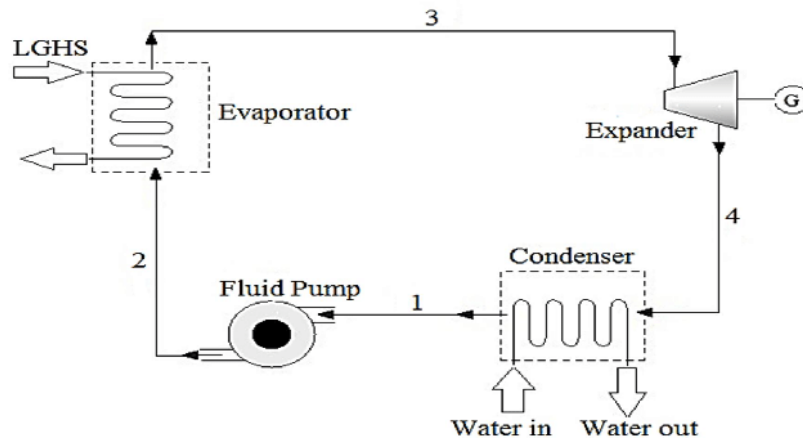
Figure 17 ORC System diagram

The pump supplies the working fluid to the evaporator, where the working fluid is heated and vaporized by the exhaust heat. The generated high-pressure vapor flows into the turbine and produces power there, and then, the low-pressure vapor is led to the condenser and condensed by air. The condensed working fluid flows into the receiver and is pumped back to the evaporator, and a new cycle begins. The heating and cooling sources are not directly in contact with the working fluid or with the turbine. For high-temperature applications like combined heat and power biomass-powered plants, high-temperature thermal oil is used as a heat carrier and a regenerator is added, to further improve the cycle performance. The typical T-S process for the investigated ORC system is shown in Figure 18.
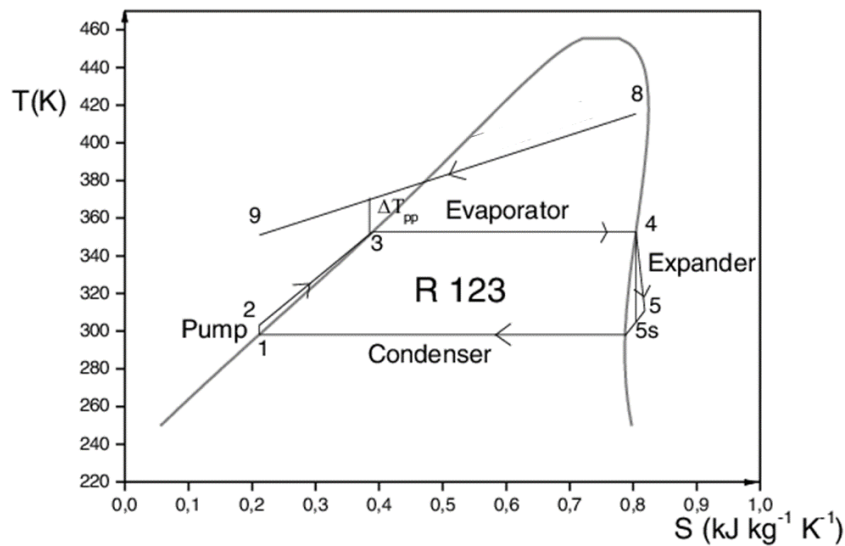
Figure 18 Typical T-S diagram for the organic Rankine cycle (ORC)

Due to different working fluids can be chosen depending on the level of heat resource temperature, it is possible to generate electrical energy from waste heat, geothermal sources, combustion of biomass or solar thermal sources. The ORC process can also produce electricity in a wide range of power outputs, from few kW up to 3 MW electric power per unit [33]. The ORC system has technical benefits as high cycle efficiency and high turbine efficiency, low mechanical stress of the turbine,

low RPM of the turbine allowing the direct drive of the electric generator without reduction gear, no erosion of the turbine blades, due to the absence of the moisture in the vapor nozzles and very long operational life of the machine etc. Furthermore, it also has practical advantages, such as simple start-stop procedures, quiet operation, minimum maintenance requirements, and good part load performance. However, the characteristic and principle of the Organic Rankine cycle will be farther discussed in the following Chapter with modelling.

Regarding the ORC systems, despite they are already a consolidated technology in the medium-large scale of electricity production, their development in cogeneration plants in the smallest range of size, suitable for residential application, is still at an early stage and represents a challenge both for industries and researchers [70]. Several works have been published on this topic. Among the most recent studies, Garcia-Saez et al. presented an energetic and economic analysis on solar-driven ORC for CHP in a residential application, considering two plant configurations (namely a solar ORC-CHP and a solar reversible heat pump), investigating several operating modes and scenarios and comparing different working fluids. They found that the implementation of this kind of systems can be convenient with positive Net Present Value (NPV) and a relatively short payback period, under certain climate conditions [71]. Yu et al. investigated the potential of the integration of an ORC with a heat pump, comparing the performance with the case of a stand-alone ORC power plant. They highlighted that the presence of appropriate operating conditions (poor thermal match between the working fluid and the waste heat for stand-alone ORC; the small ratio of latent to sensible heat for ORC's working fluid; the satisfactory value of COP of the heat pump) could lead to a significant benefit in terms of heat recovered and performance of the integrated plant [72].

2.5.   Abs-Adsorption Systems

Chillers are used in commercial and residential buildings and industrial plants to provide air conditioning, refrigeration, and process fluid cooling.
There are two basic types of chiller cycles:

- Traditional vapor compression cycle.
- Sorption cycle.

Vapor compression chillers use reciprocating, screw, or centrifugal compressors to power the cycle. The compressors are most often driven by electric motors, although they can also be powered by natural gas engines or steam turbines. Sorption chillers, which are available as either absorption or adsorption designs, are driven with thermal energy produced from a direct fired burner integrated with the chiller, or with thermal energy supplied indirectly to the chiller. Indirect thermal sources include hot water, steam, or combustion exhaust. Sorption chillers can recover thermal energy from combined heat and power (CHP) prime movers (e.g., reciprocating engines, microturbines, and combustion turbines).
Essentially, absorption is a refrigeration technology which enables to produce cold by directly using thermal energy. It is based on the phenomena of sorption, which is a collective term for the process where one substance (sorbent) takes up or holds another (sorbate) owing to the physical or chemical attraction between the pair of substances. The sorbate plays the role of refrigerant, describing the same thermodynamic cycles as in a vapor compression system. In fact, sorption systems are analogous to conventional refrigeration ones but use thermal compression instead of mechanical compression.

Thermal compression of the refrigerant basically involves two reverse processes: desorption, which consists of separating the sorbate from the sorbent by adding heat; and sorption, where the sorbate is soaked up by the sorbent. Contrary to the desorption process, sorption is an exothermic reaction.

Sorption systems can be classified into three major groups, depending on the nature of the sorbent and on whether the process occurs in an open or closed environment:

- *Absorption*: the liquid or solid sorbent experiences physical and/or chemical changes during the soaking up of the refrigerant.
- *Adsorption*: a solid sorbent attracts the refrigerant into its surface, but it does not change as a result of the process.
- *Desiccation*: the sorbent (solid or liquid) is a hygroscopic material which ab- sorbs the moisture from humid air. It is referred as an open cycle since the refrigerant (water) is discarded from the system after providing the cooling effect.

When air conditioning applications are concerned, it is commonly agreed that absorption technology is the most suitable option among sorption cooling processes, [73]. Desiccant cooling systems may be an adequate solution when having good indoor quality is essential. Moreover, their application is limited to large installations because of the high initial cost, as stated by [74]. On the other hand, adsorption systems present a maximum achievable COP comparable with absorption ones. Yet, their lower densities make them bulkier and more expensive. Nevertheless, they may be a good option when low temperature driving heat is available.
In the next sections, the two main sorption technologies, i.e. absorption and adsorption chillers, will be discussed in detail.

Absorption Chillers
By exploiting the waste heat coming from a heat source, it is possible in fact, to be able to operate a system of this type. While in compression refrigeration systems the thermal power is subtracted from the cold source at the expense of the mechanical power used to drive the compressor, in absorption systems the production of cold is guaranteed by the thermal power introduced. In absorption cycles, the mechanical power for driving the fluid circulation pump is in fact negligible [75].
Generally, an absorption machine, able to work both as a heat pump and as a chiller, is composed of 4 main elements:

- Condenser: Just like in the traditional condenser of the vapor compression cycle, the refrigerant enters the condenser at high pressure and temperature and gets condensed. The condenser is a water-cooled type.

- Expansion valve or restriction: When the refrigerant passes through the expansion valve, its pressure and temperature reduce suddenly. This refrigerant (ammonia in this case) then enters the evaporator.

- Evaporator: The refrigerant at very low pressure and temperature enters the evaporator and produces the cooling effect. In the vapor compression cycle this refrigerant is sucked by the compressor, but in the vapor absorption cycle, this refrigerant flows to the absorber that acts as the suction part of the refrigeration cycle.

- Absorber: The absorber is a sort of vessel consisting of water that acts as the absorbent, and the previously absorbed refrigerant. Thus, the absorber consists of the weak solution of the refrigerant (ammonia in this case) and absorbent (water in this case). When ammonia from

the evaporator enters the absorber, it is absorbed by the absorbent due to which the pressure inside the absorber reduces further leading to more flow of the refrigerant from the evaporator to the absorber. At high temperatures, water absorbs lesser ammonia, hence it is cooled by the external coolant to increase it ammonia absorption capacity.

In Figure 19, shown below, it is possible to observe a typical layout of the absorption cycle. In this case, the task performed by the compressor (in the traditional compression cycle) is performed by the absorber and the desorber, which therefore have the function of raising the pressure of the fluid.
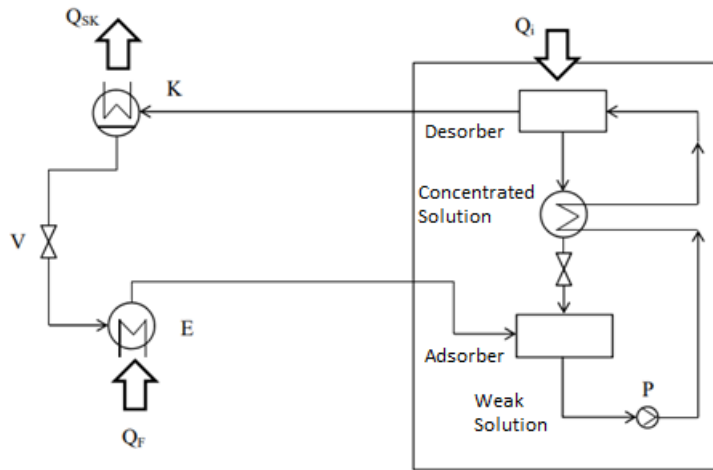
Figure 19 Absorption system layout

This is guaranteed by the thermal power introduced into the Q_i cycle. These systems require the presence of a hot source, since the thermal power must be introduced at a temperature that is higher than the ambient one.

The expression for the performance of the absorption refrigeration system is defined by (2):

$$COP_{Abs,ref} = \frac{Q_F}{Q_i + W_{pump}}$$

(2)

Where W_{pump} is the mechanical power applied by the pump and Q_F is the useful heat removed for the cooling effect.

Another feature of these systems, which differentiates them from the compression ones, is the refrigerant fluid. It consists of a mixture of two fluids which, in the most common types, are ammonia/water and water/lithium bromide. In the first case, ammonia performs the function of refrigerant fluid, while in the H_2O-BrLi group, water is the fluid entrusted with the task of extracting heat from the environment to be cooled.

Generally, in the systems that are marketed, the lithium bromide cycle uses water as a thermal source at a temperature that varies between 90 °C and 130 °C depending on the size of the absorber (the higher the temperature, the smaller the dimensions) obtaining, as a cooling effect, cold water at about 7 °C and, as performance, an Energy Efficiency Ratio (EER) with values of 0.75 ÷ 0.70. In cases of extreme refrigeration (up to -20 °C) it is necessary to use ammonia systems, which have, on the other hand, a high cost of the absorber. The use of NH_3 is motivated by its low cost and high availability on the market, on the other hand, it is not used in the home because of its high toxicity and moderate flammability.

Regarding the working pairs for absorption refrigeration systems, LiBr/H_2O and H_2O/NH_3 are the most widely used. The absorbent is the first term in the formulae whereas the absorbate is the second

term. Although other innovative working pairs have been investigated for the last years, see for instance [76], it seems that those two classical pairs will be still the reference for absorption systems in the near future, as predicted by [77]. By and large, LiBr/H$_2$O is most adequate for air conditioning purposes, while H$_2$O/NH$_3$ is more suitable for refrigeration in industrial applications.

The simplest configuration is the single-effect cycle. It is a common fact that the coefficient of performance (COP) of LiBr/H$_2$O machines working with this cycle ranges from 0.6 to 0.8. Besides, driving temperatures are between 80 and 100°C for water-cooled systems, while for air-cooled ones are about 20°C higher. This range of temperatures makes LiBr/H$_2$O single-effect cycles very appropriate for solar cooling.

By adding some extra components to the basic single-effect configuration, the double-effect cycle is able to use the input heat twice for generating a greater amount of refrigerant. Due to the higher working pressures achieved in this configuration, this cycle is not practical for refrigerants with low boiling temperatures such as ammonia. The COP obtained for LiBr/H$_2$O double-effect systems is typically between 1.1 and 1.3. In turn, the usual range of driving temperatures is 140-170°C for water-cooled machines and 160-190°C for air-cooled ones, [78]. Those temperatures make more complicated the use of solar energy as driving source; however several technologies are avail- able in the market to provide solar heat at such temperatures, [79].

As an extension of the previous configuration, the triple-effect cycle appears as a promising option to increase the performance of LiBr/H$_2$O absorption machines. Here, the input heat is used in three stages and driving temperatures above 200°C are needed. In general, COP values around 1.4-1.6 may be achieved. However, there is a major challenge associated with this cycle, the corrosion problems caused by the very high working temperatures. Triple-effect technology is currently under active development, as pointed out by [80] [81] [82] [83].

When the temperature of the available source heat is not high enough to fire a single-effect configuration, the half-effect cycle is regarded as an adequate option. The driving temperatures for water-cooled LiBr/H$_2$O systems are typically between 60 and 75°C. In turn, air-cooled systems require driving temperatures of about 20-30°C higher. In general, COP values achieved with this cycle are roughly half of a single-effect cycle, hence its name. Although this configuration can be also referred as two-stage cycle, the former name is usually preferred. The main disadvantages of this cycle are the complicated configuration and the reduced COP, around 0.3-0.4. Some interesting works studying the possibilities of this cycle are presented in [84][78][85][74].

Numerous studies have been conducted for applications of liquid absorption machines. A heat recovery system, consisting of a generator and an economizer, was developed by Fernandez-Seara et al. [86] to provide incoming thermal energy to an absorption chiller. The results showed that the energy recovered from a ship's engine is suitable for the considered application, as the temperature level and available heat exceed those required. Ouadha et al. [87] performed a thermodynamic analysis of a water-ammonia system, also considering the energy balance for marine diesel, demonstrating that this is capable of providing sufficient waste heat to operate the absorption chiller. Cao et al. [88] developed a TRNSYS model to simulate an absorption chiller used for space cooling in a cargo ship under Miami conditions, finding that the system is capable of providing comfort conditions in the route under consideration. The same authors, in [89], developed a TRNSYS model to compare the absorption system of a basic VCC system, conducting an energo-economic analysis that demonstrated the feasibility of such systems. Ezgi [90] performed a thermodynamic analysis on a LiBr / water system for both space heating and cooling on a naval surface vessel driven by the heat lost from the engine, demonstrating that the seawater-cooled system not only satisfies the actual heating and cooling loads of the vessel under examination, but also provides a surplus.

Table 4 resume the studies in literature on applications of liquid absorption machines.

Table 4 Studies in literature on applications of liquid absorption machines

ABSORPTION SYSTEM STUDIES					
Reference	**Application Sector**	**Technology**	**Chiller Type**	**Study**	**Recovery System**
[86]	Heat recovery	Absorption	NH_3/H_2O	Matematic Model	Yes
[87]	Space cooling	Absorption	NH_3/H_2O	Thermodynamic Model	No
[88]	Space cooling	Absorption	$H_2O/LiBr$	Dynamic Model	Yes
[89]	Space cooling	Absorption	$H_2O/LiBr$	Dynamic Model	Yes
[90]	Space heating and cooling	Absorption	$H_2O/LiBr$	Thermodynamic Model	Yes

Adsorption Chillers

The operating principle of solid adsorption machines is based on the ability of some materials, defined as "adsorbent materials", to be able to reversibly adsorb some vapor molecules (refrigerant or working fluid) as shown in Figure 20. The bond that it is established between the vapor molecules and the adsorbent material is of a chemical nature. The main advantage of these innovative air conditioning systems is that they are not powered by electricity but by low temperature thermal energy, obtainable without major difficulties; in fact, energy sources such as solar energy or the waste heat of internal combustion engines could be some of the technological solutions useful for the operation of these systems.
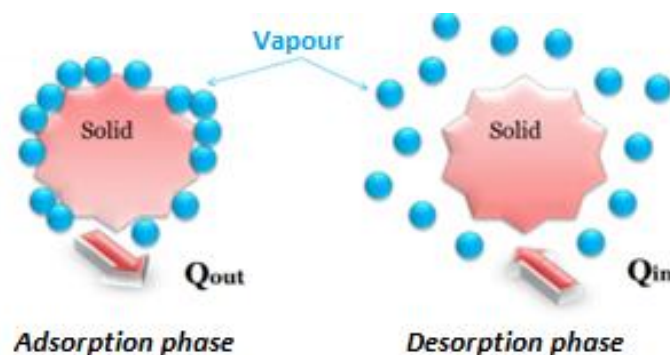
Figure 20 Adsorption phases

Basically, these machines are very similar to vapor compression systems (powered by electricity); one of the main differences is that instead of the electric compressor, a thermal compressor is used,

inside which the adsorbent materials are contained. The possibility of thermally regenerating the adsorber so that it can adsorb cyclically, several times without any alteration, is certainly an excellent technological solution to lower electricity consumption. Although the basic thermodynamic cycle of adsorption systems is characterized by COP values lower than those of vapor compression machines, these systems can become competitive when compared in terms of primary energy, justifying the possible use of adsorption machines in the field of air conditioning.

In general, an adsorption machine, able to work both as a heat pump and as a chiller, is composed of 4 main elements:

- The thermal compressor (adsorber or adsorbent bed): within which the adsorption and desorption processes of the refrigerant fluid take place.
- The condenser: where the vapor released in the desorption phase condenses, releasing heat to the external environment.
- The evaporator: where the evaporation (endothermic process) of the refrigerant fluid occurs, favored by the adsorption phase.
- The lamination valve: used to reduce the pressure from the condensation to the evaporation pressure.

Figure 21 shows the typical operating scheme of a solid adsorption system:
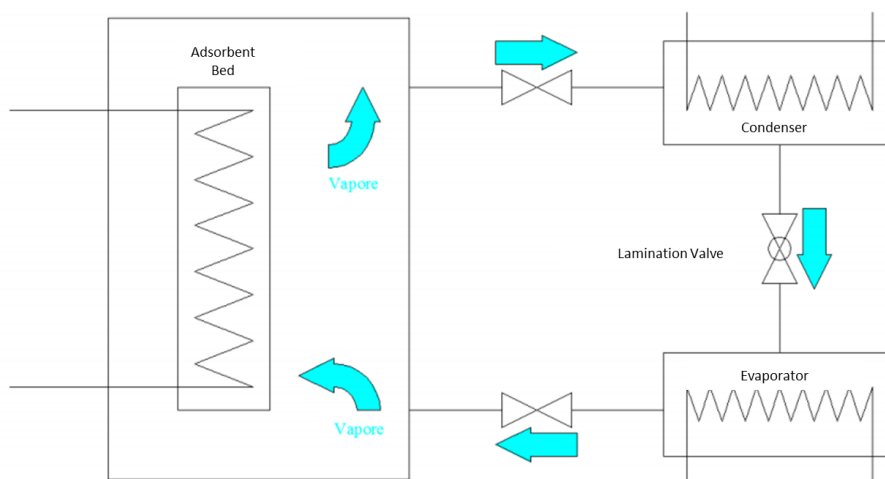
Figure 21 Schematic of an adsorption system

In the last 5 years, several studies have been carried out for the optimization of the technology at various levels:
• Studies on materials
• Studies on components
• Studies on the operational management of the system
• Studies on lab-scale systems

Sorbent Materials
The development of adsorbent materials is currently strongly correlated with the choice of the adsorbent/adsorbate pair. Since the most common adsorbates are water and ammonia, the following sections summarize the adsorbent research activities developed for the most promising types of adsorbents in recent years.

- *Silica Gels*

Silica gels historically represent one of the most used adsorbent materials for the absorption of water vapor. In fact, they represent the least expensive option for adsorption cooling applications and can easily be used for heat sources at temperatures below 100 °C (eg flat solar thermal collectors). It is an amorphous material consisting of an aggregation of primary silica particles whose dimensions and packaging determine the characteristics of the final product such as its specific surface and the distribution and volume of pores. The pore size varies from a minimum of 2 nm to a maximum of 20 nm. The properties of this material can be modified by intervening on the chemical nature and concentration of the precursors [91].

- *Zeolites*

Zeolites are crystalline alumino-silicates, characterized by a high specific surface (i.e. about 800 m^2/g) and large microporous volumes, which make these materials perfectly suitable for the adsorption of water vapor. Due to their porous structure, zeolites are generally highly hydrophilic, which allows them to achieve high adsorption capacities even at low partial pressures. This high affinity with water, of course, reflects a strong bond that requires higher temperatures to break than silica gels (i.e. more than 150 °C) [91].

- *Zeo-Like Materials*

More recently, several new microporous adsorbents have been proposed. They are often referred to as zeo-like materials, as their crystalline structure is somewhat similar to that of classical zeolites. The two classes that have shown the most promising characteristics are aluminophosphates (AlPO) and silico-aluminophosphates (SAPO). Indeed, unlike other classical adsorbents, these materials show a partially hydrophobic behavior, which is reflected in an S-shaped adsorption isotherm. This is an advantageous feature, which allows to obtain a high amount of water vapor exchange in a narrow partial pressure range. Consequently, since the overall heat storage capacity is highly dependent on water vapor exchange, these materials can guarantee very high heat storage capacities Among these two classes, the most attractive materials are known as AlPO-18 and SAPO-34. In particular, research on these materials led to the first commercial adsorbent developed specifically for closed adsorption systems (e.g. for heating, cooling and storage applications). It is known as AQSOA Z02, and is manufactured and marketed by Mitsubishi Plastic Inc. (Chiyoda-ku, Tokyo) [92].

- *Metal Organic Frameworks*

Metal Organic-Frameworks (MOFs) represent a new emerging class of adsorbent materials. These materials, still in an early stage of development, are considered the future of adsorption. Due to their structure, consisting of metal ions interconnected by organic macromolecules, it is possible to select several different compositions; giving infinite possibilities to obtain the ideal adsorbent material simply by adjusting the synthesis procedure. In fact, they are usually characterized by a high specific surface (i.e., higher than 2000 m^2/g), which guarantees the ability to reach higher absorption capacities than other adsorbent classes. Higher adsorption capacities are also obtained by adjusting the pore size, based on the adsorbate and the working field. However, as mentioned above, this class is still far from practical application, for two main reasons: their high cost, linked both to the small quantity currently produced and to the cost of raw materials, and their stability, which still requires investigation. In [93], all the advantages of this type of materials for future applications have been listed.

- *Activated carbon*

Activated carbons are carbonaceous adsorbing materials, obtained from various possible precursors (eg coconut shells, wood, charcoal), characterized by a large specific surface (1200–1300 m^2/g) and microporous volume. These materials are typically used as ammonia adsorbents and alcohols by adsorption, due to the high affinity shown for these adsorbates. Due to the competitive cost and wide

commercial availability, they are considered a promising option in the field of adsorption. In [94], the adsorption kinetics and thermodynamic analysis of cooling systems employing activated carbon-graphene / ethanol pairs have been studied, demonstrating that they possess a high cooling effect that will provide a significant direction for the development of cooling systems next generation.

- Composites
Composite adsorbents represent a hybrid method to improve the absorbency of materials. Indeed, they are based on the inclusion of inorganic salt (e.g., $CaCl_2$, LiCl, LiBr) within a porous host structure (e.g., silica gel, vermiculite). This concept was invented by the Boreskov Institute of Catalysis, in an attempt to exploit the absorption capacity of certain types of salts, avoiding one of their main limitations, namely the excessive limitation of mass transfer induced by salt agglomeration [95]. Given the wide availability of inorganic salts, it is possible to synthesize composite adsorbents that can be used with a high number of adsorbates. Typical examples are the well-known Selective Water Sorbents (SWS) which represent the broadest class of composite materials, specifically developed for water adsorption.

Studies on components
At the component level, a line of research has developed around the study and optimization of adsorbent beds. The exchange of mass and heat is essential to accelerate the dynamics of the ads/desorption reaction. In [96], I. Girnik studied the effect of the bi-dispersed adsorbent bed on the dynamics of ad/desorption in typical air-cooling conditions using two different particle sizes of AQSOA™ -FAM-Z02 adsorbent, as described in Figure 22, showed an increase in performance.
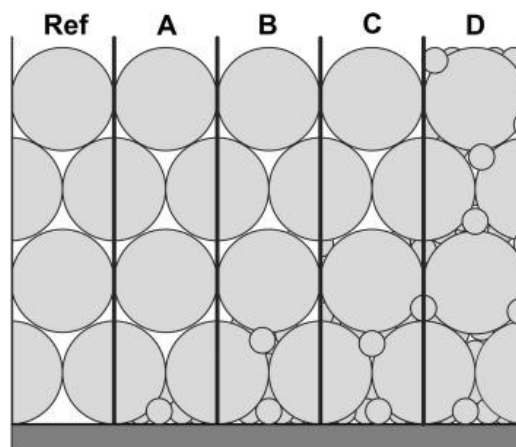
Figure 22 Diagram of the bi-dispersed layers from a reference of only coarse grains (Ref) up to the complete filling of fine grains in the unoccupied spaces (D)

An innovative adsorbent bed has been developed at the Fraunhofer-Institute Solar Energy Systems ISE (Freiburg, Germany) which uses a new type of heat exchanger based on aluminum sintered metal fibre structures brazed on flat fluid channels. The adsorption heat exchanger is coated with a silico-aluminum phosphate (SAPO-34) employing a partial transformation of the direct crystallization support (PST) [97]. The experimental characterization of the module shows a specific power at high volume (up to 82 W/L for cooling, 320W/L for heating). Although no heat is recovered between the absorption cycle and the desorption cycle, a COP of nearly 0.4 is achieved for cooling and 1.4 for heating.
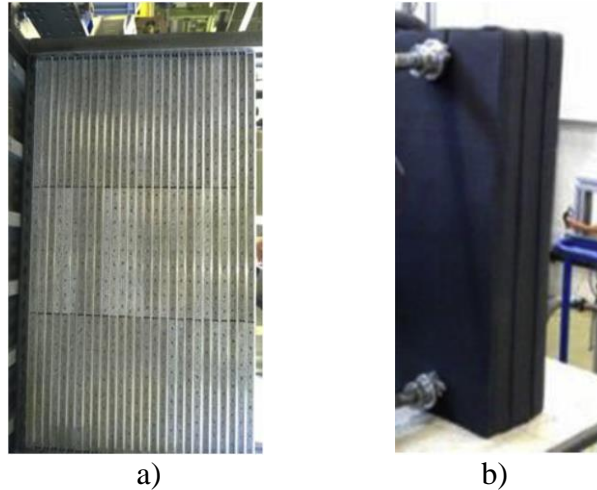
Figure 23 Views of the heat exchanger

Improving the heat transfer conditions in the adsorption bed volume is one of the crucial tasks for improving the energy efficiency of the adsorption chiller. In [98], a promising method was investigated which consists in modifying the outer surface of the heat exchanger using thermally conductive glue and thereby removing the gaps. The coating made with epoxy resins allows to an increase in the thermal conductivity and therefore the performances of the absorbent bed.

Studies on the operational management of the system

Studies have been performed on the optimization of adsorption chillers by exploiting mass recovery and heat recovery respectively. For example, a composite adsorber ($CaCl_2$-activated carbon) operating both with and without mass recovery was tested. The experimental results have shown that through the mechanism of mass recovery it is possible to obtain better performances [99].

Heat recovery is also an effective way to improve the performance of the adsorption refrigeration system thanks to its easy implementation. Three types of heat recovery (circular heat recovery is complete and serial and passive heat recovery are partial) have been applied in recent adsorption refrigerators. A theoretical analysis of three heat recovery methods was performed in [100]. The results show that serial and passive heat recovery (part type) are more optimal than circular heat recovery (complete type) when manufacturing and cost are considered.

To optimize the system, a new management strategy was studied, based on different durations of the isobaric adsorption and desorption phases of an adsorbent cooling cycle, as shown in Figure 24. This innovative management strategy, described in [101], is aimed, in particular, at achieving a high cooling power density.
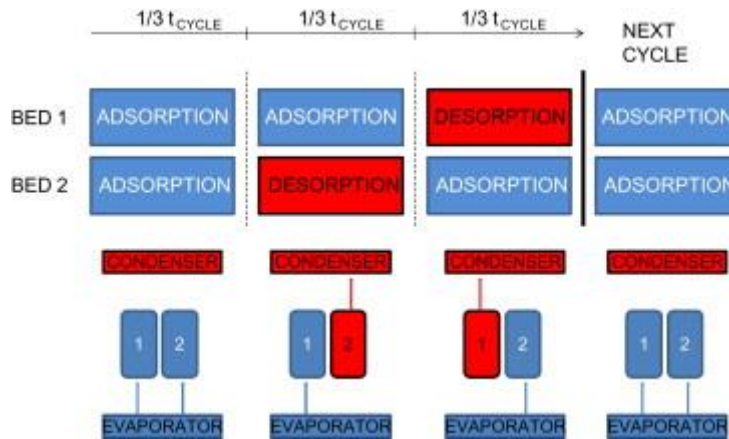
Figure 24 System management strategy by reallocating the times of the cycle phases

Studies on lab-scale systems

At the laboratories of Shanghai Jiao Tong University (Shanghai, China), as described in [102], an innovative silica gel and water adsorption chiller was built and experimentally studied that uses a mass recovery process under conditions hot water temperature below 80 °C. For the data center waste heat use case, the adsorption chiller can be well operated at supply temperatures of 51.4–61.3 °C, with COP of 0.285-0.477 and SCP (Cooling Power specification) of 71.2-108.4 W/kg while producing chilled water at 18.8-22.4 °C. For cases of glass displays and liquid crystal displays that produce residual heat utilization, COP values of 0.317-0.483 and SCP values of 95.2-146.7 W/kg can be achieved under temperature conditions hot water inlet temperatures of 56.2–74.9 °C and chilled water outlet temperatures of 14.2–16.8 °C. These experimental results indicate that the operational feasibility and good performance of the silica gel and water adsorption chiller for using ultra low temperature waste heat are confirmed.

As part of a joint study between Hokkaido University (Hokkaido, Japan) and Nihon Netsugen System Co. (Tokyo, Japan), in [103], a laboratory AHP prototype with a capacity of 1 kW was developed. A natural mesoporous material (WSS impregnated with 20% by weight of LiCl) was used as adsorbent to reduce the initial cost and inserted in corrugated aluminum heat exchangers (HEX) shown in Fig. 18. They are Foundation performance experiments were conducted and COP of 0.45 and SCP of 0.41 kW/kg were obtained under the following experimental conditions: $H_T = 80$ °C, $H_M = 30$ °C, $H_L = 15$ °C and time of cycle equal to 14 min. In addition, heat recovery was introduced and experimentally studied to reduce the amount of regeneration heat and the heat balance was evaluated. It was confirmed that two types of heat recovery could improve the COP for this AHP up to 0.54 when the outlet temperature of both adsorbers was 55 °C. The COP could be further improved to 0.57, based on the calculation for the heat balance. This AHP has the advantages of a high SCP over AHP.

In [104], at Yasouj University in Iran, an adsorption chiller with micro-nano activated carbon/methanol and powered by solar energy was designed and built. The chiller used in this study includes evaporator, condenser, adsorbent bed and compound parabolic collector. The manifolds used in this chiller are of the compound parabolic type. Unlike traditional systems which only refrigerate during the night, in this document the continuous refrigeration system with two adsorbent beds can produce cold during the day.

The main technical characteristics of the studied chillers are summarized in Table 5.

Table 5 main technical features of lab-scale prototypes

Ref	Dimensions [mmxmmxmm]	COP	SCP max [W/kg]	Adsorbent Material	Coating	Number of beds	Characteristics
[102]	1590x1060x1420	0,28-0,47	71-108	Silica gel	-	2	11 Exchangers made of aluminum with finned tubes
[103]	400×300×12	0,45	410	WSS adsorbent (natural mesoporous materials composed of silicon dioxide)	Epoxy resin	2	4 Exchangers made of aluminum
[104]		0,10-0,14	65 - 90	Nano/Micro Active carbon	-	2	Solar driven

3. DEVELOPMENT OF AN ADSORPTION CHILLER PROTOTYPE (CNR ITAE)

As discussed in Chapter 2, adsorption refrigeration machines have the fundamental characteristic of being powered by heat at low thermal levels (<100 °C) and of using environmentally friendly refrigerants (e.g., water, ethanol).

The main objective of the experimental activity is to develop and test, by means of a specific test station, an adsorption air conditioner prototype that has innovative features compared to the state of the art. The work has been funded by the project POFESR "FI-ShipS: Future Innovative Ship for Sicilian routes" in collaboration with National Council of Research, Caronte & Tourist S.p.a.

The prototype in question has been designed to be compatible with the power supply through the recovery of thermal energy deriving from the cooling circuits or from the exhaust fumes of I.C. first and/or secondary engines present on ships but also with other hot water sources such as solar energy. Initially, a feasibility analysis was conducted based on the state of the art of air conditioning systems used in the naval field and of the potential system solutions based on the use of solid adsorption machines that could present, in this context. Subsequently, the activity moved on to the design and construction of the adsorption chiller prototype. As a first step, the type of heat exchangers to be used for the construction of the adsorbers was identified. The performance of the single adsorber has been tested to choose the optimal number of exchangers to be provided to meet the required cooling capacity. The layout of the adsorber necessary for the construction of the chiller was then defined by selecting the number of beds, the type of adsorbent material and its configuration. The heat exchangers useful for making the evaporator and condenser of the chiller have been sized starting from the evaluation of the adsorber power. The chambers necessary for the realization of the prototype were designed and sized to obtain a simple and compact configuration. Finally, the P&ID graph was created for the management of the plant and a software was implemented in LabVIEW to create the control system. To test the performance of the thermally driven chiller prototype, the test station located at the "TEST CENTER" of the C.N.R. I.T.A.E.

3.1. Identification of the layout

The layout of the adsorption chiller was defined on the basis of the literature survey carried out and the required requirements.

Different configurations were considered for the construction of the adsorber. Their potential has been evaluated in terms of density of cooling capacity, costs and dimensions. We opted for a simple layout based on a number of beds equal to two and on the use of zeolite in the form of foam as an adsorbent material. Water has been chosen as refrigerant. Following the definition of its layout, the executive design of the full scale adsorbers necessary for the operation of the adsorption air conditioner was carried out. The layout of the Adsorption Prototype is showed in Figure 25.
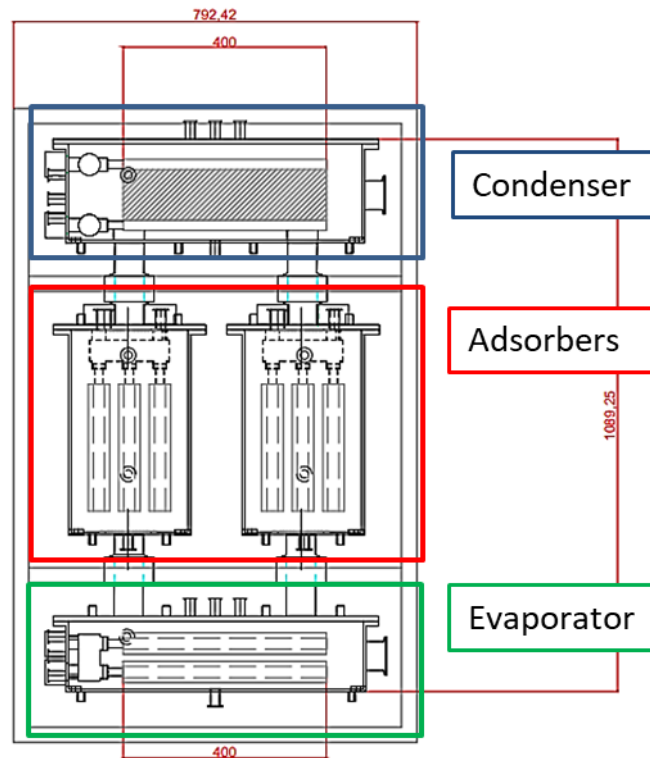
Figure 25 Layout of the Adsorption Prototype

3.2. Identification of the best sorbent material configuration

Heat pumps based on the adsorption/desorption of water vapor on micro and mesoporous materials allow an innovative approach to the rational use of energy, for a sustainable energy policy and effective climate protection, through the reduction of the environmental impact of conventional heating and cooling devices. Several adsorbent materials have shown promising water vapor adsorption capacities for such applications, among which the most widely used are silica gel and silico-aluminous zeolites. Before mentioned adsorbent materials show, however, important limitations in the application of adsorption machines. In fact, silica gel, being an amorphous material, has little structural stability to the different adsorption /desorption cycles while the traditional silico-aluminous zeolites, despite the high stability due to the crystalline structure, are very hydrophilic and therefore are characterized by the high heat of desorption which limits its use to applications where regeneration heat at high temperature is available.

Hence the need to use new adsorbent materials that have a stable crystalline structure and that are partially hydrophobic to be regenerable at moderately low temperatures. The zeolites belonging to the family of nano-porous structures based on silicon-aluminum-phosphorus, the SAPO and ALPO zeolites, possess the ideal combination of properties for the before mentioned application because they combine high absorption capacity of water vapor and low heat of regeneration. Along with the development of adsorbent materials, the adequate integration of the adsorbent is of great technical importance for the thermodynamic performance of adsorption machines with the heat exchanger (HEX) to form the adsorber (Ad-HEX), which is the key component for obtaining high heat exchange yields. The traditional configuration of the adsorbent, made using the adsorbent material in the form

43

of granules, has shown, over time, obvious limitations due to the poor contact between the adsorbent itself and the walls of the exchanger.

The use of finned exchangers, with a high surface area, coated with a thin layer of adsorbent is currently considered the most efficient method to reduce the heat exchange resistances at the adsorbent/metal surface interface and therefore obtain an improvement in the dynamic response of the adsorber with the consequent improvement of the thermodynamic efficiency of the machine. The most promising coating methods are zeolite in situ crystallization and binder-based coating processes. The direct synthesis of the adsorbent material on the surfaces of the exchangers allows to have a good thermal contact but on the other hand presents considerable difficulties of realization due to the complexity of the direct synthesis of the material, as for example happens in the case of zeolites in which the chemical reaction environments are generally aggressive for the metal surfaces of the exchanger.

The binder-based coating method is an alternative way to deposit a thin layer of adsorbent on the surface of the heat exchanger. In this case, the adsorbent material is used in the form of very fine granules or powders mixed with a polymeric phase which acts as a binder with the metal surface. The advantage of this method is the ease of execution compared to direct chemical synthesis and greater control of the thicknesses deposited by controlling some operating parameters, such as the viscosity of the adsorbent precursor/polymer mixture, the porosity of the matrix, in the case of the zeolitic foams. and the deposition rate (dip coating).

3.3. Experimental characterization of the selected sorbent material

The development activity of the zeolite foam was carried out in collaboration with the University of Reggio Calabria, through a consultancy contract, and led to the creation of different types of coating on heat exchangers (HEx) using non-traditional adsorbent materials SAPO/ALPO zeolites combined with a siloxane foam-based matrix. The composite coating was developed specifically for the intended industrial application. In particular, the experimental formulations were optimized to obtain the coating of the heat exchangers (coated HEX) with different deposition techniques. Excellent results in terms of preparation and deposition were obtained using composite coatings containing 90% by weight of zeolite. The above formulation has proved effective both with the spray deposition technique and by casting. The latter technique, in particular, was used for the construction of four heat exchangers coated with composite foams containing SAPO zeolites. More details on the consultancy activity are available in a specific scientific report.

The characterization of the zeolite foam was carried out in collaboration with the Engineering Department of the University of Palermo, as part of a consultancy contract, and concerned the morphological, microstructural, and mechanical characterization of composite coatings based on zeolite on aluminum supports and relative heat exchangers coated on the same support. In order to complete the investigation, accelerated aging tests were also conducted in a salt spray chamber with the aim of verifying the durability of the coating in critical environmental conditions.

The XRD and FTIR analyses carried out on the coating made it possible to verify that the applied material consists of zeolite SAPO-34 and PDMS (silicone). The morphological investigation showed a very particular microstructure with a closed porosity that configures the coating like a sponge with adsorbing properties. The adhesion tests showed adhesion compatible with the required application conditions. On the acquired coatings, water vapor adsorption measurements were carried out which confirmed that the matrix does not hinder the absorption capacity of the zeolite, preserving the effectiveness in the adsorption and desorption phases of the coating. Finally, accelerated aging tests for 15 days confirmed the good mechanical stability of the coating in adverse environmental conditions.

Preliminary experimental investigations were carried out to determine the most suitable composite coating formulation in terms of workability and zeolitic filler content. In particular, the action of different solvent contents (water, ethanol) was evaluated to optimize the viscosity of the mixture to be deposited on the coating. This type of investigation identifies an application parameter, viscosity, which is fundamental in the realization and therefore in the final properties of the coating.

Figure 26 shows the viscosity trend of siloxane-zeolite-solvent mixtures with increasing content of zeolitic filler obtained by a rotational viscometer at 300 rpm. The results show that as the content of zeolite increases, the composite mixture, polymer/zeolite, shows a progressive increase in viscosity as the filler content increases. In particular, at equilibrium, the composite with 95% zeolite shows a viscosity of about 0.09 Pa*s. The sample with a lower content of zeolite (80% by weight), on the other hand, shows at equilibrium a viscosity lower by more than half (0.041 Pa*s).

The use of an initial mixture that is too dense could generate problems on the homogeneity of the dispersion of the particles as well as difficulties during the deposition phase. In the case of the formulation with a high content of zeolite (95% by weight), due to the high viscosity of the initial mixture, difficulties are foreseeable in the deposition method, both using the casting technique (dip coating) and by spraying deposition. In order to facilitate the ease of deposition, viscosity values of the precursor solution lower than 0.08 Pa*s are considered suitable for the use of both deposition techniques used.
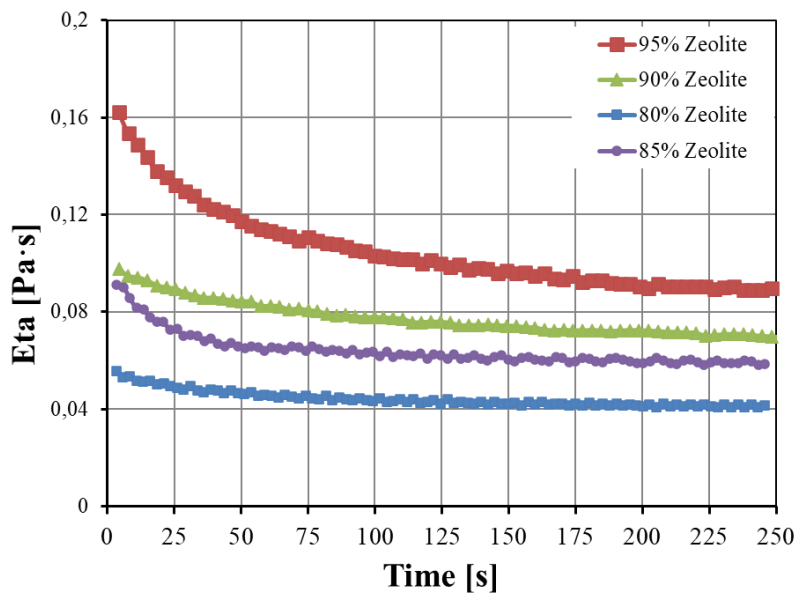
Figure 26 Viscosity trend of siloxane-zeolite-solvent mixtures with increasing content of zeolitic filler.

Figure 27 shows some reference images relating to the deposition of composite foams conducted on finned exchangers supplied by the customer (3 mm pitch) with increasing content of SAPO zeolite.
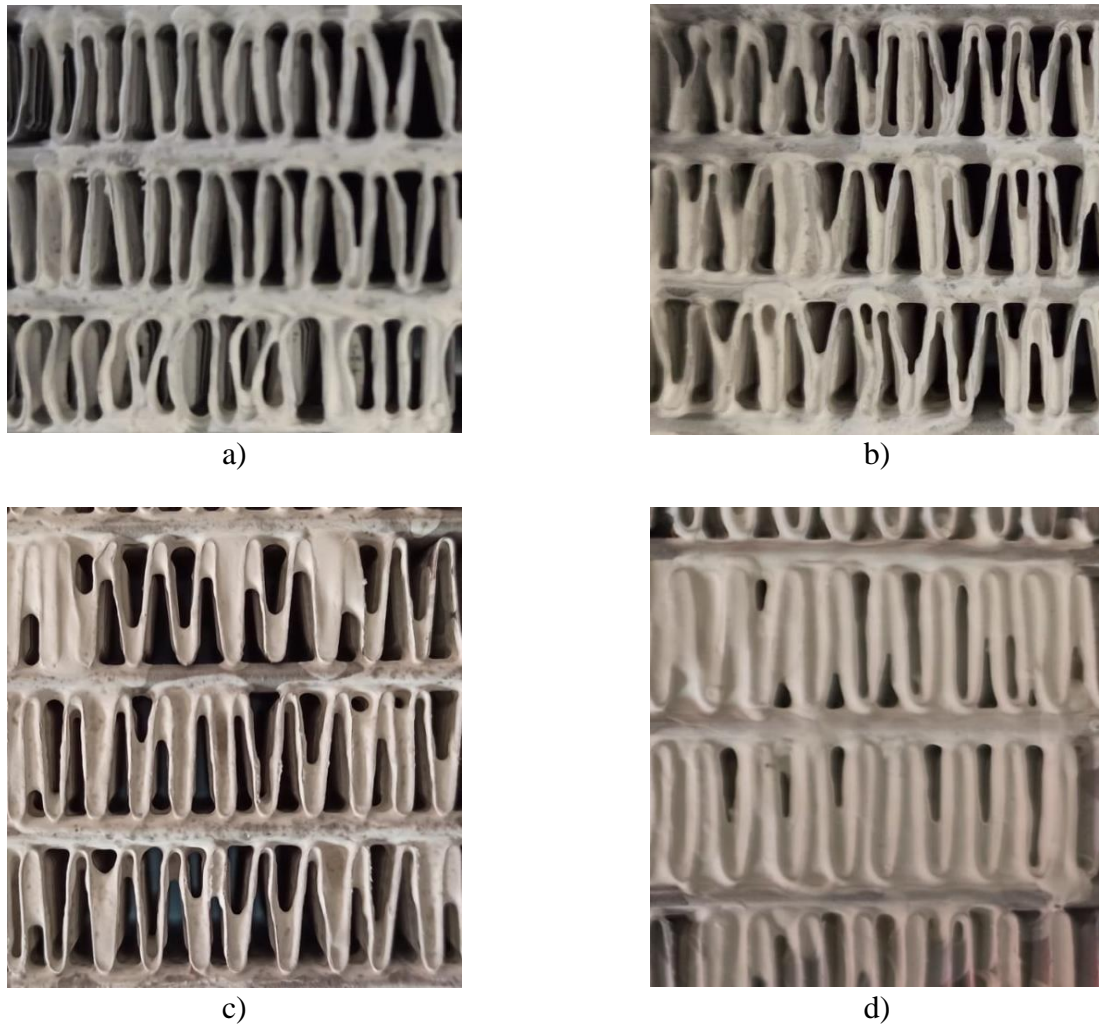
Figure 27 Deposition of composite coatings with increasing content of SAPO zeolite (80% - 95% by weight) on finned exchanger with 3 mm pitch

Foam coatings with 80% and 85% of zeolite are very regular in thickness, do not have lumps, but in consideration of the low filler content they have not been considered for depositions on full-scale heat exchangers. With these concentrations, in fact, the thermodynamic efficiency of the exchanger is limited due to a low weight ratio of zeolite / weight of the exchanger. A high filler content (formulated with zeolite content> 90%), on the other hand, leads to a very dense mixture that tends to clog the exchanger channels during the deposition and formation phase of the coating. It is noted that deposition with 90% zeolite content presents a good compromise between ease and homogeneity of deposition and content of adsorbent material.

As an integration, specimens were made deposited on aluminum foil (dimensions 50 cm x 50 cm) for all concentrations of zeolite supplied with the samples for the purpose of subsequent morphological and mechanical investigations on the coatings themselves.

Based on the preliminary deposition tests, a series of exchangers having dimensions 40x20x4 cm were created. Figure 28 shows some reference images of the exchangers made. Once the siloxane-zeolite-solvents solution had been deposited, it was dried in air for 5 minutes and then cured in an oven for 24 hours at 70 °C. The image shows that the deposition did not involve the obstruction of the channels between the fins of the exchanger and therefore does not increase the resistance to the flow of steam. However, from Figure 28-c it can be seen that there are areas of heterogeneity in the distribution of the coating. These areas do not lead to a reduction in the performance of the exchanger itself, as they are mainly located along the edges of the aluminum fins and consequently do not block

46

the channels between the fins which instead appear free and therefore do not represent an obstacle to the flow of water vapor. The enlargement of Figure 28-c confirms the above considerations, highlighting how even the channels in the apparently heterogeneous areas are still suitable for the passage of steam.

The finned area at the bottom of the exchanger (see the enlargement shown in Figure 28-c, frame in green) in fact, shows an unobstructed central channel of about 0.5 mm along which the flow of steam can take place. These exchangers have been tested at the CNR ITAE and will be used for the realization of the adsorption chiller prototype.
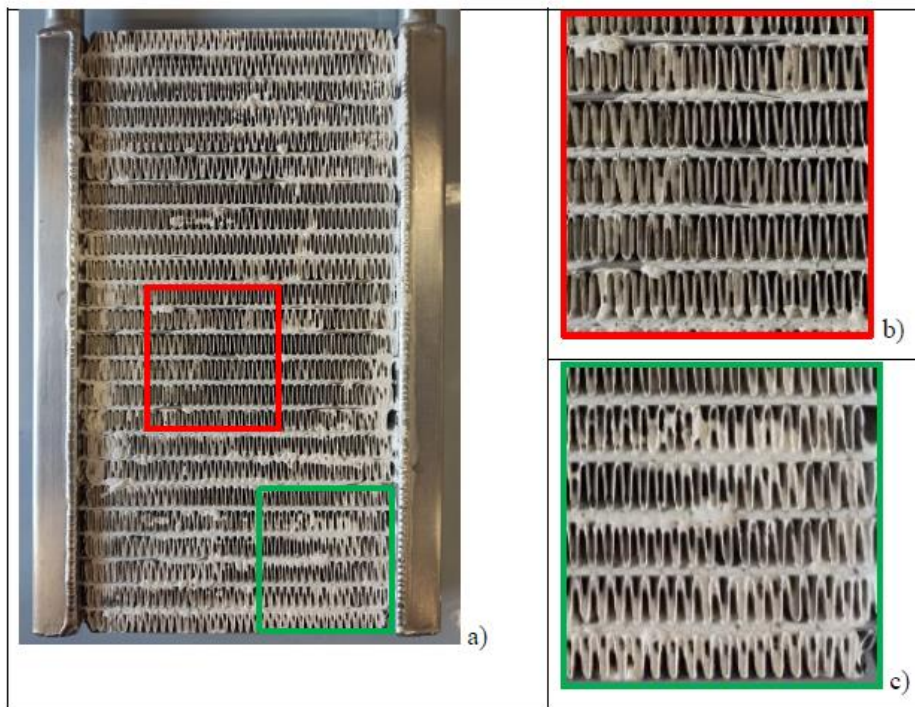
Figure 28 View of an exchanger coated with 90% by weight of SAPO zeolite (content by weight of anhydrous zeolite equal to 100g) and relative enlargements of a homogeneous zone (b - highlighted in red) and of a heterogeneous zone (c - highlighted in green)

3.4. Development and testing of components

Test Bench

To test the performance of the single heat exchanger/adsorber, a test station for adsorbers was built based on a single bed adsorption chiller at the laboratories of the "Nicola Giordano" Institute of Advanced Energy Technologies (I.T.A.E. C.N.R.). From the analysis of the results obtained from these tests it was possible to evaluate the potential of the exchanger and consequently to size the full-scale adsorber, identifying the optimal number of exchangers to be inserted in the adsorption chambers to meet the established cooling capacity.

In Figure 29 it is possible to view the test station created.

a)   b)

Figure 29 a) View of the test bench and b) single bed adsorption chiller.

The P&ID, shown in Figure 30, shows all the interconnections between the equipment, pipes, sensors and valves and their relative positions.
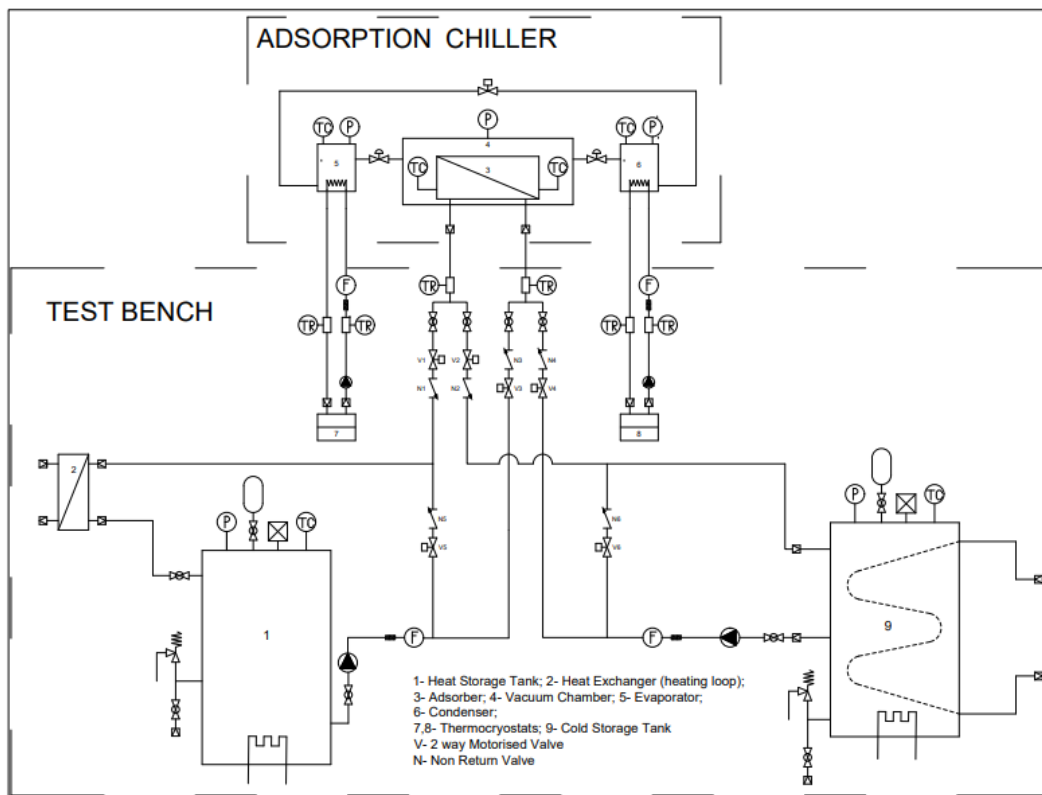
Figure 30 Final P&ID of the test station

A control software has been created in the LabVIEW environment to control and properly manage the system consisting of the test station and the single bed adsorption chiller. The latter allows you to monitor and acquire all the physical quantities useful for the operation of the machine. The software

in addition to measuring specific quantities, such as the temperatures and pressures inside the chambers, also serves to control the various operating modes, as well as to switch from one to the other thanks to the hydraulic valve system and the vacuum valves present in the system.

Figure 31 shows the screen of the synoptic and control panel created in LabVIEW and adapted for the prototype.

a)   b)
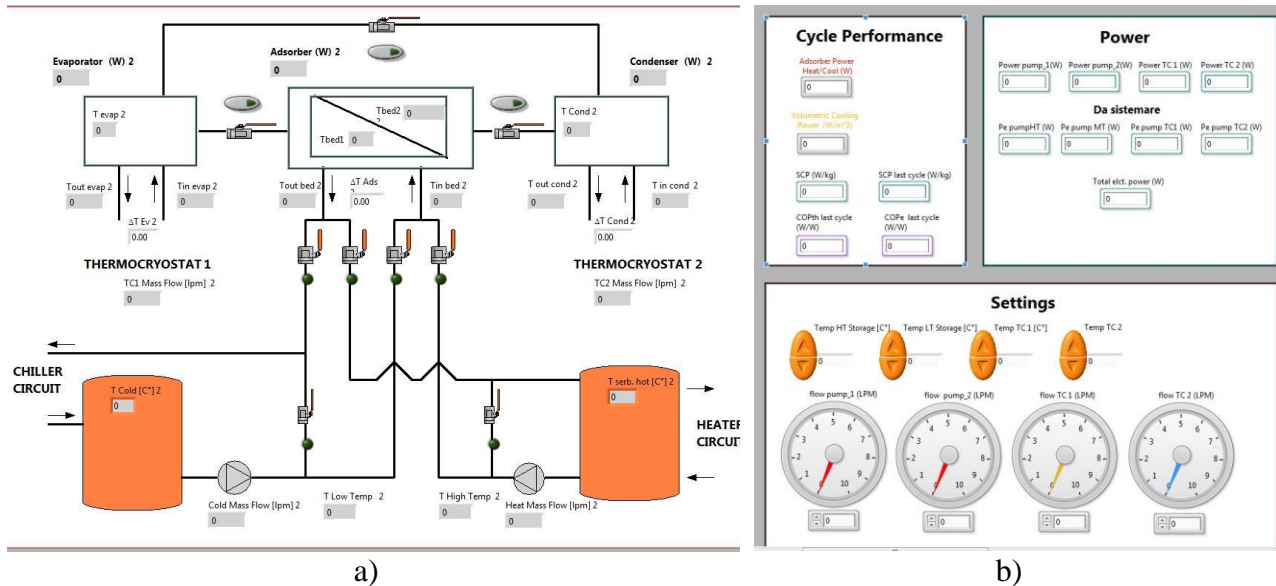
Figure 31 Synoptic and control panel of the software created in LabVIEW for the control of the machine

Design of the components

For the construction of the adsorbers, it was decided to use compact heat exchangers with flat finned aluminum tubes, characterized by dimensions and fins such as to ensure a high exchange density and at the same time a small footprint. To identify the type of heat exchangers to be used, the commercial models produced by FIRA S.p.a.[105] were considered and compared with each other and those produced by RC Racing [106], both shown in Figure 32.

a)   b)
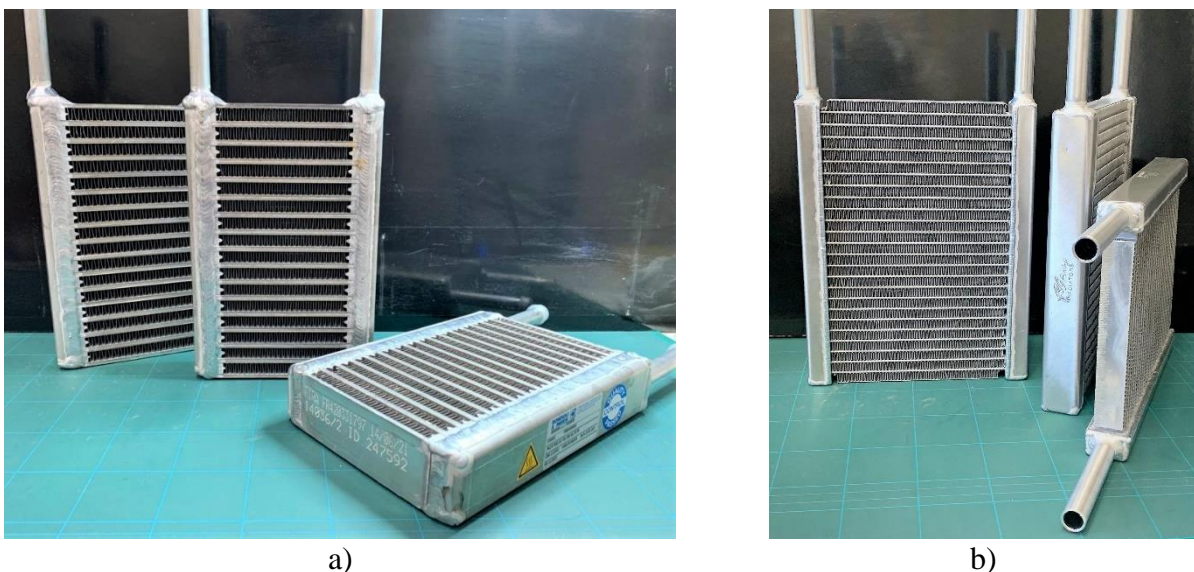
Figure 32 Heat exchangers manufactured by a) FIRA and b) RC Racing

The heat exchangers produced by FIRA are available in four different geometries. All 4 configurations have, with the same radiant mass, different geometric characteristics both in relation to the fins and to the internal channels of the exchangers.

Following an analysis of the technical specifications and performance of the two products, the exchangers produced by RC Racing were chosen.

After their purchase, they were entrusted to the University of Reggio Calabria to prepare them with zeolite foam, as shown in Figure 28.

The adsorbent zeolite foam has been inserted inside the fins of the exchangers to obtain high vapor permeability and maximize the performance of the zeolite, thus allowing an improvement in the performance of the adsorption chiller. Table 4 shows the weights of all the exchangers before and after the application of the zeolite coating.

Table 6 Features of the HExs

	HEx empty [g]	HEx coated at 80°C [g]	Coating [g]	Zeolite content (80%) [g]
HEx 1	668.6	779.6	111	88.8
HEx 2	661.7	783.4	121.7	97.4
HEx 3	665.9	789.6	123.7	99
HEx 4	672	802.8	130.8	104.6
HEx 5	666.5	814.9	148.4	118.7
HEx 6	664.4	798.2	133.8	107

The design of the adsorbent beds was carried out by evaluating the average power that the single heat exchanger is able to produce and considering the required project specifications. It was considered that a total of 6 heat exchangers will be required for the adsorbers. Subsequently, the vacuum chambers intended to contain the adsorbers were designed and, based on these, those relating to the condenser and the evaporator of the chiller. The chambers have been designed to be able to operate in sub-atmospheric pressure conditions and have been arranged in such a way as to obtain a compact configuration. The sizing of the adsorber chambers was carried out starting from the dimensions of the heat exchangers, trying to reduce the weight and total volume of the prototype, guaranteeing only the margin of space necessary for the assembly of the chambers.

The condenser and the evaporator, on the other hand, have been sized by calculating their heat exchange surface starting from the power produced by the adsorbent chambers.

The adsorbers will be made by providing three heat exchangers for each of them, while two each have been provided for the condenser and evaporator. The dimensions of the exchangers used for the adsorbers are indicated, together with those of the exchangers used in the condenser and evaporator, in Table 7 and Figure 33:

Table 7 Dimensions of the heat exchangers used

	Width [mm]	Height [mm]	Depht [mm]	Interaxis distance pipes[mm]	Diam. Pipes[mm]
HEx. Condenser	100/140	400	44/54	120	**16**
HEx. Adsorbers	160/200	250	22/42	180	**16**
HEx. Evaporator	160/200	400	22/42	180	**16**
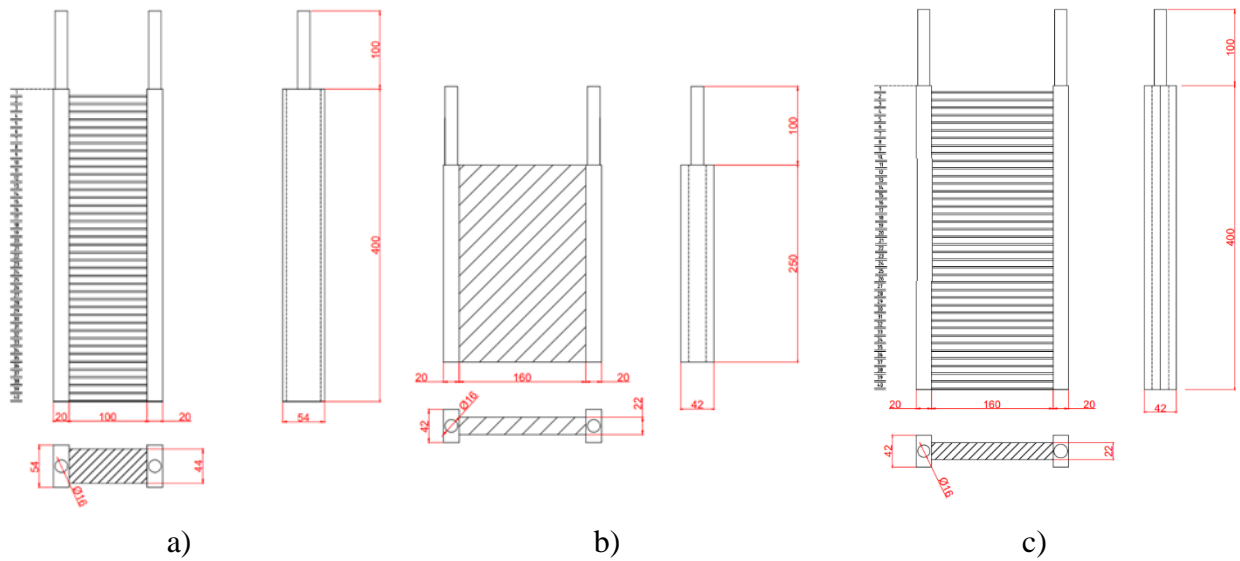
Figure 33 Dimensions of the exchangers in order from left to right respectively for a) condenser, b) absorber and c) evaporator.

3.5.   Design and manufacturing of the prototype

Once the dimensions of the heat exchangers were defined, the executive drawing of the adsorption chambers was made. The construction of the chambers, for which AISI 316 steel was chosen as the material, was entrusted to a workshop specialized in the production of vacuum components.
Figure 34 shows the side and front view of the overall layout of the adsorption chiller.

Condensatore

Comere per letti
adsorbenti

(A)   (B)

Evaporatore
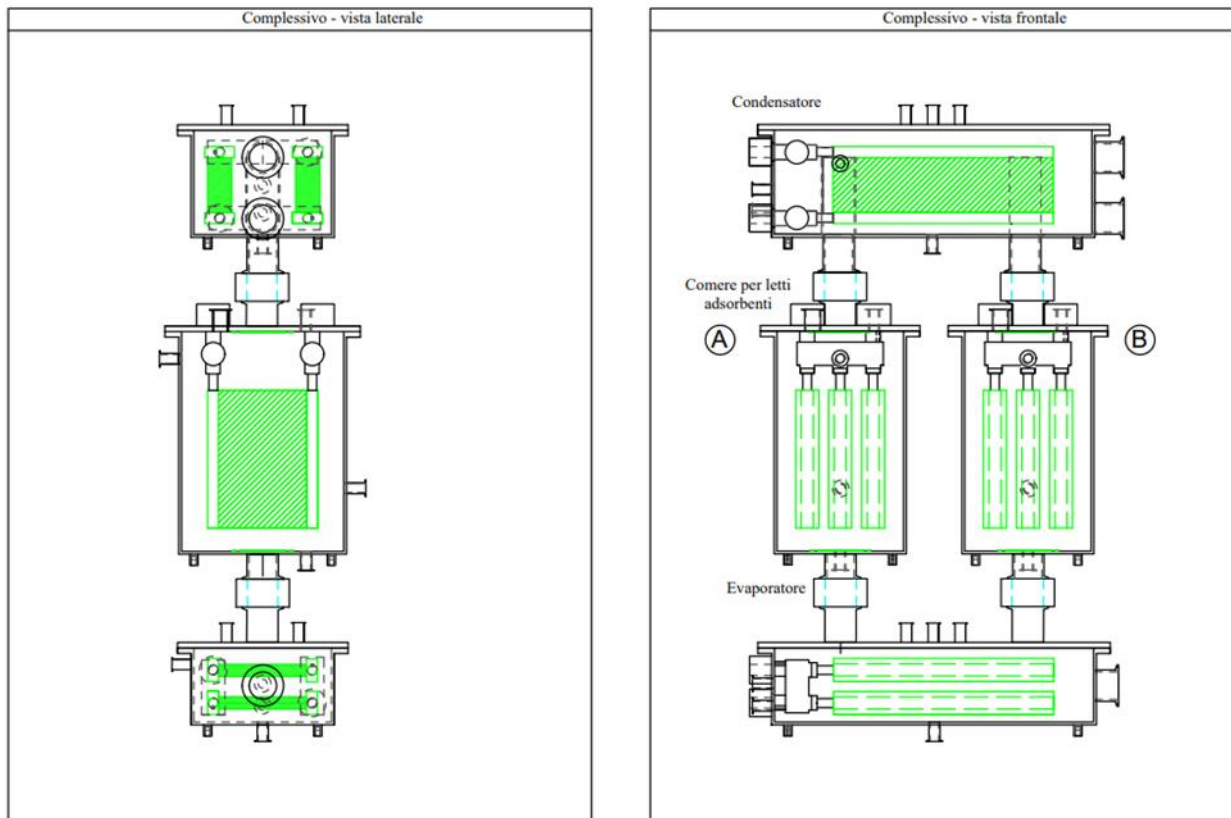
a)   b)

Figure 34 Side and front view of the designed chiller

After the design and construction phase of the vacuum chambers, the components necessary for the construction of the hydraulic and electrical circuits were selected, as well as the fundamental sensors for monitoring the functioning of the prototype.

Below are described step by step and in detail the main phases of the realization of the adsorption chiller.

The insulation of the chambers:
Considering that any heat losses could penalize the overall performance of the chiller, in order to thermally isolate the vacuum chambers from the external environment and work in stationary conditions, the insulation of the chambers was carried out. Figure 35 shows the chamber without insulation.

Figure 35 Chamber intended for making one of the two adsorbers before insulation.

The insulator is also equipped on one of the two sides with an adhesive tape to facilitate the insulation operation. Given the presence of the flanges, the insulation was cut and shaped according to the chambers by means of punches of different sizes. Once the desired shape was obtained, the thermal insulation was positioned on the vacuum chambers (Figure 36a-b).

a)   b)

Figure 36 Insulation of the rooms for the realization of the prototype

The insulation used is a flexible elastomeric foam having a thickness (s) of 1 cm and a thermal conductivity (λ) of 0.034W/mK.
It is possible to define the thermal resistance (R_i) of each layer of thickness (s_i) and conductivity thermal ($λi$) with the relation (3):

$$R_i = \frac{s_i}{\lambda_i} \tag{3}$$

The total exchange resistance R_{tot} is the sum of the thermal resistances determined so far:

$$R_{tot} = R_{int} + \sum R_i + R_{ext} \tag{4}$$

Where R$_{int}$ and R$_{ext}$ represent the surface thermal resistances.
The thermal transmittance U is calculated as (5):

$$U = \frac{1}{R_{tot}} \tag{5}$$

The heat flow through the chamber walls is calculated in (6):

$$\dot{Q} = U\,\Delta T \tag{6}$$

Where $\Delta T = (Tint - Text) = 15°C$
Table 8 resumes the benefit of the application of the insulation

Table 8 Comparison of thermal performance with/without insulation

	Without insulation	With Insulation
R$_{tot}$ **[m²K/W]**	0.536	2.056
U$_{tot}$ **[W/m²K]**	1.865	0.486
Q̇ **[W/m²]**	27.84	7,29

Adsorber chambers:
Once filled with the zeolite-based foam, the exchangers were mounted on the respective vacuum chambers by means of the hydraulic manifolds already described above. The mounting of the adsorbers on the manifolds of the vacuum chambers was carried out by means of straight brass fittings.

a)   b)

c)

Figure 37 a) and b) view of the idraulic connections and c) the superior flange

Given the vertical arrangement of the chambers, to avoid the passage of adsorbent material from the adsorbers to the evaporator located below, filters have been inserted on the lower communications flanges (DN 50). These were made by fixing squares of wire mesh inside the two adsorber chambers with specially made pins and 3 mm thick Teflon frames.

a)   b)

Figure 38 Application of the metal filters on the bottom of the adsorbers

In this way, the passage of material is avoided, guaranteeing the flow of steam through the meshes of the metal mesh.

- Condenser:

To optimize the spaces inside the condenser chamber, the two exchangers were arranged longitudinally. Between them, to prevent the liquid inside the condenser from ending up in the adsorber chambers, cylindrical bulkheads have been provided at the DN 50 connection flanges between the condenser and the adsorbers.

Figure 39 Positioning of the exchangers inside the condenser

Evaporator:

Inside the evaporator, the exchangers were instead arranged parallel to the lower surface of the chamber, again in order to optimize space.

Figure 40 Positioning of the exchangers inside the condenser

Hydraulic circuit:

For the operation and control of the two-bed adsorption system, a hydraulic circuit has been created capable of guaranteeing the various operating phases of the chiller prototype.

The test station used to test the prototype features three temperature lines:

• High temperature: to be connected to the adsorbers for the desorption phase.
• Medium temperature: to be connected to the condenser and adsorbers for the adsorption phase.
• Low temperature: to be connected to the evaporator.

The high temperature line and the medium temperature line can be identified within the hydraulic circuit that affects the adsorbers. The first is useful both for the desorption phase (connection between the adsorbers and the condenser) and for heating the bed, the second, on the other hand, is useful both for the adsorption phase (connection between the adsorbers and the evaporator) and for cool the bed. The next figure (Figure 41a) shows the P&I of the hydraulic system related to the adsorbers.

The various operating logics of the system have been implemented thanks to the installation within the hydraulic branches of two-way solenoid valves and ball valves with built-in BALLSTOP check valve. The latter have been inserted in series with the solenoid valves to ensure that the working fluid flows in a single direction.

Figure 41b shows the hydraulic branches made for the adsorbers that were mounted on the steel frame on which the prototype was made. Their fastening was achieved through the use of support collars, hooked to the frame thanks to threaded rivets.

a)   b)
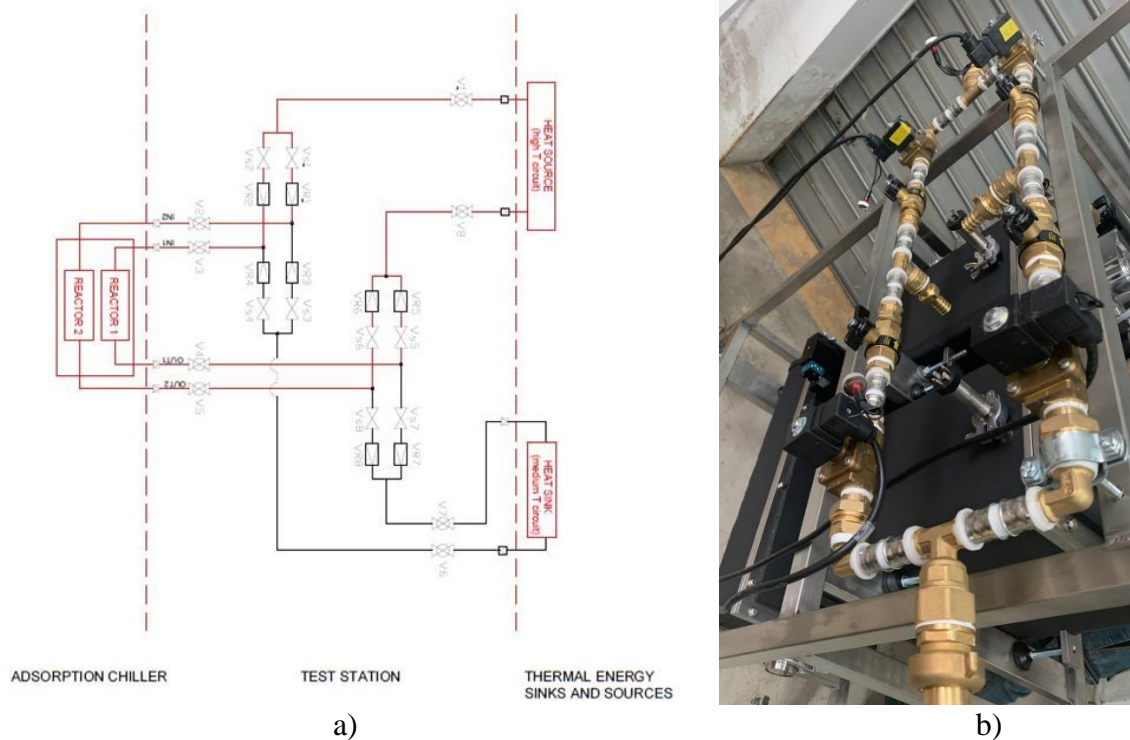
Figure 41 a) Layout and b) manufacturing of idraulic connections

- <u>Hydraulic water tightness</u>:

After the installation of the hydraulic branches, each chamber was subjected to hydraulic seal tests to avoid the risk of water leaks in the circuits. To manage and monitor the pressure values during the tightness tests, analogue pressure gauges and a hydraulic pump were used.

The water was introduced under pressure by activating the pump. The pressure was raised slowly and steadily until it reached a value higher than the operating pressures of the prototype. The hydraulic connection branches and the exchangers of the various chambers, after eliminating the air pockets present inside them, were put under pressure and left under observation for a couple of days to check the tightness of the joints and the various fittings present.

a)   b)

Figure 42 Tests of water tightness

- <u>Assembly of the chambers</u>:

After carrying out the hydraulic tests, the four insulated chambers were placed on a support frame made of stainless steel. The section of steel used was chosen once the weight of the 4 chambers necessary for the construction of the prototype was known. The overall weight was increased by 20% to create a frame that did not show any mechanical failure.

The configuration of the frame has been conceived in such a way as to limit the overall dimensions to a minimum and at the same time allow the assembly of the 4 vacuum chambers and the connected circuits (electrical and hydraulic). The frame is equipped with 4 wheels, sized according to the overall weight of the prototype, to facilitate movement within the laboratory.

a)   b)

c)

Figure 43 Manufacturing of the frame support and positioning of the chambers

Once their position has been identified, threaded feet have been inserted on the various chambers, to adjust their alignment for the purpose of their coupling, facilitating final assembly. During the assembly phase, the 4 Gate Valves KF DN 50 were inserted, useful for connecting the adsorbers with evaporator and condenser. Pneumatic operated valves produced by VAT have been selected, shown in Figure 44. The connections between the connections of the KF vacuum components and the flanges of the chambers were made through the use of O-rings (equipped with a centering ring) and clamping.

a)

b)
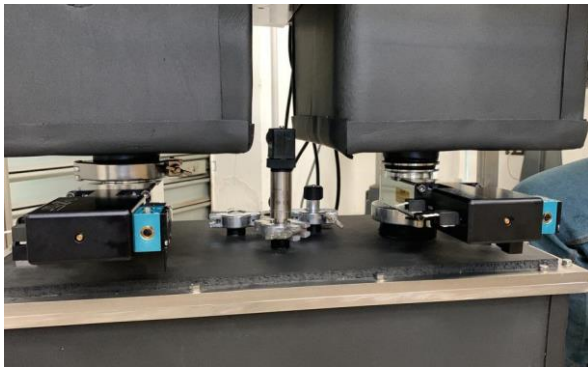
c)

d)

Figure 44 Connections between the chambers

Once the vacuum connections between the various chambers of the prototype were made, the hydraulic branches made to connect the prototype to the test station were also fixed to the frame in order to make the prototype compact and reduce the overall dimensions to a minimum. Likewise, the branches of the vacuum circuit were also fixed to the frame. The final configuration of the assembled prototype is shown in Figure 45:
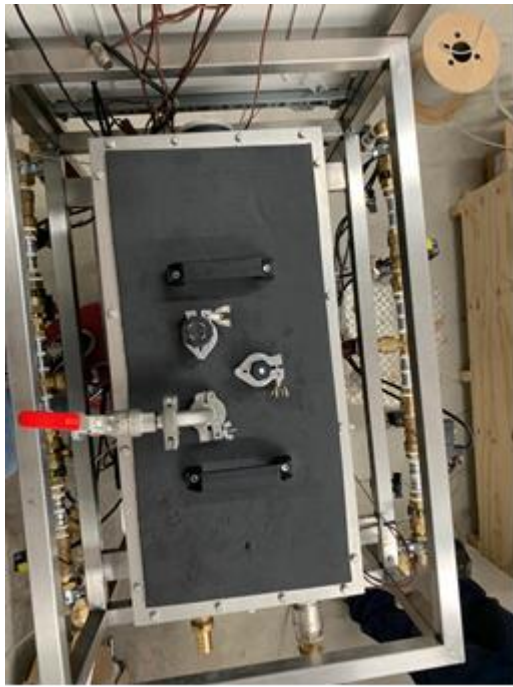
a)

b)

Figure 45 Final configuration of the assembled prototype

- Sensors:

Each prototype chamber is equipped with a pressure sensor and a temperature sensor. An Edwards transducer (model ASG2-1000) with a KF16 flange connection was chosen as the pressure sensor. It is a robust and corrosion resistant membrane meter that provides accurate, gas independent measurements from 1000 mbar to 1 mbar. This device allows accurate measurement with an accuracy of $\pm$ 0.2 full scale and 0.1% full scale stability. The selected thermocouples are of type T and class 1, with AISI 321 stainless steel sheath and have a diameter of 0.5 mm and a length of 150 mm. These were connected to the chambers through flanged bushings and shown in Figure 46 before being installed.

a)

b)
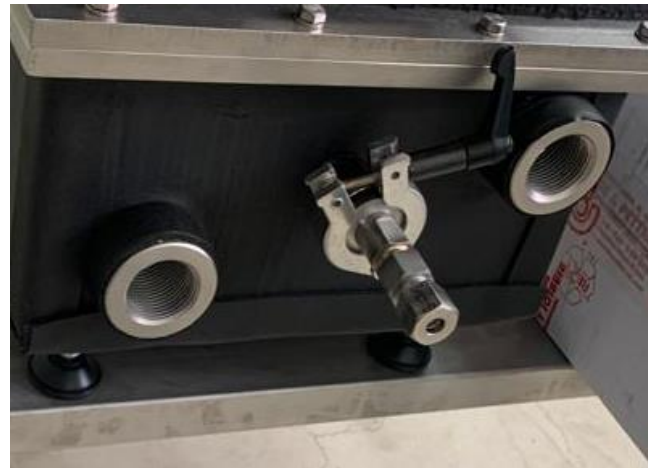
<center>c)   d)</center>

Figure 46 a) Pressure transducer, b) Termocouple c) and d) TC welded on KF25 flange

To monitor the temperature inside the adsorbers, thermocouples with double channel feedthroughs welded on KF25 vacuum flanges were used instead. In addition, to monitor the water temperature inside the hydraulic circuit, thermocouples have been inserted at each hydraulic connection of the four chambers, both at the inlets and outlets.

- Realization of electrical connections:
To allow automatic operation of the adsorption machine. an electrical panel has been built (shown in Figure 47). In the electrical panel there are a series of switches that govern the power supply of the vacuum and hydraulic valves. In addition, a string of National Instruments modules has been inserted to read the main monitored quantities. In particular, the modules used are:

• 1 A/I module: useful for reading the pressure inside the 4 vacuum chambers.
• 1 Tc module: useful for reading the various thermocouples installed inside the machine.
• 4 relay modules: useful for controlling all the valves inside the prototype.

The electrical panel, for safety reasons, has been equipped with a magneto thermic switch and an earth circuit to protect users during the test phase.
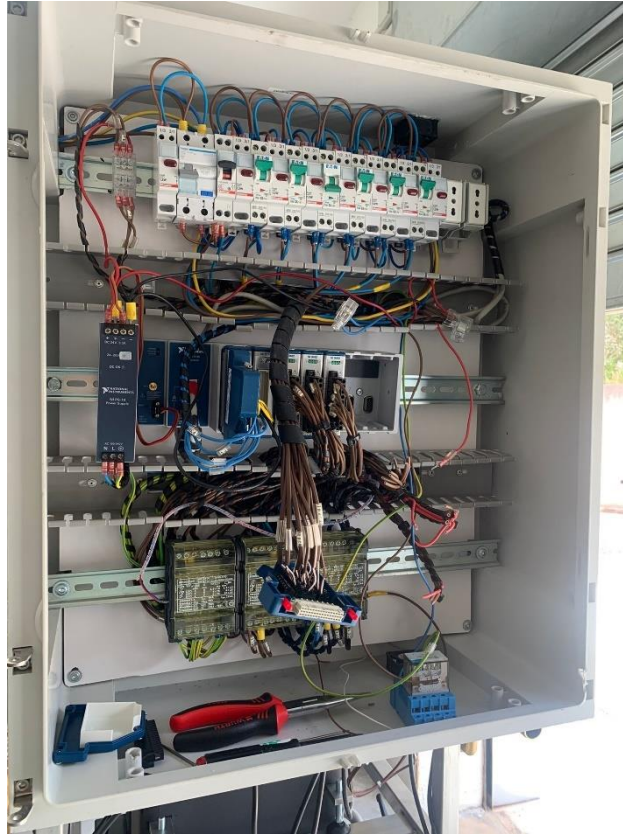
Figure 47 Prototype electrical panel

3.6.   Testing and characterization of the chiller

Full scale Test Bench for thermally driven chillers

The full scale testing rig used is specifically made to set the various temperature levels necessary for the operation of components, as described in [107][108]. It is used to evaluate the performance of the chiller. It primarily consists of heat sources and sinks connected to storages, including a 1.5 m^3 water storage that is continuously heated by a 70 kW heater (HT storage), a 1 m^3 water storage that is connected to an air-cooled chiller with a nominal power of 63 kW (LT storage), and a 0.75 m^3 storage that is filled with a 44.5 wt% water/glycol mixture and has 5 immersed resistances (33 kW each) in order to control the temperature. The HT circuit of the sorption unit is heated by the hot water storage tank; by combining the water in the hot and cold storages (HT and LT) with a motorized 3-way valve coupled to a PID regulator able to set the desired temperature level, the cooling water for the MT circuit of the sorption unit is produced. The goal set temperature can be maintained in the HT and MT circuits' inlet circuits thanks to this real-time regulation.

Variable speed pumps are fitted to control the operating flow rates in each circuit, and all the pipes are thermally insulated. Through a control panel created in the LabVIEW® environment, the monitoring and controlling system is operated. The following sensors are installed in the testing apparatus:

- Type "T" thermocouples with Class 1 tolerances for the measure of all the temperatures in the inlet/outlet pipes of every circuit and in the storages.
- Magnetic flow meters MVM250-PA with 1% of reading accuracy for the measure of all the flow rates.

- Piezoresistive differential pressure meter, to calculate pressure drops inside the circuits of the heat pumps/chillers under testing.
- Electric energy meter SINEAX DM5S with Class 1 tolerances for the measure of electric input delivered to the chillers.

The evaluated uncertainty under the examined settings is in the range of 5-8% according to the metrological characteristics of the used sensors, while the one on the EER is in the range of 2-4%. The layout of the testing bench is shown in Figure 48.
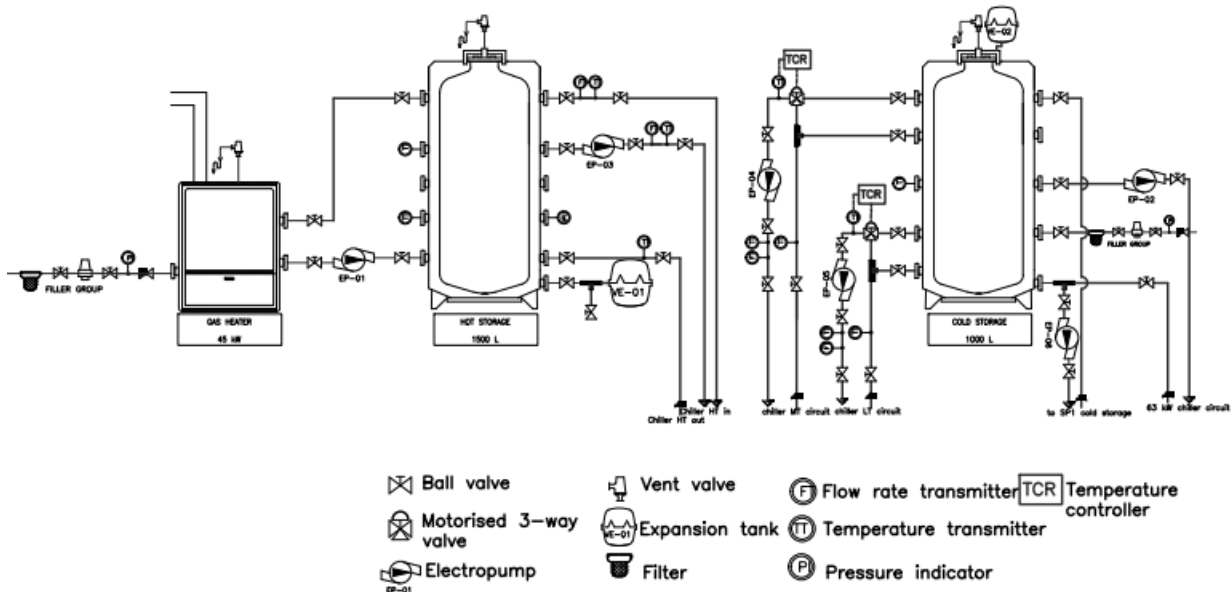
Figure 48 Layout of the test bench for thermally driven chillers located at CNR ITAE

Methodology

Once the prototype was connected, several tests were carried out to simulate the real operating conditions. The operating conditions depends on:

- The evaporator temperature: which simulates the environment to be cooled.
- The condenser temperature: which simulates the external environment suitable for heat dissipation.
- The cycle times.
- The flow rates of the three heat sources (high, medium, and low temperature).

The purpose of this variation is to find the optimal operating conditions to maximize the performance of the chiller. The most important parameter that will be evaluated will be the the average cooling capacity that will be produced by the evaporator.

The three temperature stages of an adsorption thermodynamic cycle, low temperature (T_L), middle temperature (T_M), and high temperature (T_H), represent the testing conditions, which are summarized in Table 9. They specifically relate to the typical entrance temperature of the heat transfer fluids flowing into the chiller's key parts.

Table 9 Testing conditions

Parameter	Measurement Unit	Value
Evaporation Temperature	°C	7/10/15
Heating Source Temperature	°C	70/75/80/85/90
Condensation temperature	°C	38
Total Cycle Time	min	5/10/15/20
Adsorption/Desorption duration ratio		1/2/3

The cycle time (s) is calculated as the product of the adsorption and desorption steps, and the overall cycle duration is produced by adding the durations of the two isosteric phases, which can be estimated both 20 s for isosteric heating and cooling, to the cycle time. The ratio (R) between the length of the adsorption and desorption processes is also reported in Table 9.

The performances of the adsorption chiller are assessed using the following metrics:

- Volumetric Cooling Power (VCP, kW/m³), as ratio between the useful cooling effect, the adsorber volume (V) and the total cycle time as shown in (7):

$$VCP = \frac{\sum_{ads} m_e c_p (T_{in-e} - T_{out-e}) \Delta T}{V \, \tau_{cycle}} \qquad (7)$$

- Specific Cooling Power (SCP, W/kg), as ratio between the useful cooling effect, the adsorbent mass (M) and the total cycle time as shown in (8):

$$SCP = \frac{\sum_{ads} m_e c_p (T_{in-e} - T_{out-e}) \Delta T}{M \, \tau_{cycle}} \qquad (8)$$

- Coefficient of Performance (COP), calculated as ratio between the cooling effect generated in the evaporator during the adsorption step (Q_e) and the amount of thermal energy supplied for isosteric heating and desorption phases (Q_h), as in shown in (9):

$$COP = \frac{Q_e}{Q_h} = \frac{\sum_{ads} m_e c_p (T_{in-e} - T_{out-e}) \Delta T}{\sum_{iso+des} m_h c_p (T_{in-a} - T_{out-a}) \Delta T} \qquad (9)$$

According to the theory of measurement uncertainty, the usual experimental error is computed using the extended uncertainty approach where the effect of the desired confidence level as well as the composed error contribution of each measuring equipment (u) are taken into account [109].
The extended uncertainty (U_Q) for the thermal energy (Q) supplied to the adsorber or the evaporator is calculated in (10), where the contributions of the flow meters (u_m) and the temperature sensors are clearly visible ($u_{\Delta T}$).
A gaussian distribution of errors was taken into account for each contribution, and the coverage factor (k) is chosen to achieve a confidence level of 99%.

$$U_Q = Q \, k \, \sqrt{\frac{u_m^2}{m^2} + \frac{u_{\Delta T}^2}{\Delta T^2}} \qquad (10)$$

Preliminary Results

The characterization campaign, carried out within the Project REGIONE SICILIA-PO FESR2014 Future Innovative Ship for Sicilian routes (FISHIPS), is planned on 2023 according to the project schedule and it's not included in this doctoral thesis. However, the preliminary activity is currently on going. Figure 49 shows the chiller installed in the laboratory of CNR ITAE to the full-scale test bench. The data resulted from the full characterization of the chiller will be used as a performance map to determine the best way to balance efficiency and power density for naval applications but it's also suitable for residential use.

Figure 49 Prototype connected to the full scale test bench

Different types of tests can be carried out on the prototype, varying the testing conditions described in Table 9.

In order to achieve the preliminary results of the characterization campaign, the first tests were carried out by setting the following temperatures:

• High temperature source: 90 °C;
• Medium temperature well (simulates the temperature of sea water): 28 °C;
• Low temperature source (simulates the environment to be cooled): 15 °C.

The tests were carried out by varying the cycle time and keeping the flow rate of the three temperature sources constant. The results relating to the Cooling Power for the temperature conditions 90°C/28°C/15°C are shown in Figure 50.

The maximum cooling capacity occurs for a cycle time equal to 5 min where the average cooling capacity value is 0,8 kW with a COP of 0,37. To the left of the peak, by further reducing the cycle time, the cycle power decreases as the adsorption phases (phases in which the useful effect is produced) are too short.
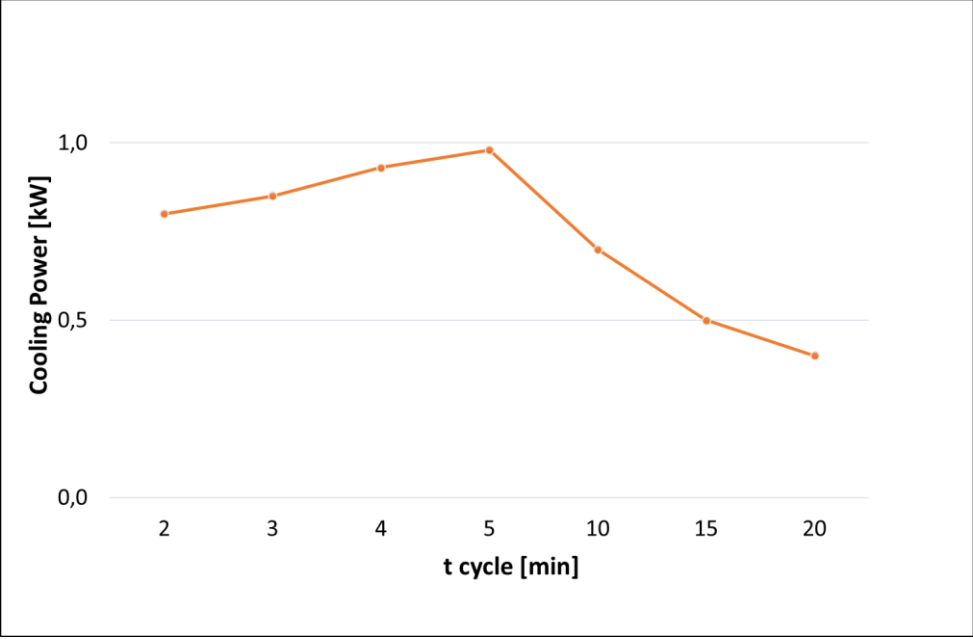
Figure 50 Cooling capacity vs the cycle time at 90/28/15 testing conditions

4. CCHP MODELLING (UNIBO-CNR ITAE)

The study of the novel solar driven Combined Cooling, Heating and Power (CCHP) system has been carried out during the first two years of PhD activity. In particular, the system is composed of a 60 m^2 flat plate solar thermal collectors' field, a 10 kW$_e$ photovoltaic plant, a 2 m^3 Thermal Energy Storage (TES), a 3 kW$_e$ micro-Organic Rankine Cycle (micro-ORC) prototype, a 4.4 kWc thermally driven Adsorption Chiller (AC) coupled with a 6 kW$_c$ auxiliary Heat Pump (HP). It has been conceived for residential applications and has been integrated with a real bioclimatic nearly zero energy building (NZEB). The building-plant system has been modelled and studied for three Italian locations, spread along the peninsula, with three different climates, Messina, Milano and Rome. An energy, environmental and economic analysis has been carried out. Within the activity of the third year, a commercial hybrid chiller has been modelled and integrated in the CCHP layout instead the adsorption prototype. The TRNSYS transient simulation software (TRNSYS version 18.00.0019) was selected to simulate the performance of the tri-generation plant. TRNSYS library has a wide range of TYPEs for the simulation of most of the energy system components while the experimental AC and ORC have been customized specifically. The AC prototype has been modelled in TRNSYS environment through a performances map created using the experimental data of the characterization while a specific subroutine for the ORC unit has been customized in Matlab.

In the next paragraphs, all the system subunits have been described in detail and, at least, the final model is presented.

ORC description

The μ-ORC test bench considered for this study is the one already presented and characterized in [110]. The system was realized by the Italian company StarEngine and it is conceived for being applied in the residential sector wherever a heat source temperature between 60 °C and 90 °C is available. Briefly, it consists of a recuperated cycle running with R134a and driven by a piston expander prototype, rated for a maximum power output of 3 kW [111]. The other main components are two brazed plate heat exchangers as evaporator and recuperator, a shell and tube condenser and an external gear pump. The expander is rigidly coupled with a permanent magnet generator, whose three-phase output line is connected to a variable resistive load. The condenser is fed with tap water that is stored in a cold tank and circulated with a centrifugal pump. However, future analysis will be also performed with an air condenser (already
available at the laboratory), as this can be more suitable to be implemented in a domestic facility.

The controlled variables of the test bench are:
- the hot and cold water temperature;
- the hot and cold water flow rate;
- the feed pump rotating frequency, which affects the working fluid flow rate and, consequently, the evaporating pressure of the Rankine cycle;
- the number of electric loads actually connected to the generator, which determines the value of the equivalent load impedance and has an influence on the expander torque and rotating frequency.

Hot water temperature is controllable by means of the electro-resistance of the boiler and by mixing the water with a colder stream in a three-way valve. Cold water temperature can be modified in a certain range using a compression chiller integrated in the cooling line. The hot and cold water flow rate can be regulated in the range 1-2.6 l/s by switching the pump mode and by partially closing the valves in the water circuits. The number of loads connected to the generator is adjustable by step of

600 W up to 3000 W of nominal power to dissipate. For this study, a constant value of the number of loads has been considered.

The previous work of Bianchi et al. [110] described the full experimental characterization of the system behavior in the range of hot source temperature between 65 °C and 85 °C, varying by step the feed pump rotating frequency and thus the working fluid flow rate and evaporation pressure. A selection of the experimental data obtained during the test campaign has been applied here for implementing the ORC sub-model and validating the results of the integrated tri-generation model.

a)   b)
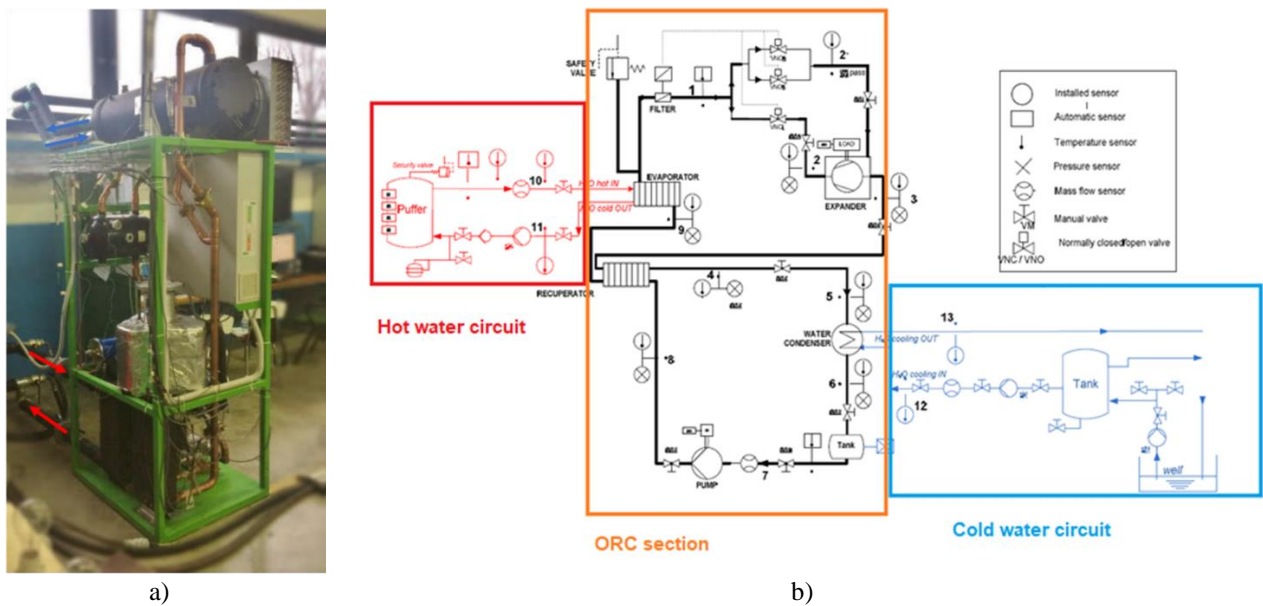
Figure 51 a) View and b) Schematic of the ORC prototype

AC description

The adsorptive chiller, designed and realized at CNR-ITAE, shown in Figure 52, has an architecture with 3 adsorbers connected, by pneumatic vacuum valves, to a single evaporator and condenser. The main features are summarized in Table 10.
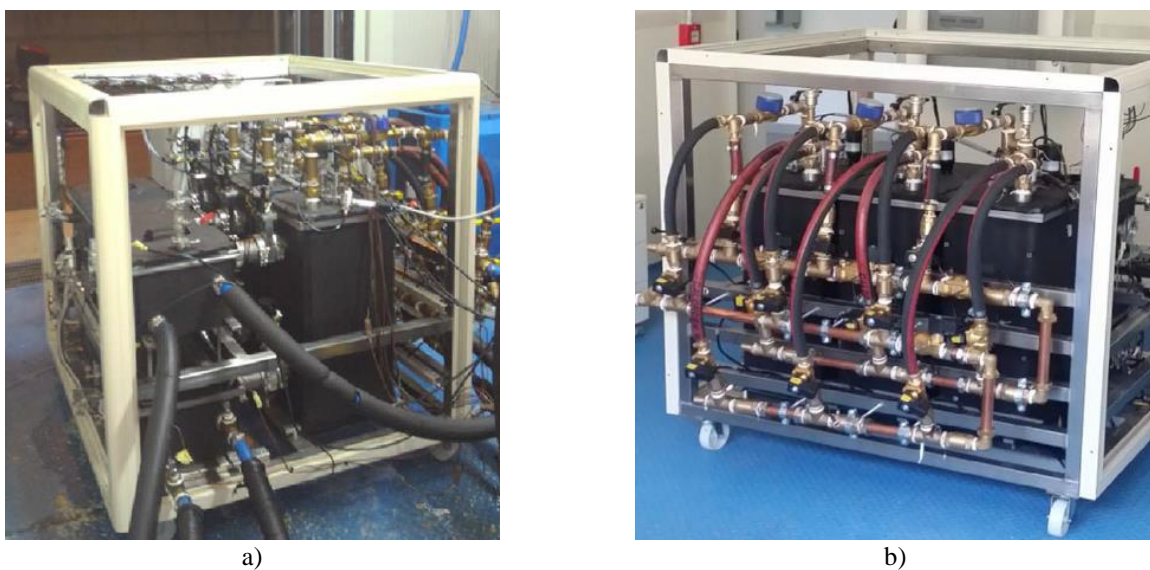

a)   b)

Figure 52 Views of the adsorptive chiller prototype.

69

Table 10 Main features of the adsorption chiller

Dimensions [mm]	$860 \times 790 \times 690$	Adsorbent material N°1: coating	Mitsubishi AQSOA FAM Z02
Volume [m^3]	0.47	Adsorbent material N°2: grains	Microporous Silica Gel
Weight [kg]	270	Nominal average cooling power [kW]	4.4
Nominal COP	0.35	Nominal volumetric cooling power [kW/m3]	9.36

The chiller's volume and weight are 0.47 m^3 and 270 kg respectively and it is able to deliver an Average Cooling Power (ACP) of 4.4 kW under nominal boundary conditions (TH = 90 °C, TL = 18 °C and TM = 25 °C) with a Volumetric Cooling Power (VCP) of 9.36 kW/m^3 and COP 0.35. The selection of the most appropriate HEx layout has been carried out to have high specific heat transfer surface area [cm^2/cm^3], to be compact, lightweight and to be able to host a good amount of sorbent material. All these constraints are required to obtain high value of cooling power density. The adsorbers' manufacturing was based on customized aluminum finned flat tubes heat exchangers, since this layout demonstrated to be highly performing. The complete description of the adsorption chiller can be found in [112,113]. HExs have triangular louvered fins spaced 360 fins/m and a specific heat transfer area of 15.49 cm^2/cm^3. The adsorption chiller prototype has been designed with an innovative architecture with three adsorbers connected to a single evaporator and condenser as shown in Figure 53.
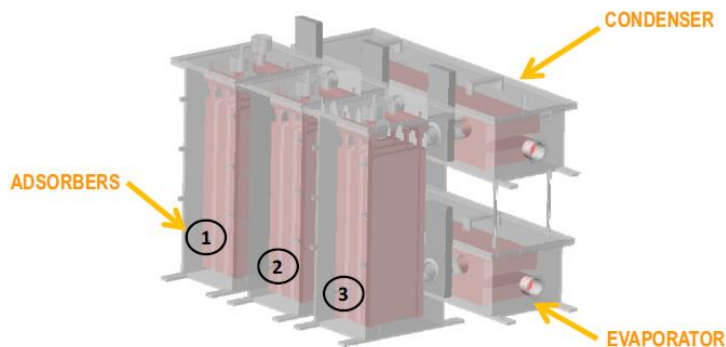
Figure 53 Schematic layout of a 3-Adsorbers based chiller

4.1. Identification of the Best Layout

Figure 54 shows the concept layout of the integrated ORC-AC system in tri-generative arrangement. A solar field is supposed to be the primary source, nevertheless the plant is able to work with any low temperature power supply. In this configuration, the water heated in the solar collectors is used to feed, in cascade, the ORC cycle and the adsorption chiller. The system would be also equipped with a thermal energy storage (TES) used as heat buffer, which is provided with electro-resistances as supplementary thermal source. In this section, the main features of the implemented model are depicted.
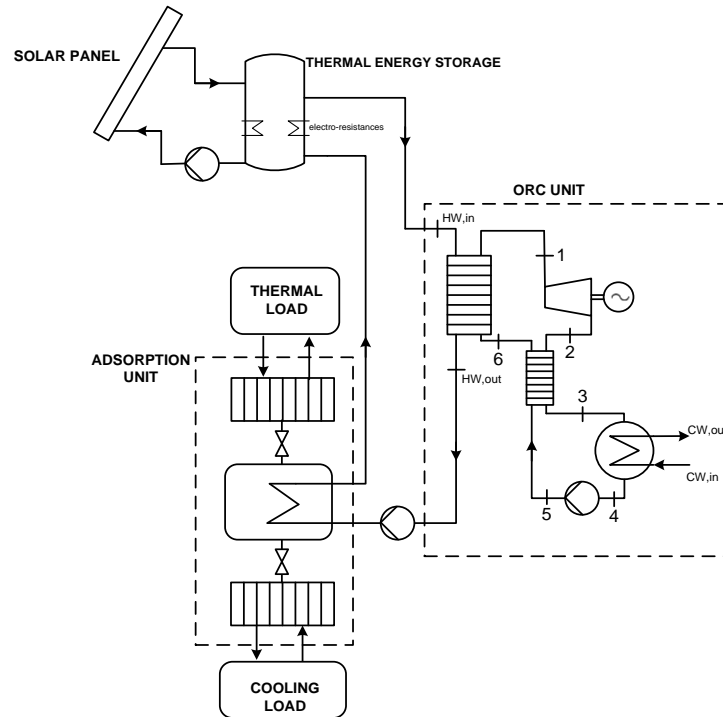
Figure 54 Micro-CCHP concept layout.

Figure 55 shows the concept layout of the coupled ORC-AC system in tri-generative arrangement. The prototype plant under analysis consists of: a 60 m^2 flat plate solar thermal collectors plant, a 10 kW$_e$ photovoltaic solar plant, a 3 kW$_e$ Organic Rankine Cycle power unit, a 4.4 kW$_c$ adsorption chiller and an auxiliary 6 kW$_c$ reversible heat pump. A 2 m^3 thermal energy storage (TES) is used as heat buffer, which is provided with electro-resistances as supplementary thermal source, and fan coils as terminals for the distribution system. The size of the auxiliary Heat Pump is chosen on the basis of the thermal and cooling loads of the buildings. If the thermal power available from AC system is not enough to meet the load, additional heating or cooling power is supplied by the Heat Pump with a nominal seasonal COP$_h$ of 4, during the heating period, and a nominal seasonal COP$_c$ of 3 in the cooling period. Flow rates of ORC-AC and distribution circuits have been fixed depending on the location, thus on the variability of thermal and cooling demands of the building. Considering available technologies, the hydronic air-conditioning system is the most suitable and it was considered for both heating and cooling periods for the proposed application. The input water temperature to the fan coils has been fixed at 40 °C and 10 °C during heating and cooling period respectively. The features of the main components of the system are summarized in Table 11:

Table 11 Characteristics of the main components

Design specifications	Value
Solar collectors area	60 m^2
PV peak electric power	10 kW$_e$
ORC system nominal capacity	3 kW$_e$
Adsorption chiller nominal capacity	4.4 kW$_c$
Heat Pump nominal capacity	6 kW$_c$
TES volume	2 m^3
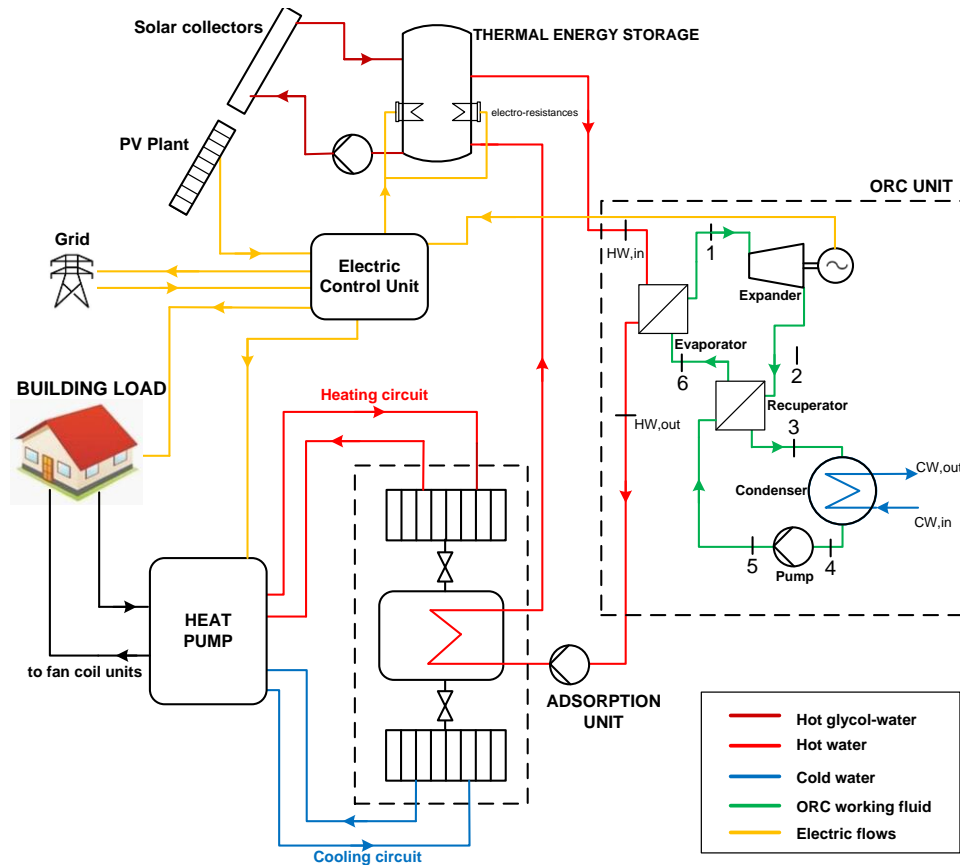
Figure 55 Schematic layout of the Micro CCHP system and Electric power flow diagram

The thermal solar field heats up the water stored in a 2 m^3 thermal energy storages interacting with ORC-AC circuit. The circulation pump of the solar circuit is operated when the outlet water temperature from solar collectors exceeds the tank average temperature.

The tank is insulated with a material of thermal loss coefficient equal to 0.54 W/m^2 K. The water inside TES is kept over 68 °C during CCHP operating hours to supply the ORC unit. If the temperature inside the TES is lower than 68 °C, also the auxiliary electric resistances are turned on in order to keep the water temperature in the required range. The water, leaving the ORC, supplies the AC unit in series with the ORC. During winter, the AC works as a heat pump to keep the supply temperature to the fan coils at 40 °C. In summer, the chiller mode is turned on to keep the supply temperature to the fan coils at 10 °C. The operating strategy is based on following the thermal loads while electrical energy available from ORC and PV plant is mainly used to meet the electric load of the building and to drive the auxiliaries of the plant. If the electric production is not enough to meet the load, the needed part is drawn from the grid. Instead, if the "production" exceeds the demand, the surplus electricity is fed into grid. The electronic control unit works to balance the electric power.

4.2. Dynamic Model of The ORC Subsection

The ORC sub-model has been developed in MATLAB environment considering an empirical approach using empirical correlations derived from data obtained by experimental characterization. It performs basic balances for each iteration in order to obtain the power exchanged for each component. The thermodynamic properties of the working fluid in every section of the circuit are calculated by means of the open source CoolProp library [110] using temperature and pressure as input values.

The following assumptions have been considered for the ORC sub-model:
- heat losses at heat exchangers are neglected
- pressure losses along the circuit are neglected
- constant value of temperature difference at evaporator hot terminal (ΔT_{app})
- constant value of recuperator effectiveness (ε_{REC})
- constant value of pinch-point temperature difference at condenser (ΔT_{PP})
- constant value of expander electro-mechanical efficiency ($\eta_{m,el}$)

The assumption of a constant ΔT_{app} is justified by the high difference between the flow rates of organic fluid and hot water (which is at least one order of magnitude higher), resulting in a value of ΔT_{app} quite low and with little fluctuations; low variations have been observed also on recuperator effectiveness in most conditions during experiments; finally, the constant ΔT_{PP} value is consistent with experimental data in the range of operating conditions here analyzed.

The input variables depend on the operating conditions of the ORC system and of the cooling system and are:
- hot water temperature at the evaporator inlet, $T_{HW,I}$;
- cold water temperature at the condenser inlet, $T_{CW,I}$;
- hot and cold water flow rate, $\dot{V}_{HW}$, $\dot{V}_{CW}$
- superheating degree at expander inlet, ΔT_{SH}.

Among the operating range considered for this system, the superheating temperature remains very close to the hot source temperature, due to the considerable difference between the flow rate of the water and the one of the working fluid (one order of magnitude). Therefore, once the hot source temperature is fixed and the superheating degree at the expander inlet is imposed by design, the evaporation pressure (p_{ev}) is fully determined as function of the evaporation temperature, which is computed by (12).
The input value of superheating degree is used to obtain the evaporation pressure of the cycle, according to (11):

$$p_{ev} = p_{sat}(T_1 - \Delta T_{SH}) \tag{11}$$

where the saturation pressure is calculated via Coolprop and the difference $T_1 - \Delta T_{SH}$ corresponds to the evaporation temperature. Superheating degree is a design variable, whose value should be taken low in order to exploit the whole available pressure difference, but high enough to avoid wet expansion problems.
Similarly, the condensing pressure (p_{cond}) is obtained as function of the condensing temperature, which is calculated using the pinch point temperature difference between condensing working fluid

and cooling water outlet, ΔT_{PP} (13). Please refer to Figure 54 for the enumeration of the cycle's sections.

$$T_{ev} = T_1 - \Delta T_{SH} \tag{12}$$

$$T_{cond} = T_{CW,out} + \Delta T_{PP} \tag{13}$$

The relation between the evaporation pressure and the working fluid mass flow rate ($\dot{m}_{ORC}$), which is affected by the feed-pump rotating speed, is assumed linear and it is obtained by interpolating the calibration points shown in Figure 56.
The working fluid mass flow rate is computed using an empirical correlation, reported in (14), as function of the evaporation pressure.

$$\dot{m}_{ORC} = \frac{p_{ev} - a}{b} \tag{14}$$

where the empirical coefficients a and b have been obtained from experimental trend of mass flow rate. All the above-mentioned constant quantities are collected in Table 12.

Table 12 Constant parameters for ORC submodel

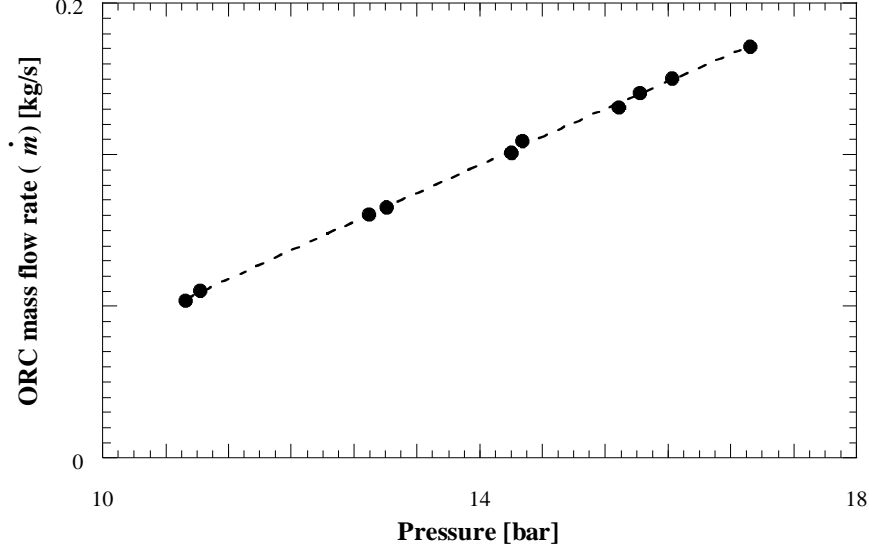| Parameter	Value
ΔT_{app}	2 °C
ε_{REC}	0.65
ΔT_{PP}	4 °C
ΔT_{SH}	3 °C
$\eta_{m,el}$	0.9
a	7.015
b	72.35

Figure 56 ORC mass flow rate versus evaporation pressure [110]

The expander behavior is taken into account by means of the total expander efficiency (η_{exp}), defined by (15), where η_{exp} is decomposed in two elements: the isentropic thermal efficiency ($\eta_{\text{is,th}}$) and the electromechanical efficiency (η_{em}), that accounts for the frictions and for the generator losses. This formula is also used to calculate the enthalpy value at the expander outlet.

$$\eta_{exp} = \eta_{is,th} \cdot \eta_{em} = \frac{(h_1 - h_2)}{(h_1 - h_{2,is})} \cdot \frac{\dot{W}_{exp,el}}{\dot{W}_{exp,th}} \tag{15}$$

The subscripts *el* and *th* refer to electrical and thermodynamic power, respectively. The thermodynamic states in the different sections of the layout are determined by the thermal balances over the system components, using the recuperator effectiveness, ε_{REC}, and thermal power, $\dot{Q}_{REC}$, expressed by (16)(17):

$$\varepsilon_{REC} = \frac{T_6 - T_5}{T_2 - T_5} \tag{16}$$

$$\dot{Q}_{REC} = \dot{m}_{ORC} \cdot (h_2 - h_3) = \dot{m}_{ORC} \cdot (h_6 - h_5) \tag{17}$$

The electrical power output is then obtained as the product of working fluid mass flow rate, enthalpy difference over the expander and the expander electromechanical efficiency. The hot water temperature at the evaporator outlet, which is used as heat input to the adsorption chiller placed at the bottom of the μ-ORC, is estimated through the thermal balance applied to the evaporator. In order to evaluate the net efficiency of the system, the electrical power absorbed by the feed pump must be subtracted to the expander power output. Pump electric consumption ($\dot{W}_{pump,el}$) is calculated by dividing the hydraulic power by the pump total efficiency, which is expressed by (18). The term ρ_{ORC} represents the density of the working fluid evaluated at the pump suction.

75

$$\eta_{pump} = \frac{\dot{m}_{ORC}/\rho_{ORC} \cdot (p_{ev} - p_{cond})}{\dot{W}_{pump,el}} \qquad (18)$$

The expander thermodynamic power ($P_{t,exp}$) and the pump consumption (P_{Pump}) are calculated according to (19) and (20).

$$P_{t,exp} = \dot{m}_{ORC} \cdot (h_1 - h_2) \qquad (19)$$

$$P_{Pump} = \dot{m}_{ORC} \cdot (h_5 - h_4) \qquad (20)$$

where h_n is the enthalpy at the point n of the cycle.

The net electric power produced is then obtained as the difference of the expander electrical power output ($P_{el,exp}$) and the pump electric consumption ($P_{el,Pump}$) and is expressed by (21):

$$P_{el,ORC} = P_{el,exp} - P_{el,Pump} = P_{el,exp} \cdot \eta_{m,el} - P_{Pump}/\eta_{m,el} \qquad (21)$$

Where $\eta_{m,el}$ is the electro-mechanical efficiency.

4.3. Dynamic Model of The AC Subsection

The adsorption chiller has been modelled using Type 909 relying on user-provided performance data files obtained in a previous full characterization of the prototype carried out at ITAE labs [114]. A specific test bench has been devoted for thermally driven chillers and results highlighted the influence of the temperature difference between condenser (T_M) and evaporator (T_L) on the overall performance of the chiller. An average cooling power (ACP) between 3.4 and 4.4 kW, and a volumetric cooling power (VCP) of 7.25–9.36 kW/m^3, with a COP of 0.3–0.35, have been calculated from results at working conditions of T_H = 90 °C, T_L = 15÷18 °C and T_M = 25÷28 °C [115]. Thus, normalized capacity and COP ratios of the Type have been obtained as a function of the hot water inlet temperature, the cooling water inlet temperature and the chilled water inlet temperature.
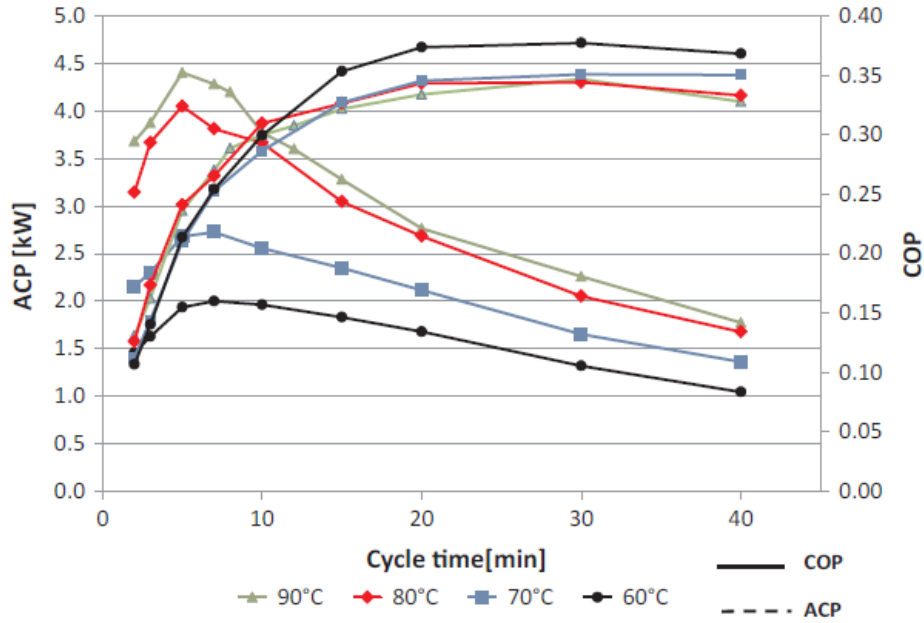
Figure 57 Experimental performance data obtained by a full characterization at CNR-ITAE[114]

The cooling power delivered from the chiller is equal to (22):

$$Q_c = COP_c \cdot Q_H \qquad (22)$$

where COP_c is the coefficient of performance at current conditions during the cooling season and Q_H is the energy provided to the chiller by the inlet hot water flow stream.
The heating power delivered from the chiller is equal to Eq. (23):

$$Q_h = COP_h \cdot Q_H \qquad (23)$$

where COP_h is the coefficient of performance at current conditions during the heating season.
The outlet water temperature to fan coils has been fixed at 40°C during the hot season varying the chilled water mass flow rate as a function of the COP and the inlet cooling temperature from fan coils.

4.4.   First CCHP Model

The proposed system consists of 80 m² flat-plate type solar field, a 3m³ storage tank, a 3 kWe ORC plant and a 4,4 kWc adsorption chiller. The main components of the model are: Type 1b for the solar field; Type 4 for the Thermal Energy Storage (TES), Type 155 for calling Matlab subroutine, Type 909 for the adsorption chiller. Type 909, a standard AC, was modified integrating a map of performances obtained by an experimental characterization activity fully described in [107]. Weather data in terms of solar radiation and environment temperature have been taken from Meteonorm database on an hourly basis. The TRNSYS model of the tri-generation system, shown in Figure 58, was simulated using experimental performance data obtained by a full characterization of ORC and AC prototypes, at University of Bologna and at CNR - ITAE respectively [116].
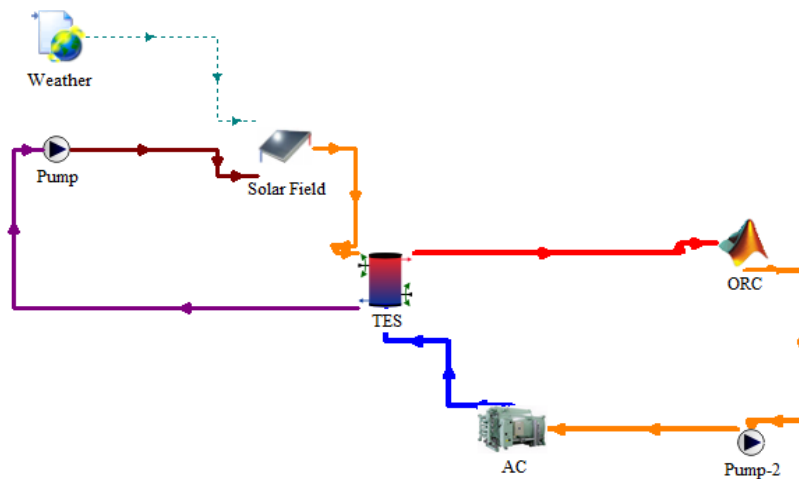
Figure 58 First CCHP model

4.5. NZEB Model

The studied building, shown in Figure 59, is a single-family detached house located in Linguaglossa, a small town in the Metropolitan City Area of Catania (South Italy), with a net conditioned area of around 251.2 m^2. The surface to volume ratio (S/V) is equal to 0.13. The location is in the D climatic zone with heating degree days (HDD) equal to 1760, according to classification specified by the Italian legislative decree 412/93 [117]. The winter period is considered from November 1st to April 15th. It has been designed as a bioclimatic house in a way that allows occupants to benefit from natural advantages of its site and, nowadays, it's a typical example of high efficiency building characterized by maximum thermal comfort and energy saving.

a)   b)

Figure 59 Building (a) North and (b) South views [118]

Location	Linguaglossa (CT)
Minimum annual temperature [°C]	7,6
Maximum annual temperature [°C]	23,4
Mean annual temperature [°C]	15
Latitude	37° 50' N
Longitude	15° 08' E
Climatic Zone	D
Degree days	1,760

The solutions selected for **building envelope** takes into account new interesting wooden made materials. The value of wood as a building material from the point of view being ecological is easily understood: it comes from one source, the trees, whose renewal, whose reproducibility, is determined by essentially from the only energy source, to date, which can be defined as unlimited, the sun.
A wooden building is relatively quick and easy to build; it has excellent structural performance, even excellent in terms of seismic resistance; fire behavior, contrary to what many think, predictable and even better, in some ways yes, compared to other non-combustible building materials; an element high durability, obviously in the face of correct design. From the point of view of economic feasibility, one of the main advantages of the building process is the reduction of construction times education. The choice of the cross-layered load-bearing panel system allows you to build the entire building mainly dry, with simple tools and small hardware. The comparison of the unit cost
of this system with that of a reinforced concrete structure to and brick solves the agon of economy to the advantage of wood.

The external and internal walls are made of a larch slab insulated with an air layer and mineral wool wood panels. They also are covered with gypsum fiberboards. Figure 60a and Table 13 describe layers of the external walls in terms of different parameters ("s" thickness, "λ" thermal conductivity, "cp" specific heat, "r" density) and the total transmittance is calculated. Roof and floor are wooden made too and insulated with woodfibre boards. Figure 61a and Table 15 describe roof properties while main features of the floor are shown in Figure 61b and Table 16.
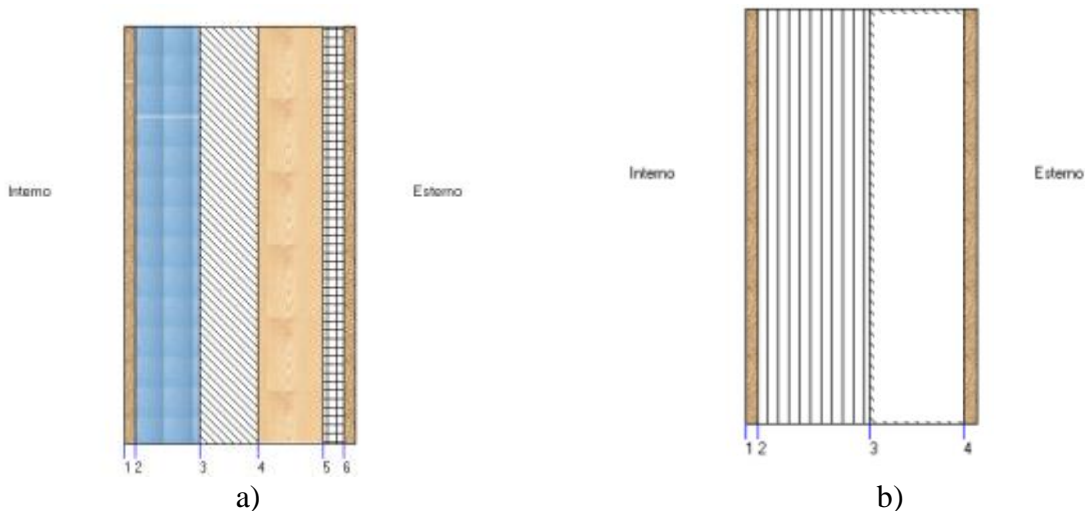
a)   b)

Figure 60 Layers of a) External and b) Internal walls

Table 13 External Walls layers characteristics

Material	s [m]	λ [W/mK]	r [kg/m^3]	c [kJ/kgK]
FERMACELL	0,13	0,32	1150	1,1
Air layer	0,08	0,51	1,3	1
Larch	0,071	0,15	627	1,6
PAVATherm	0,08	0,04	150	2,7
ERACLIT	0,025	0,9	400	1,55
Plaster	0,015	0,7	1400	0
Total Transmittance [W/m^{2}K]	**0,318**			

Table 14 Internal Walls layers characteristics

Material	s [m]	λ [W/mK]	r [kg/m^3]	c [kJ/kgK]
FERMACELL	0,125	0,32	1150	1,1
Larch	0,071	0,15	627	1,6
Air layer	0,04	0,1	1300	1
FERMACELL	0,125	0,32	1150	1,1
Total Transmittance [W/m^{2}K]	**1,22**			

a)   b)
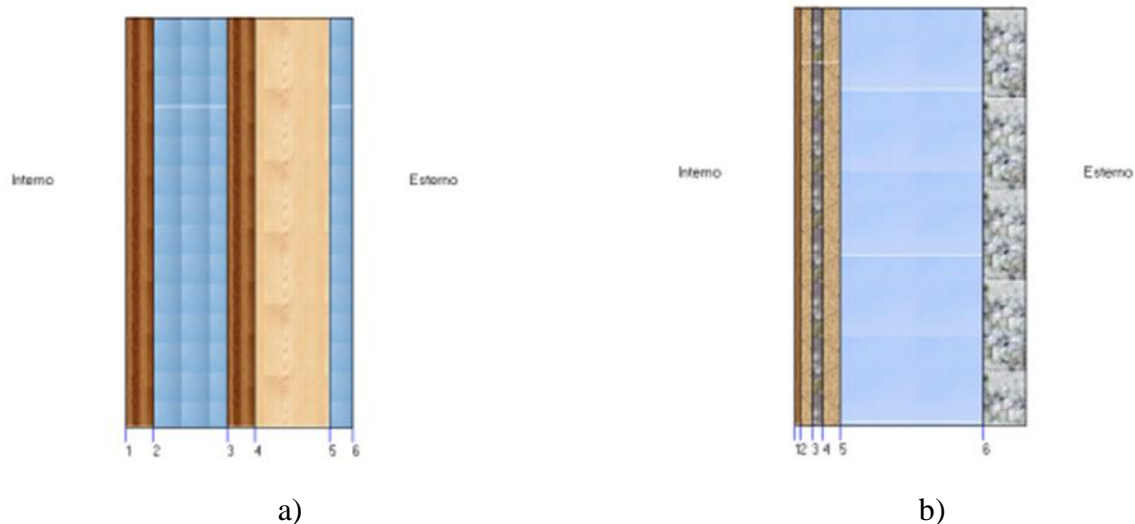
Figure 61 a) Roof and b) Floor

Table 15 Roof properties

Material	s [m]	λ [W/mK]	r [kg/m³]	c [kJ/kgK]
Larch	0,03	0,15	627	1,6
Air layer	0,08	0,42	1300	1
Larch	0,03	0,15	627	1,6
PAVATherm	0,08	0,04	150	2,7
Air layer	0,025	0,1	1300	1
Covering	0,001	110	7100	0
Total Transmittance [W/m²K]	**0,332**			

Table 16 Floor properties

Material	s [m]	λ [W/mK]	r [kg/m³]	c [kJ/kgK]
Larch	0,02	0,15	627	1,6
Screed	0,04	0,9	1800	0
PAVATherm	0,04	0,04	150	2,7
Screed	0,06	0,9	1800	0
Crawl space	0,5	0,026	1,3	0
Subfloor screed	0,15	0,19	400	0
Total Transmittance [W/m²K]	**0,047**			

The building is provided with different-sized windows with double-glazing low emissivity and aluminum frames with thermal break. Thermal properties of windows are described below in Table 17, while Table 18 reports thermal properties for different opaque surfaces of the building envelope.

Table 17 Thermo-physical parameters for windows

Table 17 Thermo-physical parameters for windows

Parameter	Value
Glass thermal transmittance, U_g	2.320 W/m^{2}K
Frame thermal transmittance, U_f	3.7 W/m^{2}K
Thermal resistance of the shading, $R_{shading}$	0.3 m^{2}K/W
Total thermal transmittance, U_{tot}	1.479 W/m^{2}K

Table 18 Main characteristics of the building envelope

Building	Total transmittance [W/m^{2}K]	Thickness [m]
External walls	0.318	0.4
Internal walls	1.22	0.36
Roof	0.332	0.25
Floor	0.047	0.81
Windows	1.479	-

The building was realized by means of Trnsys3d for SketchUp [119] and imported as 3D model into the Type 56, as shown in Figure 62.

The building volume was divided into four thermal zones according to classifications and requirements specified by the Standard UNI 10339 [120]. The Air Change Rate has been fixed to 0.5 h^{-1}, in order to guarantee the required comfort conditions fixed by the standard UNI EN 15251 [121]. The dwelling is occupied by a family with four people (two working adults and two young students). Standardized factors of ASHRAE Standard 90.1-2004 have been used for occupancy and plug-loads that were modelled with typical schedules for residential kind of use [122]. LED lamps (50–90 lm/W) have been chosen to model light equipment. Indeed, an hydronic air-conditioning system have been chosen, according to TABULA WebTool [123] reporting the most diffused technologies in the last years used in residential buildings. Type 600 have been used to model 2-pipe fan coils able to deliver heating and cooling energy to the air stream inside the building.
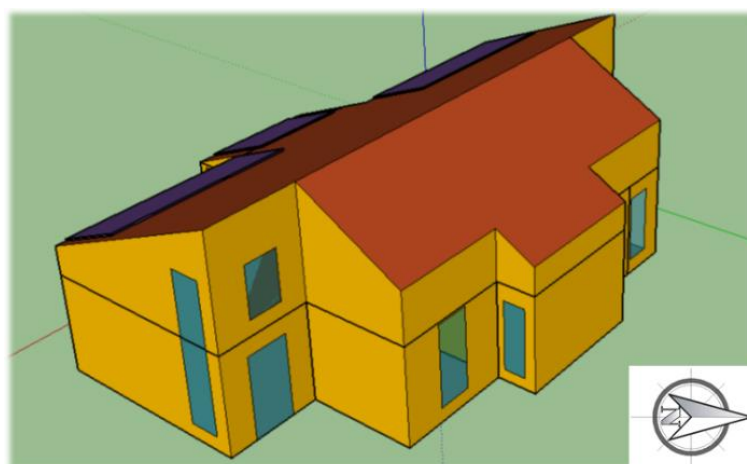

Figure 62 Building 3D model

The building performances have been simulated in Messina, Rome and Milan. These cities are characterized by different climatic conditions well representing the variability of Italian climates. Weather data and reference heating periods for each location are showed in Table 19.

During the winter, the heating set point temperature is 20 °C with an Upper dead band of 2 °C and a Lower dead band of -0.5 °C. The daily heating schedule is characterized by the reference zone and in particular:

ZONE B: 8 hours from 8.00 to 10:00, from 17:00 to 23:00.

ZONE D: 12 hours from 8.00 to 14:00, from 17:00 to 23:00.

ZONE E: 14 hours from 8.00 to 16:00, from 17:00 to 23:00

Table 19 Weather data and reference heating periods for each location

Location	Messina	Rome	Milan
Minimum annual temperature [°C]	11.8	7.7	1.9
Maximum annual temperature [°C]	26.5	24.4	23.8
Mean annual temperature [°C]	18.5	15.7	13.1
Latitude	38°11'39"48 N	41°53′35″N	45°28′01″N
Longitude	15°33'1"80 E	12°28′58″E	9°11′24″E
Climatic Zone	B	D	E
Heating Period	1 December-31 March	1 November-15 April	15 October-15 April
Degree days	707	1415	2404

In summer, the house is cooled at 26 °C with an Upper dead band of 2 °C and a Lower dead band of -3 °C. The same daily schedule is considered for all locations because a reference daily cooling period isn't defined by Italian law. Therefore, the dwelling is cooled from 8:00 to 20:00 every day during the cooling season.

4.6.   Integrated Building-Plant CCHP Model

The CCHP plant and the building, described in the previous section, have been implemented in TRNSYS 18 dynamic simulation software [124], as shown in Figure 63.
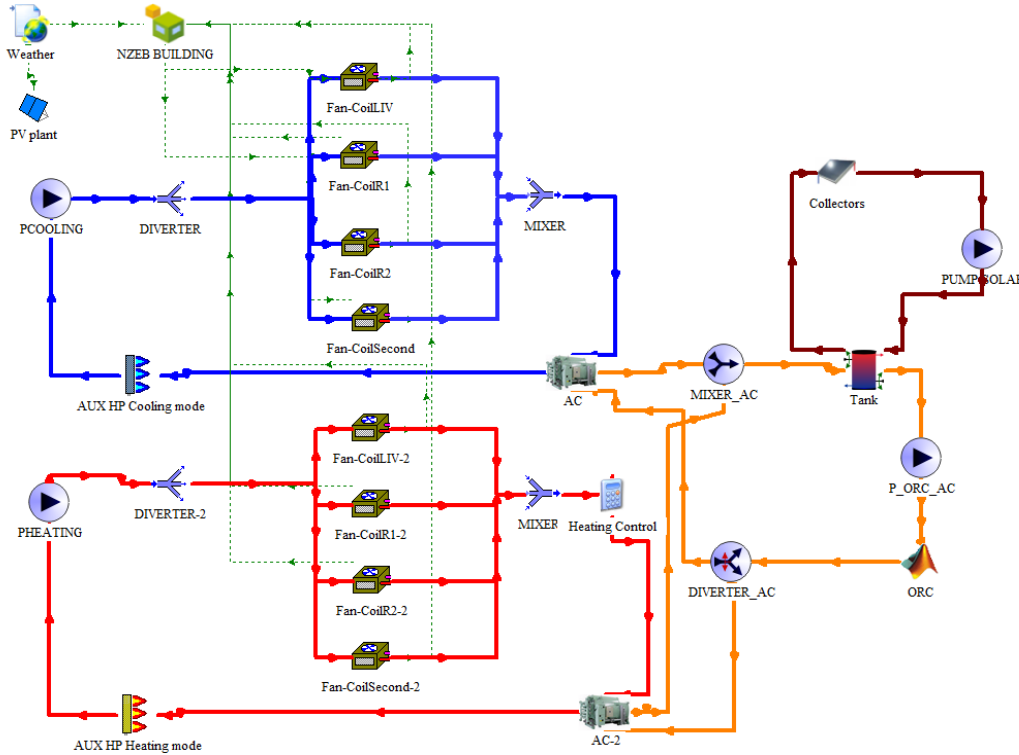

Figure 63 Scheme of the TRNSYS model

TRNSYS simulations are constructed by connecting individual component models (known as Types) together into a complete model. Many components of the CCHP system have been modelled by means of existing Types from TRNSYS libraries while a specific subroutine for the ORC unit has been customized in Matlab [125]. The main components of the model are: Type 56 for the Building; Type 1b for the solar field; Type 194 for the PV plant; Type 4 for the Thermal Energy Storage (TES); Type 155 for calling Matlab subroutine; Type 909 for the adsorption chiller; Types 1246 and 659 for the Heat Pump during cooling and heating mode respectively; Type 600 for the Fan-coils. Types used for the model of ORC and AC units were modified with User-provide files that reply to experimental performance data obtained by a full characterization of the real ORC and AC prototypes, at University of Bologna and at CNR - ITAE respectively. Weather data in terms of solar radiation and ambient temperature have been taken from Meteonorm database [126] on an hourly basis.

Type 1 models a flat plate solar thermal collector using a quadratic efficiency equation from the well-known Hottel-Whillier equation:

$$\eta_{FPC} = a_0 - a_1 \frac{(\Delta T)}{I_T} - a_2 \frac{(\Delta T)^2}{I_T} \qquad (24)$$

84

where a_0, a_1 and a_2 are three coefficients which depend on the type and model of the collectors; I_T is the Irradiation and ΔT is equal to the difference between the collector inlet temperature (T_i) and the ambient temperature (T_a).

The thermal power delivered to the fluid is described by (25):

$$Q_{FPC} = \dot{m}_{FPC} \cdot c_p \cdot \left(T_{FPC,out} - T_{FPC,in}\right) \qquad (25)$$

The water flow rate of the solar circuit $\dot{m}_{FPC}$ has been set at 100 kg/h and the pump is controlled by a thermostat. The controller turns on the pump only when the outlet temperature from solar collectors ($T_{FPC,out}$) is higher than the average temperature of the TES (T_{TES}).

Photovoltaic panels have been modelled by means of Type 194 using parameters and reference conditions from commercial modules.

4.7.   Future Strategies of Optimization - Integration of a Commercial Hybrid Chiller

Different innovative technologies are available for reducing the CO_2 emissions of the industrial sector through energy efficient processes.

The possibility of integrating thermal and electric chillers into hybrid units is thus one of the popular options put forth in recent years by manufacturers and in the scientific literature.

The chillers produced by FAHRENHEIT as commercial machines were considered. FAHRENHEIT is a company, based in Germany, founded in 2002 as a spin-off of the Fraunhofer Institute for Solar Energy Systems (ISE). The company, a pioneer in adsorption technology, designs and manufactures advanced and innovative adsorption cooling devices to provide energy efficient cooling solutions [127].

FAHRENHEIT adsorption chillers can be used wherever residual heat is available, leading to a new dimension of energy efficiency as they do not rely on electricity for cooling. Its chillers and adsorption modules find application in industrial manufacturing, air conditioning, data centers, solar cooling and various other applications. They can also lead to significant savings in energy and CO_2 emissions in mobile applications such as automobiles and transport cooling systems.

The commercial hybrid chiller considered consists of two units connected in parallel: an adsorption unit employing silica gel/water as working pair and a compression chiller using R134A as the refrigerant. It consists of a "parallel" connection of a thermally driven unit and a traditional vapour compression unit with a total cooling capacity of 46.7kW and a COP_{th} up to 0.65. The connection between them is made through a hydraulic circuit. The useful effect to the user is the cooling effect at the evaporator of the compression chiller (ChT circuit). The integrated compression chiller covers peak and bridge loads and provides additional fault tolerance and optimal energy efficiency. The nominal adsorption and compression cooling capacities achieve values up to 16.7kW and 30kW respectively with a total cooling capacity of 46.7kW and a COP_{th} up to 0.65.

The additional compressor has the rated capacities:

P=30.0 kW at LT_out 16°C
P=25.4 kW at LT_out 12°C
P=21.3 kW at LT_out 7°C

The schematic of the hybrid chiller is presented in Figure 64.
It allows to exploit the benefits and main peculiarities of both components:

- sorption systems have electricity consumption extremely low and need limited maintenance. Use of Water as a refrigerant with 0 GWP and 0 Ozone Depletion Potential (ODP)
- electric chillers offer high precision in temperature regulation and fast response to temperature fluctuations.
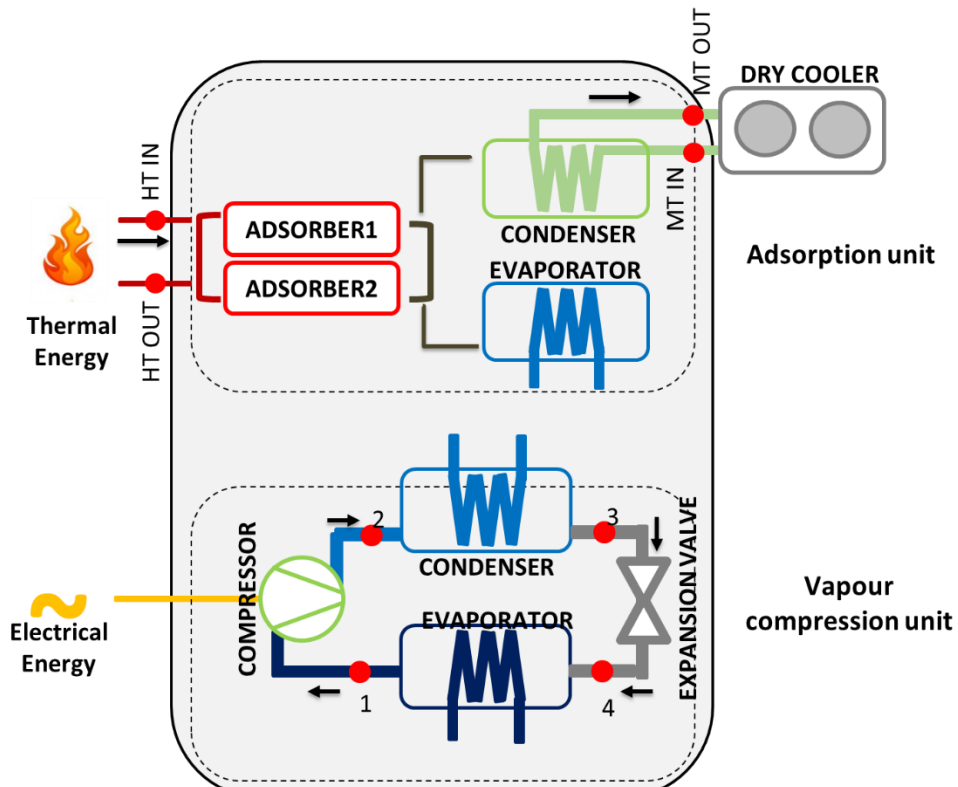

Figure 64 Schematic of the Hybrid chiller

5. RESULTS

5.1.   Results first CCHP Model

This section presents the most representative results obtained from the experimental setup and the simulations. Due to the large quantity of results and variables, the analysis is focused on a thermodynamic analysis, efficiency and energy flows. The performance of the plants has been evaluated in terms of electric and thermal energy production on a monthly and yearly basis. Furthermore, the following efficiencies have been assessed:

- the solar field efficiency (η_{SF}), defined as the ratio between the output power from the solar collector and the input solar power;
- the electric efficiency of the ORC ($\eta_{ORC,el}$), defined as the ratio between the output electric power and the inlet thermal power to the ORC;
- the coefficient of performance (COP), i.e. the ratio between the cooling power and the input thermal power of the adsorption chiller.
- the global efficiency (η_{global}), defined as the ratio between the useful electric, thermal, cooling energy and the inlet thermal energy from the solar field and the auxiliary heater.

As expected, the output energy from the 80 m^2 solar field, located in Rome, is much lower than the input solar radiation, while it is equal to the input energy to the TES because of the plant configuration. Consequently, the mean annual conversion efficiency of the solar field is about 33%. Figure 65 report the monthly energy balance of the plant. As reported, the load is fixed and increase in summer season with the useful solar energy achieving the best performances.
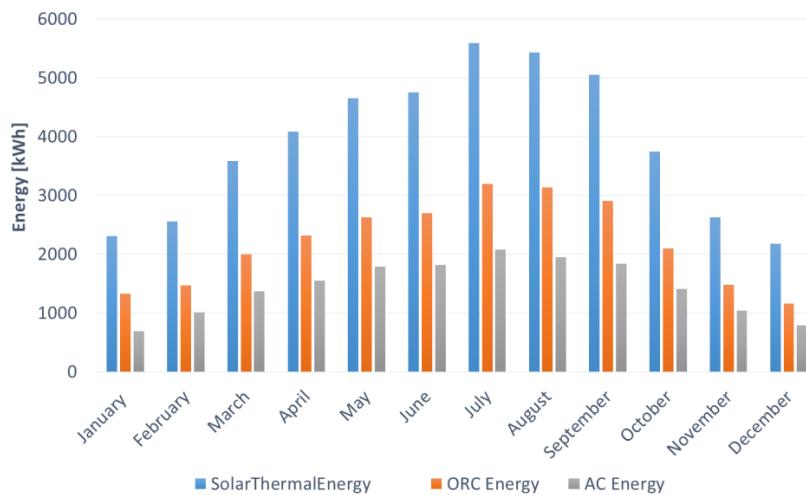

Figure 65 Monthly energy balance of the plant.

Figure 66 reports the yearly energy balance of the plant. The different sectors of the pie chart refer to the energy input to the AC and ORC subsystems and to the losses in the TES. It is evident that a global efficiency decrease is due to thermal losses and irreversibilities.
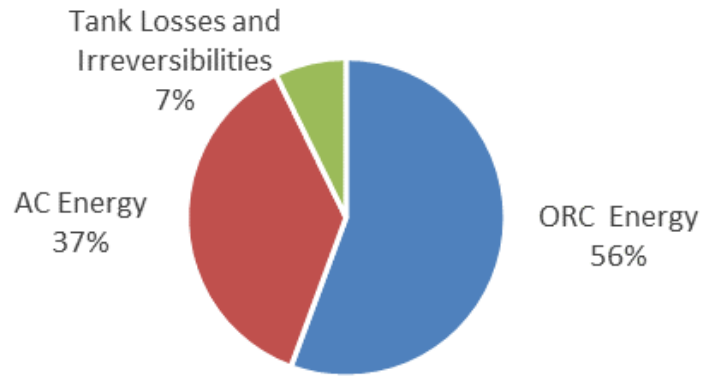
Figure 66 Yearly thermal energy balance

The performance of the plant has been then analyzed on an hourly basis for typical working days in winter and summer as reported in Figure 67. As expected, the thermal energy collected from the solar field during a typical winter day is lower than in a typical summer day, and it's evident a large raise of the $T_{in,ORC}$ in the summer case. In this case the exceeding energy is stored in the TES. The ORC is switched on when the TES average temperature reaches upper bound and works till the temperature decreases down to the bound (65 °C).
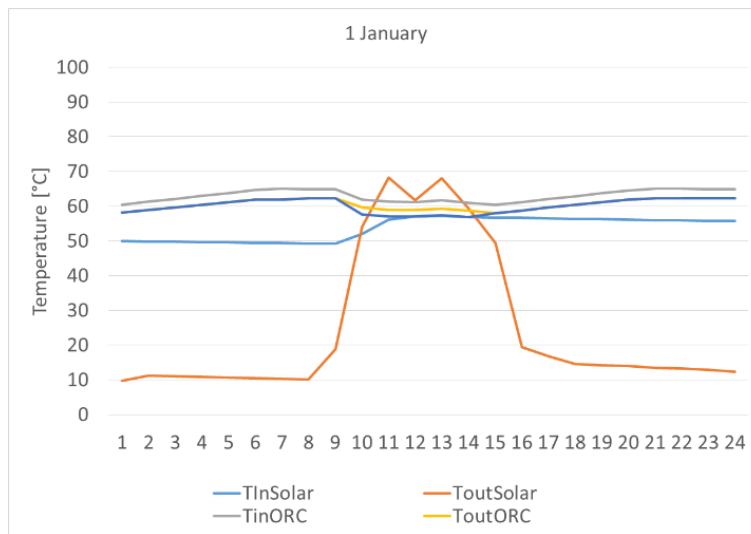
a)
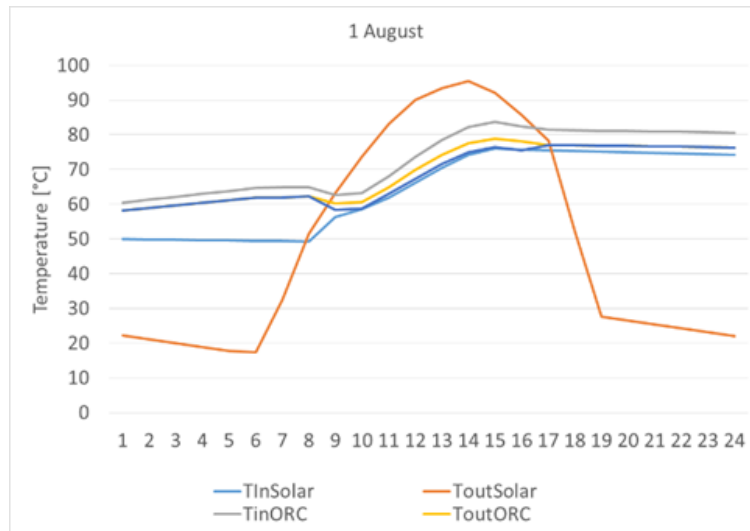
b)

Figure 67 Daily trend of temperature for typical days in (a) winter and in (b) summer.

Table 20 summarizes the main performances parameters of the system. The yearly global efficiency of the plant achieves 63%.

Table 20 CCHP Performances

| Solar Radiation	140.6 MWh
Solar Energy	46.5 MWh
η_{SF}	33%
AUX Energy	973 kWh
ORC Thermal Energy Input	26426 kWh
ORC Electrical Energy	2114 kWh
$\eta_{ORC,el}$	8%
AC Thermal Energy Input	17611 kWh
AC Thermal Energy Output	22681 kWh
AC Cooling Energy	5070 kWh
COP_{AC}	0.29
η_{global}	63%

5.2. Results Integrated Building-CCHP Model

The most representative results obtained from the simulations of the Integrated Building-Plant CCHP Model are presented in this section. The performances of the plants have been evaluated in terms of electric and thermal energy production on a monthly and yearly basis.

Thermal and electric loads

The building has been simulated in Messina, Rome and Milan. These cities are characterized by different climatic conditions and, thus, there is a high variability of thermal and cooling loads for each location. Figure 68 shows that the cooling energy demand of the building located in Messina is significantly higher than the other cities because of the high value of irradiation during summer period. On the contrary, due to the longest heating period and the lowest mean temperatures, the building located in Milan has the highest value of annual heating demand.

The base load of energy demand is covered by the AC unit while the peak of the load profile is delivered by the reversible HP. The CCHP system located in Messina covers almost completely the small heating demand but only the 35% of the cooling demand. The HP and AC working hours for Messina result comparable during the whole year and it is evident the AC results undersized. In Rome, the AC unit covers the 94% and 44% of the heating and cooling demand respectively. Finally, in Milan, the auxiliary HP covers only peaks of load profile during the coldest months while, in summer, the AC covers the entire cooling load. A summary of annual Heating and Cooling energy demand for each location is reported in Table 21.
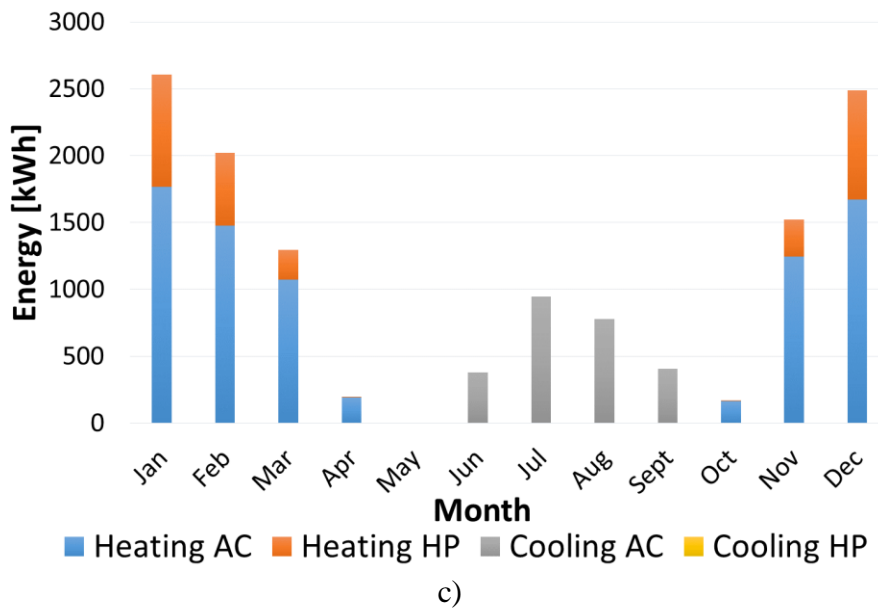

a)

b)

c)
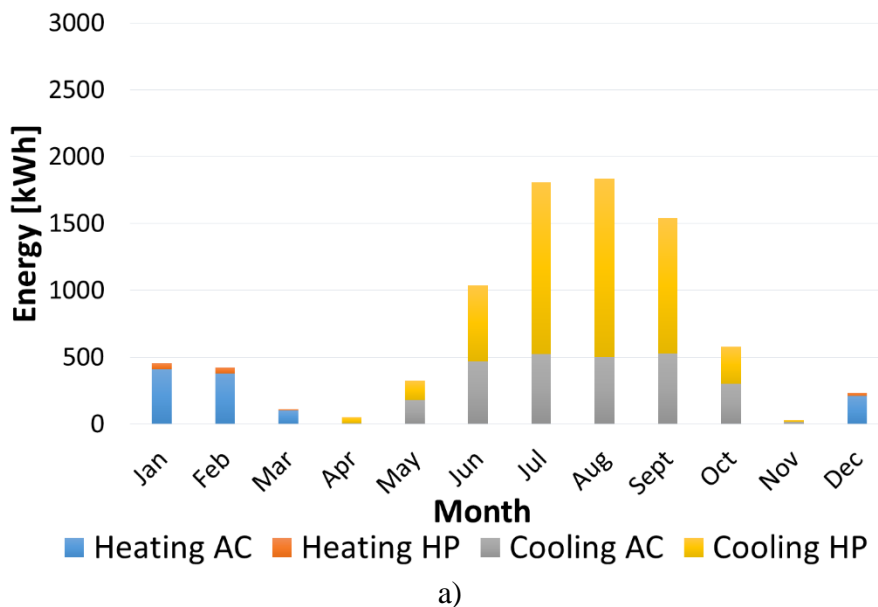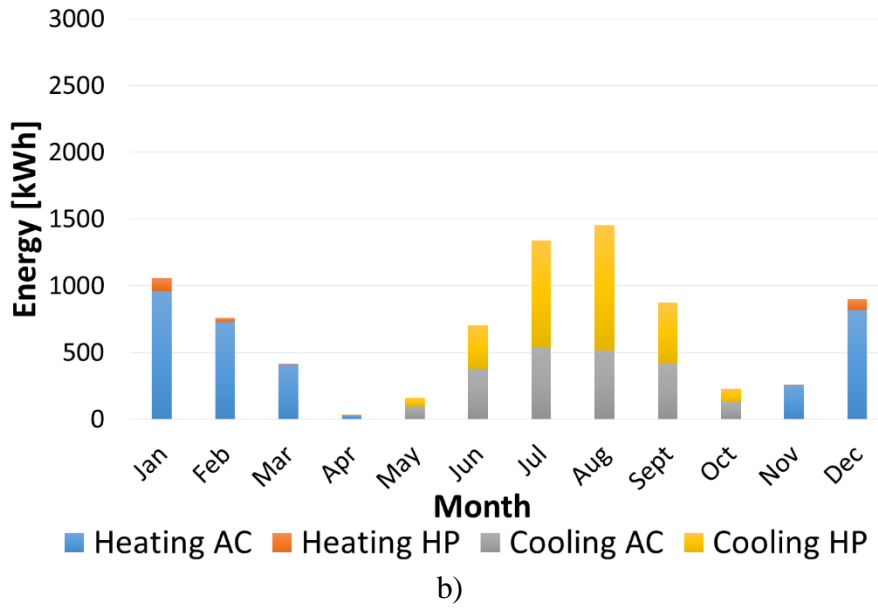
Figure 68 Monthly distribution of Heating and Cooling energy demand for a) Messina b) Rome and c) Milan

Table 21 Summary of Heating and Cooling energy demand on annual basis for different locations

	Messina	Rome	Milan
Total Heating Energy [kWh$_h$]	1222	3415	10281
AC Heating Energy [kWh$_h$]	1100	3197	7581
HP Heating Energy [kWh$_h$]	122	218	2700
Total Cooling Energy [kWh$_c$]	7163	4757	2503
AC Cooling Energy [kWh$_c$]	2520	2073	2503
HP Cooling Energy [kWh$_c$]	4643	2684	0
h$_{AC}$	2246	2366	2603
h$_{HP}$	2113	1532	940

Figure 69a-c and Figure 70a-c report the following daily performance trends in winter and summer season respectively: the amount of solar radiation incident upon the total collector area (I_{tot}); the output thermal power delivered from the Flate Plate Collectors (Q_FPC); the auxiliary thermal power delivered to the TES from the electric resistances (Q_TES_aux); the input thermal power to supply the ORC (Q_ORC_in); the input thermal power to supply the AC (Q_AC_in); the output electric power produced by the ORC (P_ORC_el). During the heating period, the typical winter day considered in Figure 69 shows that the input solar power is not enough to supply the CCHP and there is a high amount of backup energy during working hours. The load profile depends on the location and, thus, from the heating schedule of each climatic zone. For the city of Messina, the CCHP plant is turned off during the night and works mostly in the late afternoon. Figure 69.b shows the working strategy of the CCHP plant and the control unit turns off the ORC according to the building thermal load profile. On the contrary, in Milan, the heating request is high and quite constant during the day as shown in Figure 69c. In the last case, the most of all energy request is obtained from conversion of PV electrical energy in thermal energy to charge the TES. In summer, as shown in Figure 70, for Rome and Messina, the solar energy production is higher and capable to deliver a consistent fraction of the energy required by CCHP system ranging from the 36% and 42%. In Milan, this fraction is about the 14% due to a lower irradiation. During cooling season, the CCHP works all day long in all three cities and turned off in the night. In all configurations, the net ORC electric power is about 1.2 kW$_e$ because supplied from the TES at a fixed temperature of 68°C.
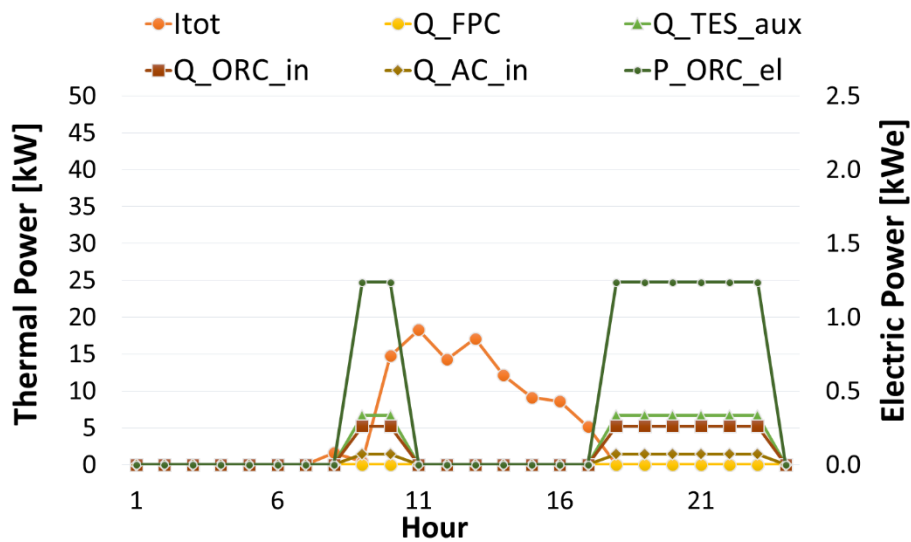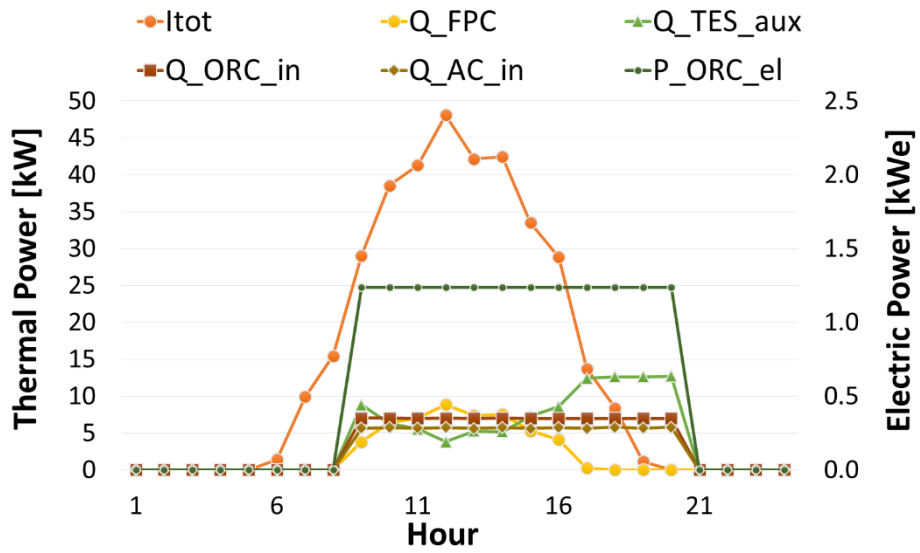

a)
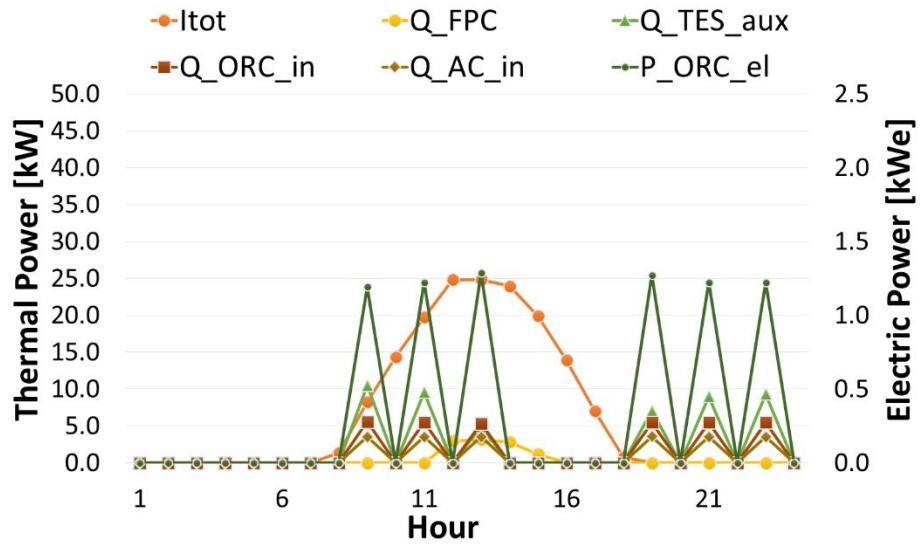
b)
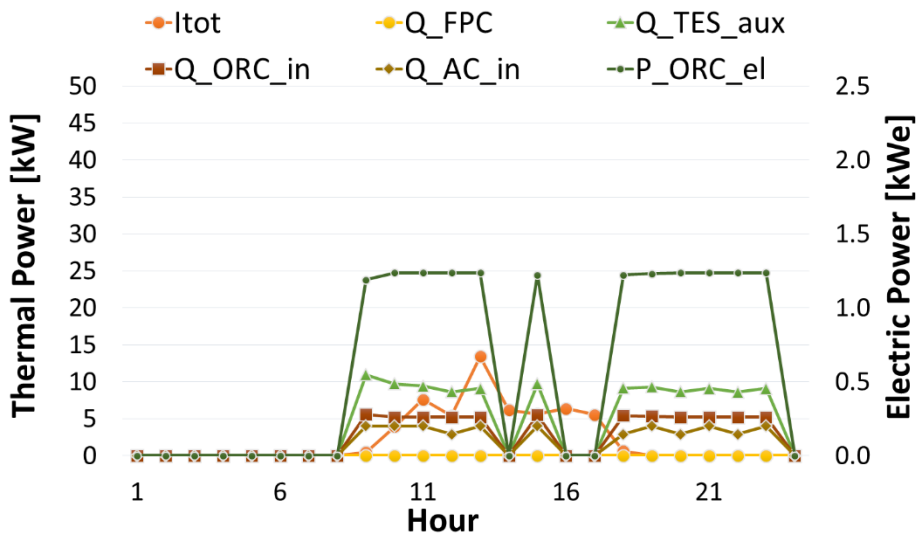
c)

Figure 69 Daily trend of the plant performances for a typical winter day a) in Messina b) in Rome and c) in Milan

a)
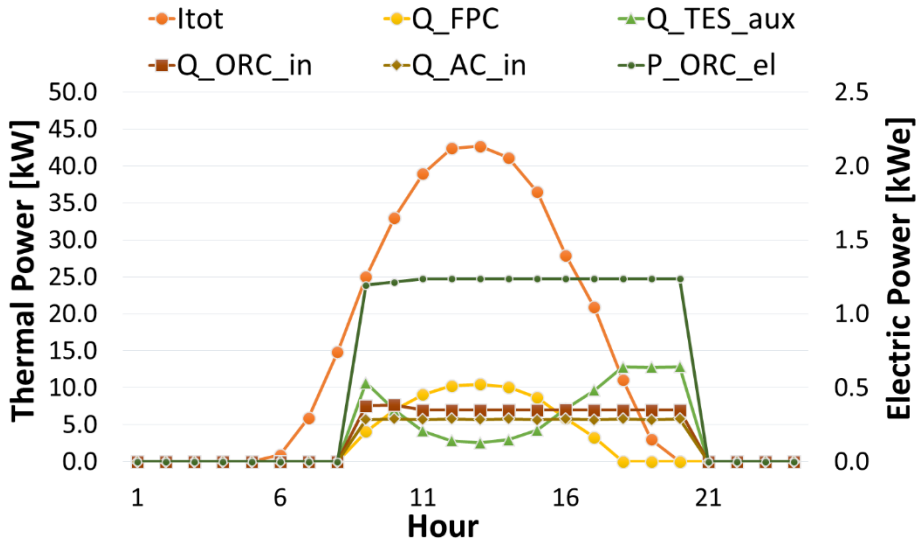
b)
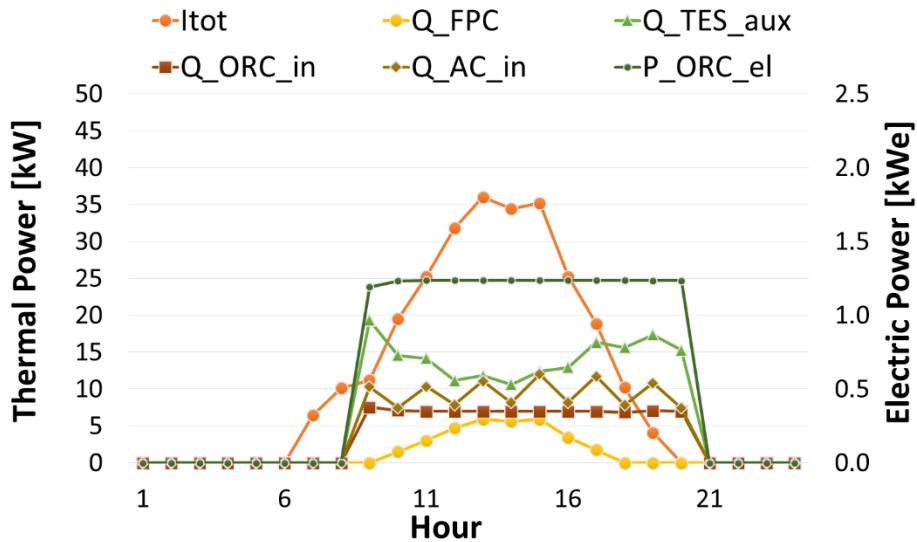
c)

Figure 70 Daily trend of the plant performances for a typical summer day a) in Messina b) in Rome and c) in Milan

The electrical balance of the entire system for each location is shown in Figure 71 and summarized in Table 22. The building load is quite constant all over the year and covered for the 16% by the ORC electric energy production. This fraction can be increased using different management strategies of the CCHP. The rest of the electric load, composed by the electrical energy consumed by resistances of the TES and the auxiliary HP electric energy, is covered by the PV production and the electric energy imported from the Grid. For the city of Milan, the PV plant results undersized due to the lower irradiation thus a high amount of electricity is imported from the grid; however, the self-consumption index results the highest with a value of 58%. In the middle seasons, when the CCHP is turned off because there is no thermal load, the surplus of the PV production is fed into the grid.
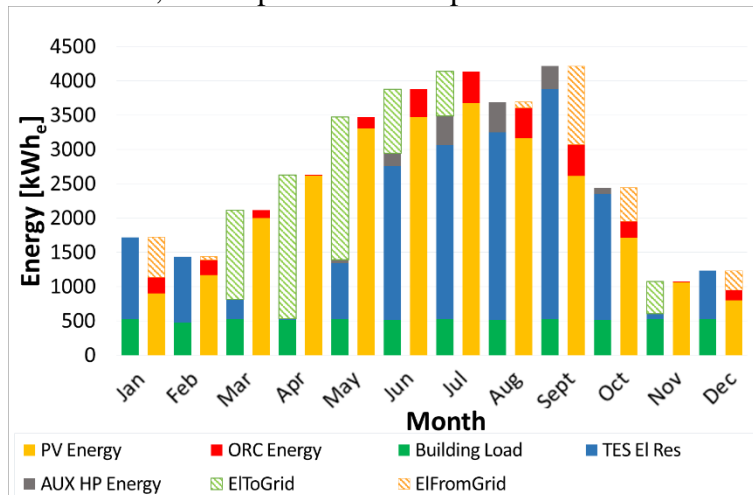
a)
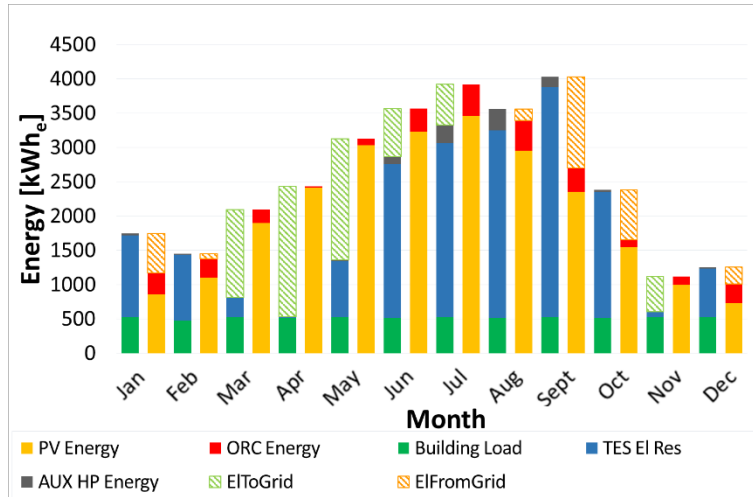
b)
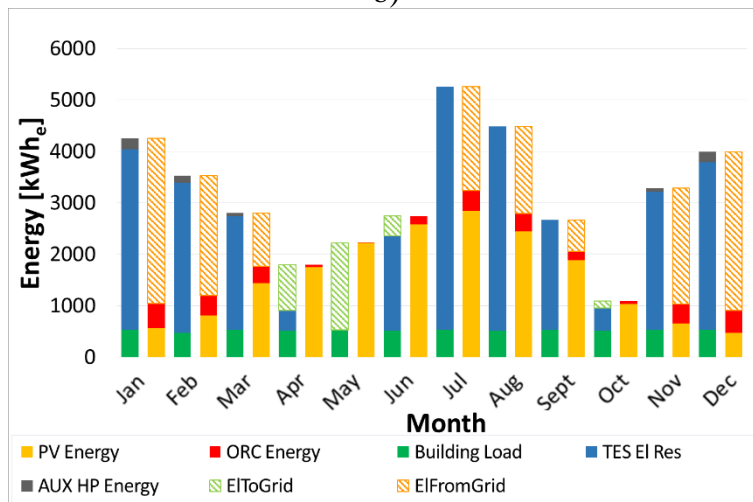
c)

Figure 71 Electrical Energy contributions for a) Messina b) Rome and c) Milan on monthly basis

Table 22 Electrical performances on annual basis for different locations

	Messina	Rome	Milan
Building load [kWh$_e$]	6203	6203	6203
HP Electrical Energy [kWh$_e$]	1579	950	940
TES Backup Electrical Energy [kWh$_e$]	16753	18888	28104
PV Electrical Energy [kWh$_e$]	26480	24547	18674
ORC Electrical Energy [kWh$_e$]	1069	1059	1071
Electric Energy from the Grid [kWh$_e$]	12862	14285	21590
Electric Energy to the Grid [kWh$_e$]	17762	15842	9162
Self-consumption index	40%	42%	58%

In order to compare the performances of the proposed CCHP system, efficiencies of the main components are reported in Table 23.

Also the global efficiency of the system ($\eta_{global,CCHP}$) is defined as the ratio between the useful electric, thermal, cooling energy and the inlet thermal energy from the solar field and the auxiliary energy:

$$\eta_{global,CCHP} = \frac{E_{heating} + E_{cooling} + E_{el,ORC}}{E_{FPC} + E_{el,HP} + E_{el,TES}}$$ (26)

Table 23 Global CCHP performances on annual basis for different locations

	Messina	Rome	Milan
η_{FPC}	11%	10%	7%
Seasonal $COP_{h,AC}$	1.3	1.3	1.3
Seasonal $COP_{c,AC}$	0.26	0.26	0.26
$\eta_{ORC,el}$	7%	7%	7%
$\eta_{global,CCHP}$	32%	32%	42%

The results have been compared to similar studies. Cioccolanti et al. proposed an experimental small scale prototype system composed of a 50m² CPC solar field, a 3.5 kWe ORC plantand a 17 kWc absorption chiller in [128]. Results showed a global efficiency value of 24.4% and the ORC unit reaches a mean electric efficiency of 4% during the whole year and a value of operating working hour limited to 650h due to a the limited area of the collectors of 50 m². Calise et al. designed and simulated a prototype of a small-scale solar CHP system based on evacuated flat-plate solar collectors and Organic Rankine Cycle and an average electric efficiency of 10% was found for the ORC. [129]. They can be comparable and show energy performances similar to this case study.

Energy and environmental analysis

The energy, environmental and economic performance of proposed system are compared with those achieved by the reference system based on separated energy production. In the reference system, the electric, cooling, and heating demand of the buildings are satisfied by the local electric grid, AC a compression chiller with a COP_c of 3.0, and gas fired boiler with a thermal efficiency of 0.92, respectively. The average Italian efficiency of thermo-electric power plant mix is equal to 0.44.

The primary energy savings of the overall system:

$$PES = \frac{PE_{ref} - PE_{CCHP}}{PE_{ref}}$$ (27)

Where the primary energy consumed by the reference system is:

$$PE_{ref} = PE_{heat} + PE_{cool} + PE_{FromGrid} = \frac{E_{heat}}{\eta_{boiler}} + \frac{E_{cool}}{EER_{ref} \cdot \eta_{Grid}} + \frac{E_{el,load}}{\eta_{Grid}}$$ (28)

The primary energy consumed by the simulated CCHP system is:

$$PE_{CCHP} = PE_{FromGrid} - PE_{ToGrid} = \frac{E_{FromGrid}}{\eta_{Grid}} - \frac{E_{ToGrid}}{\eta_{Grid}}$$ (29)

In Eq. (28) and (29), $PE_{FromGrid}$ represents the primary electric energy withdrawn from the grid, while, in equation (29) in case of insufficient electric production, PE_{ToGrid} represents the electric energy fed to the electric grid, in case of overproduction.

The environmental performance of the CCHP system is evaluated on the basis of on the equivalent dioxide emissions reduction ($CO_{2,avoided}$) respect to the reference system calculated in (30):

$$CO_{2,avoided} = f_{CO_2} \cdot (PE_{ref} - PE_{CCHP}) \qquad (30)$$

Where f_{CO2}, the Italian CO_2 emission factor, is set at 0.39 kg_{CO2}/kWh [130].

Results of the energy and environmental analysis are shown in Table 24.

Table 24 Energy and environmental analysis of CCHP, for different location

Location	PES	$CO_{2,avoided}$
Messina	1.53	11713 kg_{CO2}
Rome	1.16	9213 kg_{CO2}
Milan	-0.01	-73 kg_{CO2}

In particular, the PES is negative for Milan. Due to a lower Irradiation, the electric energy production is not enough to feed the auxiliary heat pump for covering the heating demand and, thus, the PV plant results undersized.

Economic analysis

In this section the energy, environmental and economic results as well as the sensitivity analysis are presented.

The initial investment cost related to CCHP plant (IC_{CCHP}) is calculated summing the cost of all main components of the system, Furthermore, an installation cost of 15% has been taken into account. All specific costs have been taken from literature and the breakdown of the costs is showed in Table 12. Unitary price of electric energy of 0.19 EUR/kWh$_e$ and of natural gas of 0.80 EUR/Sm^3 were considered as average seasonal values in Italy and were used to calculate the economic annual cost of the reference system.

The Electricity is exchanged with the grid by means of a specific feed-in policy mechanism ("Scambio Sul Posto", SSP) designed to provides economical compensation to PV system owners. Under SSP, the plant operator pays the supplier for the electricity consumed, while the Italian Electric Grid Manager (GSE) gives credit for the electricity fed in. The balance is calculated once a year and this method can lead to a surplus on behalf of the plant operator [131].

Table 25 Breakdown of the costs of the CCHP system

Component	Specific Cost	Total Cost
PV system	1700 EUR/kW	17000 EUR
Flat Plate Collectors	300 EUR/kW	18000 EUR
TES	2000 EUR	2000 EUR
Adsorption Chiller	1700 EUR/kW	7500 EUR
ORC	5000 EUR/kWe	15000 EUR
Heat Pump	6000 EUR	6000 EUR
Total sum		64000 EUR
Installation Cost		+15%
Total IC$_{CCHP}$		73500 EUR

The Net Present Value (NPV) has been calculated in order to analyze the profitability of the investment according to (31):

$$NPV = \sum_{k=0}^{n} \frac{F_k}{(1+i)^k}$$ (31)

Where F_k is the net cash inflow-outflows during a single period k, "i" is the discount rate of return fixed at 0.04, and n is the amount of years of the useful life of the plant.
Initially, the Simple Pay Back (SPB) has been evaluated without considering any type of incentives, in order to perform the economic analysis according to (32):

$$NPV = \sum_{k=0}^{SPB} \frac{F_k}{(1+i)^k} = 0$$ (32)

Considering Table 26and Figure 72, a SPB over 25 years has been obtained. This payback period is not acceptable. However, in Italy the economic feasibility of these systems is supported by economic incentives.
Thus the SPB$_{inc}$ has been evaluated, taking into account an incentive about the covering of 65% of the initial investment cost related to the CCHP plant [132];

a)

b)
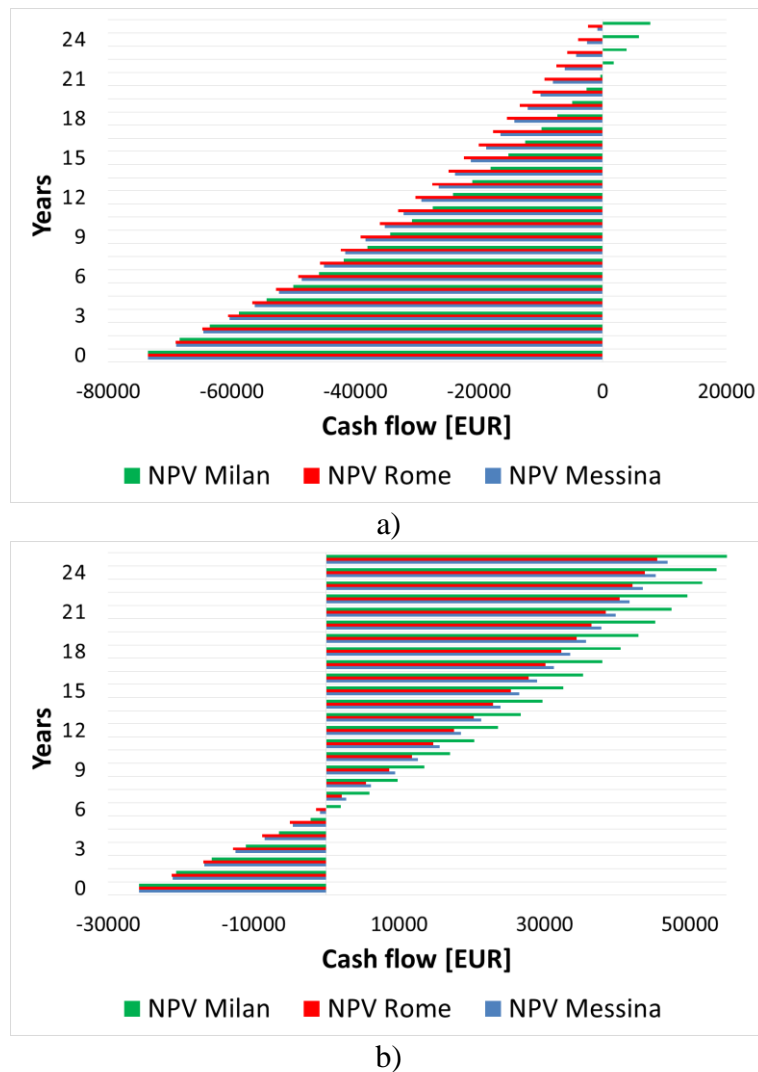
Figure 72 NPV for different locations a) without incentives and b) with incentives

Table 26 Economic analysis of CCHP, for different locations without incentives and with incentives

Location	NPV (25 y)	SPB	NPV$_{inc}$	SPB$_{inc}$
Messina	-853 EUR	>25 y	47000 EUR	6 y
Rome	-2342 EUR	>25 y	45500 EUR	7 y
Milan	7750 EUR	22 y	55500 EUR	6 y

It's reasonable considering an economic feasibility with a SPB of 10 years. The minimum incentive to achieve this value is about the 50% of the initial investment cost. Thus, the CCHP feasibility can be evaluated also taking in account other values for nations with different economic support mechanisms.

The overall economic performances have been compared to other works as well as done in the energy analysis. Taking in account as reference systems the previous works [128,129], values of PBT results over 25 years and 13 years respectively. Considering a government's financial support, the PBT can achieve values of 13 years and 5 years for the considered configurations. Therefore, it can be concluded that results above have been successfully validated on the basis of similar works available in literature.

6. CONCLUSIONS

In this work, a small scale solar CCHP system conceived for the residential sector has been investigated by means of a dynamic model in TRNSYS. The system is based on a 3 kW$_e$ ORC and a 4.4 kW$_c$ thermally driven Adsorption Chiller experimental prototypes and a solar field is supposed to be the primary source. Nevertheless, the plant is able to work with any low temperature power supply. The water heated in the solar collectors is used to feed a 2 m^3 thermal energy storage used as heat buffer, which is provided with electro-resistances as supplementary thermal source to supply the ORC unit and in cascade, the adsorption chiller. The system is also equipped with an auxiliary 6 kW$_c$ reversible heat pump to cover the peak of the thermal energy demand from the building. The main innovation of the model is the integration of the micro-ORC unit with the adsorption chiller, implemented on TRNSYS by user-defined types that use performance data obtained by a full experimental characterization of ORC and AC prototypes, which are installed and currently working at University of Bologna and at CNR - ITAE respectively. The dynamic performances of the considered system have been evaluated with respect to a real "nearly zero energy building" (NZEB) located in three different cities representative of the Italian climatic zones: Messina, Rome and Milan. Results of simulations, which have been carried out on hourly basis, revealed the great influence of solar radiation and weather conditions on the effectiveness of the system. The CCHP plant works for about 2400 hours per year on average with different load profiles and can achieve a global efficiency ranging between 32% and 42%.

A techno-economic analysis was carried out and the payback period of the analyzed solution results in more than 25 years unless economic support mechanisms are considered. If the initial cost is supported by economic incentives, the economic analysis shows that the proposed CCHP system can achieve a Pay Back Time of 6 years with a Net Present Value of 50 kEUR at 25 years. The economic feasibility of the CCHP system can be achieved also for different government's financial support considering a minimum economic incentive of 50% of the initial investment cost.

On the experimental side, a novel Adsorption Chiller prototype has been designed and realized. Each component has been modelled, manufactured, and tested on a dedicated test bench. The final prototype has been at least assembled and is currently under characterization by means of the full-scale test station located at the "TEST CENTER" of the C.N.R. I.T.A.E. to define a complete performance map in the typical operating conditions of the application subject of this project. Preliminary tests have been carried out and the maximum Cooling Capacity is achieved at the cycle time of 5 minutes.

In conclusion, this PhD activity has highlighted the potential of solar driven micro-CCHP systems for residential applications, and its economic feasibility if government's financial support is available; moreover, the proposed model can be adopted as a tool for the design of similar systems by redefining the different subsystems according to the desired technology.

Future activities will be dedicated to validation of the proposed model by means of a lab-scale installation at the CNR ITAE labs. Also, many strategies of optimization of the studied CCHP system will be analyzed to achieve better performances, including the possibility of integration of hybrid chillers.

REFERENCES

[1]   International Energy Agency (IEA), Global Energy Review: CO2 Emissions in 2021, (2021).

[2]   International Energy Agency (IEA), Energy Efficiency Report, (2021).

[3]   International Energy Agency (IEA), Energy efficiency 2020, Paris, n.d. https://www.iea.org/reports/energy-efficiency-2020.

[4]   Eurostat, Energy Balance, (2017). http://ec.europa.eu/eurostat/web/energy/data/energy-balances.

[5]   IPCC, Climate Change 2022, 2022. https://www.ipcc.ch/report/ar6/wg3/.

[6]   Directive 2010/31/EU of the European Parliament and of Council of 19 May 2010 on the energy performance of buildings (recast), Off. J. Eur. Union. (2010) 13–25.

[7]   DIRECTIVE 2012/27/EU OF THE EUROPEAN PARLIAMENT AND OF THE COUNCIL of 25 October 2012 on energy efficiency, Off. J. Eur. Union. (2012) 1–56. https://eur-lex.europa.eu/LexUriServ/LexUriServ.do?uri=OJ:L:2012:315:0001:0056:en:PDF.

[8]   E. Commission, D.-G. for Energy, Clean energy for all Europeans, Publications Office, 2019. https://doi.org/doi/10.2833/9937.

[9]   Directive (EU) 2018/844 of the European Parliament and of the Council of 30 May 2018, Off. J. Eur. Union. (2018). https://eur-lex.europa.eu/legal-content/EN/TXT/?uri=uriserv:OJ.L_.2018.156.01.0075.01.ENG.

[10]   E. Commission, COMMUNICATION FROM THE COMMISSION TO THE EUROPEAN PARLIAMENT, THE COUNCIL, THE EUROPEAN ECONOMIC AND SOCIAL COMMITTEE AND THE COMMITTEE OF THE REGIONS - A Renovation Wave for Europe - greening our buildings, creating jobs, improving lives, (2020).

[11]   E. Commission, COMMUNICATION FROM THE COMMISSION TO THE EUROPEAN PARLIAMENT, THE EUROPEAN COUNCIL, THE COUNCIL, THE EUROPEAN ECONOMIC AND SOCIAL COMMITTEE AND THE COMMITTEE OF THE REGIONS The European Green Deal, (2019). https://eur-lex.europa.eu/legal-content/EN/TXT/?qid=1576150542719&uri=COM%3A2019%3A640%3AFIN.

[12]   E. Commission, Proposal for a DIRECTIVE OF THE EUROPEAN PARLIAMENT AND OF THE COUNCIL on the energy performance of buildings (recast), (2021).

[13]   E. Commission, COMMISSION RECOMMENDATION (EU) 2019/1019 of 7 June 2019 on building modernisation, Off. J. Eur. Union. (2019).

[14]   I. Official Gazette, Legislative Decree no. 192 of 19 August 2005, (2005).

[15]   I. Official Gazette, Legislative Decree 311/2006, (2006).

[16]   I. Official Gazette, DECREE OF THE PRESIDENT OF THE ITALIAN REPUBLIC DPR 59, (2009).

[17]   E. Negro, T. Cardinale, N. Cardinale, G. Rospi, Italian Guidelines for Energy Performance of Cultural Heritage and Historical Buildings: The Case Study of the Sassi of Matera, Energy Procedia. 97 (2016) 7–14. https://doi.org/https://doi.org/10.1016/j.egypro.2016.10.008.

[18]   I. Official Gazette, Law no. 90/2013, (2013).

[19]   Gestore dei Servizi Energetici – GSE, Guida alla Cogenerazione ad Alto Rendimento CAR, aggiornamento dell'edizione 1, (2018).

[20]   Gestore dei Servizi Energetici – GSE S.p.A, Sintesi nuovo decreto Certificati Bianchi, DM 11 gennaio 2017, (2017).

[21]   European Union, DIRECTIVE 2004/8/EC OF THE EUROPEAN PARLIAMENT AND OF THE COUNCIL, Off. J. Eur. Union. (2004).

[22]   J.R. Oliver, A Micro-Cooling, Heating, And Power (M-CHP) Instructional Module, 2005.

[23]   Y.A. Çengel, Thermodynamics : an engineering approach, Sixth edition. Boston : McGraw-

Hill Higher Education, [2008] ©2008, n.d.
https://search.library.wisc.edu/catalog/9910062108002121.

[24]   I.E. Agency, Energy Balances of OECD Countries 2010, 2010.
https://doi.org/https://doi.org/https://doi.org/10.1787/energy_bal_oecd-2010-en-fr.

[25]   International Energy Agency (IEA), Tracking Industrial Energy Efficiency and CO2
Emissions, (2007). https://www.iea.org/reports/tracking-industrial-energy-efficiency-and-
co2-emissions.

[26]   International Energy Agency (IEA), Combined Heat and Power, (2008).

[27]   U.S. ENVIRONMENTAL PROTECTION AGENCY, Combined Heat and Power - A Guide
to Developing and Implementing Greenhouse Gas Reduction Programs, (2014).

[28]   International Energy Agency (IEA), Distributed Generation in Liberalised Electricity
Markets, (2002).

[29]   K.S. and T.U. Nishio, M., J. Itoh, A thermodynamic approach to steam-power system design,
Ind. Eng. Chem. Process Des. Dev. (1980).

[30]   L. Dong, H. Liu, S. Riffat, Development of small-scale and micro-scale biomass-fuelled CHP
systems – A literature review, Appl. Therm. Eng. 29 (2009) 2119–2126.
https://doi.org/https://doi.org/10.1016/j.applthermaleng.2008.12.004.

[31]   J.A. Orlando, R. of Heating, A.-C. Engineers, Cogeneration Design Guide, American Society
of Heating, Refrigerating and Air-Conditioning Engineers, 1996.
https://books.google.it/books?id=u%5C_AeAQAAIAAJ.

[32]   U.S.E.P.A. and Environmental Analysis, i., " I. Eastern Research Group, Energy, Biomass
Combined Heat and Power: Catalog of Technologies, US Environ. Prot. Agency, Comb.
Heat Power Partnersh. (2007).

[33]   R.K. and G.T. Simader, G. R., Micro CHP systems: state of the art, Eur. Comm. Austrian
Fed. Minist. Econ. Labour. (2006).

[34]   Energy Nexus Group, Technology Characterization: Microturbines, (2002).

[35]   Department of Trade and Industry, Microgeneration strategy, 2006.

[36]   M. Banjac, D. Djukanovic, M. Petrovic, Techno-economic analysis of gas turbine-based
CHP plant operation under a feed-in tariff system, Therm. Sci. 24 (2020) 150.
https://doi.org/10.2298/TSCI200103150B.

[37]   H.I. Onovwiona, V.I. Ugursal, Residential cogeneration systems: review of the current
technology, Renew. Sustain. Energy Rev. 10 (2006) 389–431.
https://doi.org/https://doi.org/10.1016/j.rser.2004.07.005.

[38]   G. Marinitsch, F. Biedermann, Development of a hot gas heat exchanger and a cleaning
system for a 35kWel hermetic four cylinder Stirling engine for solid biomass fuels, (2005).

[39]   P. Rasmussen, M. Nielsen, S. Kær, S. Andreasen, Experimental study and modeling of
degradation phenomena in HTPEM fuel cell stacks for use in CHP systems, (2009).

[40]   J. Wang, N. He, J. Fei, Z. Ma, Z. Ji, Z. Chen, N. Nie, Y. Huang, Flexible and wearable fuel
cells: A review of configurations and applications, J. Power Sources. 551 (2022) 232190.
https://doi.org/https://doi.org/10.1016/j.jpowsour.2022.232190.

[41]   M. Liu, Y. Shi, F. Fang, A new operation strategy for CCHP systems with hybrid chillers,
Appl. Energy. 95 (2012) 164–173.
https://doi.org/https://doi.org/10.1016/j.apenergy.2012.02.035.

[42]   J. Carles Bruno, A. Valero, A. Coronas, Performance analysis of combined microgas turbines
and gas fired water/LiBr absorption chillers with post-combustion, Appl. Therm. Eng. 25
(2005) 87–99. https://doi.org/https://doi.org/10.1016/j.applthermaleng.2004.05.002.

[43]   M.V. Oro, R.G. de Oliveira, E. Bazzo, An integrated solution for waste heat recovery from
fuel cells applied to adsorption systems, Appl. Therm. Eng. 136 (2018) 747–754.
https://doi.org/https://doi.org/10.1016/j.applthermaleng.2018.01.081.

[44]   P. Colonna, S. Gabrielli, Industrial trigeneration using ammonia–water absorption
refrigeration systems (AAR), Appl. Therm. Eng. 23 (2003) 381–396.

https://doi.org/https://doi.org/10.1016/S1359-4311(02)00212-0.

[45] B. Le Lostec, N. Galanis, J. Millette, Simulation of an ammonia–water absorption chiller, Renew. Energy. 60 (2013) 269–283. https://doi.org/https://doi.org/10.1016/j.renene.2013.05.027.

[46] Z. He, T. Ding, Y. Liu, Z. Li, Analysis of a district heating system using waste heat in a distributed cooling data center, Appl. Therm. Eng. 141 (2018) 1131–1140. https://doi.org/https://doi.org/10.1016/j.applthermaleng.2018.06.036.

[47] N. Fumo, P.J. Mago, L.M. Chamra, Emission operational strategy for combined cooling, heating, and power systems, Appl. Energy. 86 (2009) 2344–2350. https://doi.org/https://doi.org/10.1016/j.apenergy.2009.03.007.

[48] J.-J. Wang, Y.-Y. Jing, C.-F. Zhang, Z. (John) Zhai, Performance comparison of combined cooling heating and power system in different operation modes, Appl. Energy. 88 (2011) 4621–4631. https://doi.org/https://doi.org/10.1016/j.apenergy.2011.06.007.

[49] X.Q. Kong, R.Z. Wang, X.H. Huang, Energy optimization model for a CCHP system with available gas turbines, Appl. Therm. Eng. 25 (2005) 377–391. https://doi.org/https://doi.org/10.1016/j.applthermaleng.2004.06.014.

[50] G. Yang, X. Zhai, Optimization and performance analysis of solar hybrid CCHP systems under different operation strategies, Appl. Therm. Eng. 133 (2018) 327–340. https://doi.org/https://doi.org/10.1016/j.applthermaleng.2018.01.046.

[51] X. Song, L. Liu, T. Zhu, T. Zhang, Z. Wu, Comparative analysis on operation strategies of CCHP system with cool thermal storage for a data center, Appl. Therm. Eng. 108 (2016) 680–688. https://doi.org/https://doi.org/10.1016/j.applthermaleng.2016.07.142.

[52] D. Haeseldonckx, L. Peeters, L. Helsen, W. D'haeseleer, The impact of thermal storage on the operational behaviour of residential CHP facilities and the overall CO2 emissions, Renew. Sustain. Energy Rev. 11 (2007) 1227–1243. https://doi.org/https://doi.org/10.1016/j.rser.2005.09.004.

[53] S. Garimella, M.J. Ponkala, A. Goyal, M.A. Staedter, Waste-heat driven ammonia-water absorption chiller for severe ambient operation, Appl. Therm. Eng. 154 (2019) 442–449. https://doi.org/https://doi.org/10.1016/j.applthermaleng.2019.03.098.

[54] H. Nami, A. Anvari-Moghaddam, Small-scale CCHP systems for waste heat recovery from cement plants: Thermodynamic, sustainability and economic implications, Energy. 192 (2020) 116634. https://doi.org/https://doi.org/10.1016/j.energy.2019.116634.

[55] M. Wegener, A. Malmquist, A. Isalgue, A. Martin, P. Arranz, O. Camara, E. Velo, A techno-economic optimization model of a biomass-based CCHP/heat pump system under evolving climate conditions, Energy Convers. Manag. 223 (2020) 113256. https://doi.org/https://doi.org/10.1016/j.enconman.2020.113256.

[56] M. Deymi-Dashtebayaz, M. Norani, Sustainability assessment and emergy analysis of employing the CCHP system under two different scenarios in a data center, Renew. Sustain. Energy Rev. 150 (2021) 111511. https://doi.org/https://doi.org/10.1016/j.rser.2021.111511.

[57] Y. Li, R. Tian, M. Wei, F. Xu, S. Zheng, P. Song, B. Yang, An improved operation strategy for CCHP system based on high-speed railways station case study, Energy Convers. Manag. 216 (2020) 112936. https://doi.org/https://doi.org/10.1016/j.enconman.2020.112936.

[58] V. Zare, H. Rostamnejad Takleh, Novel geothermal driven CCHP systems integrating ejector transcritical CO2 and Rankine cycles: Thermodynamic modeling and parametric study, Energy Convers. Manag. 205 (2020) 112396. https://doi.org/10.1016/J.ENCONMAN.2019.112396.

[59] M.J. Dehghani, C. Kyoo Yoo, Modeling and extensive analysis of the energy and economics of cooling, heat, and power trigeneration (CCHP) from textile wastewater for industrial low-grade heat recovery, Energy Convers. Manag. 205 (2020) 112451. https://doi.org/https://doi.org/10.1016/j.enconman.2019.112451.

[60] M. Soltani, M. Chahartaghi, S. Majid Hashemian, A. Faghih Shojaei, Technical and

economic evaluations of combined cooling, heating and power (CCHP) system with gas engine in commercial cold storages, Energy Convers. Manag. 214 (2020) 112877. https://doi.org/https://doi.org/10.1016/j.enconman.2020.112877.

[61] X. Wang, G. Shu, H. Tian, R. Wang, J. Cai, Operation performance comparison of CCHP systems with cascade waste heat recovery systems by simulation and operation optimisation, Energy. 206 (2020) 118123. https://doi.org/https://doi.org/10.1016/j.energy.2020.118123.

[62] H. Cho, P.J. Mago, R. Luck, L.M. Chamra, Evaluation of CCHP systems performance based on operational cost, primary energy consumption, and carbon dioxide emission by utilizing an optimal operation scheme, Appl. Energy. 86 (2009) 2540–2549. https://doi.org/https://doi.org/10.1016/j.apenergy.2009.04.012.

[63] E. Tayyeban, M. Deymi-Dashtebayaz, M. Gholizadeh, Investigation of a new heat recovery system for simultaneously producing power, cooling and distillate water, Energy. 229 (2021) 120775. https://doi.org/https://doi.org/10.1016/j.energy.2021.120775.

[64] M. Bianchi, A. De Pascale, P.R. Spina, Guidelines for residential micro-CHP systems design, Appl. Energy. 97 (2012) 673–685. https://doi.org/10.1016/j.apenergy.2011.11.023.

[65] M.M. Maghanki, B. Ghobadian, G. Najafi, R.J. Galogah, Micro combined heat and power (MCHP) technologies and applications, Renew. Sustain. Energy Rev. 28 (2013) 510–524. https://doi.org/10.1016/j.rser.2013.07.053.

[66] A. Akisawa, T. Miyazaki, T. Kashiwagi, Theoretical analysis of the optimal configuration of co-generation systems and competitiveness of heating/cooling technologies, Energy. 35 (2010) 4071–4078. https://doi.org/10.1016/j.energy.2010.06.015.

[67] E. Cardona, A. Piacentino, F. Cardona, Matching economical, energetic and environmental benefits: An analysis for hybrid CHCP-heat pump systems, Energy Convers. Manag. 47 (2006) 3530–3542. https://doi.org/10.1016/j.enconman.2006.02.027.

[68] G. Angrisani, A. Akisawa, E. Marrasso, C. Roselli, M. Sasso, Performance assessment of cogeneration and trigeneration systems for small scale applications, Energy Convers. Manag. 125 (2016) 194–208. https://doi.org/10.1016/j.enconman.2016.03.092.

[69] G. Angrisani, C. Roselli, M. Sasso, F. Tariello, Dynamic performance assessment of a micro-trigeneration system with a desiccant-based air handling unit in Southern Italy climatic conditions, Energy Convers. Manag. 80 (2014) 188–201. https://doi.org/10.1016/j.enconman.2014.01.028.

[70] J.S. Pereira, J.B. Ribeiro, R. Mendes, G.C. Vaz, J.C. André, ORC based micro-cogeneration systems for residential application - A state of the art review and current challenges, Renew. Sustain. Energy Rev. 92 (2018) 728–743. https://doi.org/10.1016/j.rser.2018.04.039.

[71] I. Garcia-Saez, J. Méndez, C. Ortiz, D. Loncar, J.A. Becerra, R. Chacartegui, Energy and economic assessment of solar Organic Rankine Cycle for combined heat and power generation in residential applications, Renew. Energy. 140 (2019) 461–476. https://doi.org/10.1016/j.renene.2019.03.033.

[72] H. Yu, T. Gundersen, X. Feng, Process integration of organic Rankine cycle (ORC) and heat pump for low temperature waste heat recovery, Energy. 160 (2018) 330–340. https://doi.org/https://doi.org/10.1016/j.energy.2018.07.028.

[73] Y. Fan, L. Luo, B. Souyri, Review of solar sorption refrigeration technologies: Development and applications, Renew. Sustain. Energy Rev. 11 (2007) 1758–1775. https://doi.org/https://doi.org/10.1016/j.rser.2006.01.007.

[74] D.S. Kim, C.A. Infante Ferreira, Analytic modelling of steady state single-effect absorption cycles, Int. J. Refrig. 31 (2008) 1012–1020. https://doi.org/https://doi.org/10.1016/j.ijrefrig.2007.12.014.

[75] R.J. Dossat, Principles of Refrigeration, fourth edi, Prentice Hall, 1997.

[76] A. Cera-Manjarres, D. Salavera, A. Coronas, Vapour pressure measurements of ammonia/ionic liquids mixtures as suitable alternative working fluids for absorption refrigeration technology, Fluid Phase Equilib. 476 (2018) 48–60.

https://doi.org/https://doi.org/10.1016/j.fluid.2018.01.006.

[77] F. Ziegler, State of the art in sorption heat pumping and cooling technologies, Int. J. Refrig. 25 (2002) 450–459. https://doi.org/https://doi.org/10.1016/S0140-7007(01)00036-6.

[78] M. Izquierdo, M. Venegas, P. Rodríguez, A. Lecuona, Crystallization as a limit to develop solar air-cooled LiBr–H2O absorption systems using low-grade heat, Sol. Energy Mater. Sol. Cells. 81 (2004) 205–216. https://doi.org/https://doi.org/10.1016/j.solmat.2003.11.002.

[79] T.S. Ge, R.Z. Wang, Z.Y. Xu, Q.W. Pan, S. Du, X.M. Chen, T. Ma, X.N. Wu, X.L. Sun, J.F. Chen, Solar heating and cooling: Present and future development, Renew. Energy. 126 (2018) 1126–1140. https://doi.org/https://doi.org/10.1016/j.renene.2017.06.081.

[80] M.H. Vasilis Fthenakis, Rolf Frischknecht, Marco Raugei, Hyung Chul Kim, Erik Alsema, and M. de Wild-Scholten, Methodology Guidelines on Life-Cycle Assessment of Photovoltaic Electricity, IEA PVPS Task 12, Subtask 20, LCA Rep. IEA-PVPS T12-032011. (2011).

[81] J.-S. Kim, F. Ziegler, H. Lee, Simulation of the compressor-assisted triple-effect H2O/LiBr absorption cooling cycles, Appl. Therm. Eng. 22 (2002) 295–308. https://doi.org/https://doi.org/10.1016/S1359-4311(01)00084-9.

[82] Y. Kaita, Simulation results of triple-effect absorption cycles, Int. J. Refrig. 25 (2002) 999–1007. https://doi.org/https://doi.org/10.1016/S0140-7007(01)00100-1.

[83] K. Wang, O. Abdelaziz, P. Kisari, E.A. Vineyard, State-of-the-art review on crystallization control technologies for water/LiBr absorption heat pumps, Int. J. Refrig. 34 (2011) 1325–1337. https://doi.org/https://doi.org/10.1016/j.ijrefrig.2011.04.006.

[84] K. Sumathy, Z.C. Huang, Z.F. Li, Solar absorption cooling with low grade heat source — a strategy of development in South China, Sol. Energy. 72 (2002) 155–165. https://doi.org/https://doi.org/10.1016/S0038-092X(01)00098-6.

[85] M. Izquierdo, M. Venegas, N. García, E. Palacios, Exergetic analysis of a double stage LiBr–H2O thermal compressor cooled by air/water and driven by low grade heat, Energy Convers. Manag. 46 (2005) 1029–1042. https://doi.org/https://doi.org/10.1016/j.enconman.2004.06.016.

[86] J. Fernández-Seara, A. Vales, M. Vázquez, Heat recovery system to power an onboard NH3-H2O absorption refrigeration plant in trawler chiller fishing vessels, Appl. Therm. Eng. (1998). https://doi.org/10.1016/S1359-4311(98)00001-5.

[87] A. Ouadha, Y. El-Gotni, Integration of an ammonia-water absorption refrigeration system with a marine Diesel engine: A thermodynamic study, in: Procedia Comput. Sci., 2013. https://doi.org/10.1016/j.procs.2013.06.099.

[88] T. Cao, H. Lee, Y. Hwang, R. Radermacher, H.H. Chun, Performance investigation of engine waste heat powered absorption cycle cooling system for shipboard applications, Appl. Therm. Eng. 90 (2015) 820–830. https://doi.org/10.1016/j.applthermaleng.2015.07.070.

[89] T. Cao, H. Lee, Y. Hwang, R. Radermacher, H.H. Chun, Modeling of waste heat powered energy system for container ships, Energy. (2016). https://doi.org/10.1016/j.energy.2016.03.072.

[90] C. Ezgi, Design and thermodynamic analysis of an H2O-LiBr AHP system for naval surface ship application, Int. J. Refrig. (2014). https://doi.org/10.1016/j.ijrefrig.2014.08.016.

[91] Y.I. Aristov, Challenging offers of material science for adsorption heat transformation: A review, in: Appl. Therm. Eng., 2013. https://doi.org/10.1016/j.applthermaleng.2011.09.003.

[92] ZEOLITE AQSOA|Products|Mitsubishi Chemical Corporation., Available Online: Https://Www.m-Chemical.Co.Jp/En/Products/Departments/Mcc/Aquachem/Product/1201185_8078.Html,. (n.d.).

[93] A. Karmakar, V. Prabakaran, D. Zhao, K.J. Chua, A review of metal-organic frameworks (MOFs) as energy-efficient desiccants for adsorption driven heat-transformation applications, Appl. Energy. (2020). https://doi.org/10.1016/j.apenergy.2020.115070.

[94]   M.J. Rupa, A. Pal, B.B. Saha, Activated carbon-graphene nanoplatelets based green cooling system: Adsorption kinetics, heat of adsorption, and thermodynamic performance, Energy. (2020). https://doi.org/10.1016/j.energy.2019.116774.

[95]   L.G. Gordeeva, I.S. Glaznev, E. V. Savchenko, V. V. Malakhov, Y.I. Aristov, Impact of phase composition on water adsorption on inorganic hybrids "salt/silica," J. Colloid Interface Sci. (2006). https://doi.org/10.1016/j.jcis.2006.05.009.

[96]   I.S. Girnik, Y.I. Aristov, Making adsorptive chillers more fast and efficient: The effect of bi-dispersed adsorbent bed, Appl. Therm. Eng. (2016). https://doi.org/10.1016/j.applthermaleng.2016.06.016.

[97]   U. Wittstadt, G. Füldner, E. Laurenz, A. Warlo, A. Große, R. Herrmann, L. Schnabel, W. Mittelbach, A novel adsorption module with fiber heat exchangers: Performance analysis based on driving temperature differences, Renew. Energy. (2017). https://doi.org/10.1016/j.renene.2016.08.061.

[98]   K. Grabowska, J. Krzywanski, W. Nowak, M. Wesolowska, Construction of an innovative adsorbent bed configuration in the adsorption chiller - Selection criteria for effective sorbent-glue pair, Energy. 151 (2018) 317–323. https://doi.org/10.1016/j.energy.2018.03.060.

[99]   L.W. Wang, R.Z. Wang, Z.S. Lu, C.J. Chen, J.Y. Wu, Comparison of the adsorption performance of compound adsorbent in a refrigeration cycle with and without mass recovery, Chem. Eng. Sci. (2006). https://doi.org/10.1016/j.ces.2006.01.018.

[100]   Q.W. Pan, R.Z. Wang, L.W. Wang, Comparison of different kinds of heat recoveries applied in adsorption refrigeration system, Int. J. Refrig. (2015). https://doi.org/10.1016/j.ijrefrig.2015.03.022.

[101]   Y.I. Aristov, A. Sapienza, D.S. Ovoshchnikov, A. Freni, G. Restuccia, Reallocation of adsorption and desorption times for optimisation of cooling cycles, Int. J. Refrig. (2012). https://doi.org/10.1016/j.ijrefrig.2010.07.019.

[102]   Q. Pan, J. Peng, R. Wang, Experimental study of an adsorption chiller for extra low temperature waste heat utilization, Appl. Therm. Eng. (2019). https://doi.org/10.1016/j.applthermaleng.2019.114341.

[103]   F. He, K. Nagano, J. Togawa, Experimental study and development of a low-cost 1 kW adsorption chiller using composite adsorbent based on natural mesoporous material, Energy. (2020). https://doi.org/10.1016/j.energy.2020.118365.

[104]   S. Edin Hamrahi, K. Goudarzi, M. Yaghoubi, Experimental study of the performance of a continues solar adsorption chiller using Nano-activated carbon/methanol as working pair, Sol. Energy. (2018). https://doi.org/10.1016/j.solener.2018.08.030.

[105]   FIRA S.p.A., https://bondioli-pavesi.com/, (n.d.).

[106]   RC RACING, https://www.rcracing.it/, (n.d.).

[107]   A. Sapienza, V. Palomba, G. Gullì, A. Frazzica, S. Vasta, A new management strategy based on the reallocation of ads-/desorption times: Experimental operation of a full-scale 3 beds adsorption chiller, Appl. Energy. (2017). https://doi.org/10.1016/j.apenergy.2017.08.036.

[108]   V. Palomba, G.E. Dino, A. Frazzica, Coupling sorption and compression chillers in hybrid cascade layout for efficient exploitation of renewables: Sizing, design and optimization, Renew. Energy. 154 (2020) 11–28. https://doi.org/https://doi.org/10.1016/j.renene.2020.02.113.

[109]   E.O. Doebelin, Measurement Systems: Application and Design, McGraw-Hill, 2004. https://books.google.it/books?id=nFr0wAEACAAJ.

[110]   M. Bianchi, L. Branchini, N. Casari, A. De Pascale, F. Melino, S. Ottaviano, M. Pinelli, P.R. Spina, A. Suman, Experimental analysis of a micro-ORC driven by piston expander for low-grade heat recovery, Appl. Therm. Eng. 148 (2019) 1278–1291. https://doi.org/10.1016/j.applthermaleng.2018.12.019.

[111]   M. Bianchi, L. Branchini, A. De Pascale, F. Melino, S. Ottaviano, A. Peretto, N. Torricelli, Application and comparison of semi-empirical models for performance prediction of a kW-

size reciprocating piston expander, Appl. Energy. 249 (2019) 143–156. https://doi.org/10.1016/j.apenergy.2019.04.070.

[112] A. Sapienza, S. Santamaria, A. Frazzica, A. Freni, Influence of the management strategy and operating conditions on the performance of an adsorption chiller, Energy. 36 (2011) 5532–5538. https://doi.org/10.1016/j.energy.2011.07.020.

[113] S. Santamaria, A. Sapienza, A. Frazzica, A. Freni, I.S. Girnik, Y.I. Aristov, Water adsorption dynamics on representative pieces of real adsorbers for adsorptive chillers, Appl. Energy. 134 (2014) 11–19. https://doi.org/10.1016/j.apenergy.2014.07.053.

[114] A. Sapienza, V. Palomba, G. Gullì, A. Frazzica, S. Vasta, A new management strategy based on the reallocation of ads-/desorption times: Experimental operation of a full-scale 3 beds adsorption chiller, Appl. Energy. 205 (2017) 1081–1090. https://doi.org/10.1016/j.apenergy.2017.08.036.

[115] A. Sapienza, G. Gullì, L. Calabrese, V. Palomba, A. Frazzica, V. Brancato, D. La Rosa, S. Vasta, A. Freni, L. Bonaccorsi, G. Cacciola, An innovative adsorptive chiller prototype based on 3 hybrid coated/granular adsorbers, Appl. Energy. 179 (2016) 929–938. https://doi.org/10.1016/j.apenergy.2016.07.056.

[116] W. Lombardo, S. Ottaviano, L. Branchini, S. Vasta, A. De Pascale, A. Sapienza, A dynamic model of a solar driven trigeneration system based on micro-ORC and adsorption chiller prototypes, in: AIP Conf. Proc., 2019. https://doi.org/10.1063/1.5138831.

[117] Decree 412/93, (n.d.). http://www.gazzettaufficiale.it/eli/id/1993/10/14/ 093G0451/sg.

[118] Segheria Vecchio s.n.c., (n.d.). https://www.segheriavecchio.it/case-blog/casa-mazza.

[119] SketchUp 3D design Software, (n.d.). https://www.sketchup.com/.

[120] UNI – Italian Committee for Standardization. Standard UNI 10339: Air conditioning systems for thermal comfort in buildings. General, classification and requirements. Offer, order and supply specifications, (1995).

[121] UNI – Italian Committee for Standardization. Standard UNI EN 15251: Indoor environmental input parameters for design and assessment of energy performance of buildings addressing indoor air quality, thermal environment, lighting and acoustics, (2008).

[122] American Society of Heating, Refrigerating and Air-Conditioning Engineers (ASHRAE) Standard 90.1-2004, (n.d.).

[123] TABULA WebTool, (2016). http://episcope.eu/building-typology/webtool.

[124] TRNSYS – Transient System Simulation Tool, (n.d.). http://www.trnsys.com/.

[125] H. Kakiuchi, S. Shimooka, M. Iwade, K. Oshima, M. Yamazaki, S. Terada, H. Watanabe, T. Takewaki, Water vapor adsorbent FAM-Z02 and its applicability to adsorption heat pump, Kagaku Kogaku Ronbunshu. 31 (2005) 273–277. https://doi.org/10.1252/kakoronbunshu.31.273.

[126] Oker-Chemie GmbH, (n.d.). http://www.oker-chemie.de/pdfs/Mat_SIO_01_SW_englisch.pdf.

[127] Fahrenheit, (n.d.). https://fahrenheit.cool/en/.

[128] L. Cioccolanti, R. Tascioni, E. Bocci, M. Villarini, Parametric analysis of a solar Organic Rankine Cycle trigeneration system for residential applications, Energy Convers. Manag. 163 (2018) 407–419. https://doi.org/10.1016/j.enconman.2018.02.043.

[129] F. Calise, M.D. D'Accadia, M. Vicidomini, M. Scarpellino, Design and simulation of a prototype of a small-scale solar CHP system based on evacuated flat-plate solar collectors and Organic Rankine Cycle, Energy Convers. Manag. 90 (2015) 347–363. https://doi.org/10.1016/j.enconman.2014.11.014.

[130] IEA, Statistics, CO2 Emissions from Fuel Combustion, (2015).

[131] Scambio sul posto, (n.d.). https://www.gse.it/servizi-per-te/fotovoltaico/scambio-sul-posto.

[132] Conto termico, (n.d.). https://www.gse.it/servizi-per-te/efficienza-energetica/conto-termico.